MSc in Geo-Engineering
MSc thesis

"CPT-based method to determine the lateral capacity of monotonically loaded rigid piles in sand"

Sebastian Matias Bascunan Chaparro

Delft University of Technology
Geo-Engineering

Dr. K.G. Gavin	TU Delft
Ir. K. Reinders	TU Delft
Dr. F. Pisanò	TU Delft
Ir. K. Kaltekis	Fugro
Ir. B.F.J. van Dijk	Arcadis

Preface

This thesis is written as the final requirement in order to obtain the M.Sc. degree in Geo-Engineering at the Technical University of Delft. The research was completed in 9 months from December 2018 to August 2019 and it was a joint task between the university and FUGRO Nederland B.V. where most of the research was conducted at. The supervision was led by Professors Kenneth Gavin and Kristina Reinders from the university, Kostas Kaltekis from FUGRO and Bas van Dijk from ARCADIS.

FUGRO is the world's leading Geo-data specialist, collecting and analysing comprehensive information about the Earth and the structures built upon it. Through integrated data acquisition, analysis and advice, the company unlocks insights from Geo-data to help clients design, build and operate their assets in a safe, sustainable and efficient manner (FUGRO website, 2019).

This thesis is a valuable document for any person who is interested in the prediction of the lateral response of the soil – monopile system subjected to monotonic loads. A new CPT-based method was calibrated by using the data extracted from pile load tests performed in Dunkirk as part of the PISA project and 3D finite element analysis by means of PLAXIS. Three out of the four known soil reactions involved in the lateral behaviour of monopiles, horizontal force and moment at the base and the moment along the shaft, were defined in terms of the tip resistance obtained from the cone penetration test results. The fourth reaction, the $p - y$ curves, was used according to the formulation proposed by Dyson & Randolph.

This research would have not been able to see the light if I had not been helped by different people along the process. First of all, I would like to thank my entire committee for all the hours they spent checking my report, answering my questions, being part of the meetings and replying all the e-mail I sent. Many thanks to the people at FUGRO, for all the good moments I spent at the office, the scientific and non-scientific conversations and all the support they gave me all the time, especially Kostas who was my supervisor and helped me with the calibration of the model and the obtention of the soil parameters. From Arcadis, Bas van Dijk showed always an extensive knowledge in every step of this thesis, from the soil model to the lateral response of the soil. From TU Delft, many thanks to Ken for always showing me the right path to follow and Kristina for reading and correcting my thesis and helping me with the structural analysis of the monopile. Also, I am very thankful to Federico for taking the time to read and comment on this thesis. Finally, special thanks to Professor David Igoe from Trinity College Dublin for providing me with the MATLAB routine that was used to prove the validity of the proposed method.

All the people who supported me in this endeavour: my classmates, bartenders all around Delft and of course all the good friends that I made here. Being away from your home country is sometimes hard and without the support of these beautiful people, everything would have been harder.

Finally to my family, without you, I could not have done it. Thank you for everything now and always.

Executive summary

Monopiles are commonly used as foundations for offshore wind turbine generators (WTGs). Due to the rapid growth of the offshore wind energy sector, there is increasing demand for WTGs of larger capacities which evidently leads to demand for monopiles with larger diameters. European Wind Energy Association's (EWEA) new Central Scenario expects 320 GW, which means the 32% of the total energy, of wind energy capacity to be installed in the European Union in 2030, 254 GW of onshore wind and 66 GW of offshore wind. An industry-standard approach for assessing pile lateral response is the $p - y$ method; however, this method was initially developed and empirically validated for long slender piles with length over diameter ratios (L/D) larger than 10 and thus its applicability to large diameter monopiles is doubtful which becomes relevant by taking into account the fact that the foundation may account for up to 35% of the installed costs.

The joint academia-industry project, Pile Soil Analysis (PISA) project resulted in an improved understanding of the lateral loading response of large diameter monopiles. Based on pile load test (PLT) data and numerical modelling, a method was developed to derive four soil reaction components from advanced finite element method (FEM) calculations to be used in a one-dimensional (1D) design framework. These four components are: base horizontal force (shear), base moment, side horizontal force and side moment.

Cone penetration test (CPT) based approaches have been shown to provide excellent predictions for the response of laterally loaded flexible piles where the $p - y$ response dominates. Four different $p - y$ methods, Novello (1999), Dyson & Randolph (2001), Li, Igoe & Gavin (2014) and Suryasentana & Lehane updated (2016), were compared in order to determine which fits better the lateral behaviour of long piles embedded in the Dunkirk sand. The method proposed by Dyson & Randolph shows the best match for this specific deposit. In this thesis, an approach to determine the additional components of the soil reaction curves for rigid monopiles is proposed. The results are compared to soil reaction curves are extracted from 3D FEM models, and compared to field tests on monopiles in sand within the serviceability state limit (SLS).

To extract the four soil reactions, appropriate sand parameters were calibrated and then tested. Some of the properties are CPT-based and the rest obtained from formulations proposed by several authors.

The base horizontal force (shear) was assumed as a frictional reaction depending on the vertical stress, the plugged area of the pile, a frictional factor related to the soil-structure interaction and an inverse correlation with L/D. A bi-linear relation is proposed to describe the horizontal force at the base.

The moment at the base was assumed related to the horizontal force and the pile diameter. As the horizontal force, a bi-linear force was defined to describe the curves extracted from the 3D FEM analysis.

The side moment was related to the side force obtained from the formulation proposed by Dyson & Randolph, the pile diameter and a frictional factor depending on the soil-structure interaction. As the $p - y$ curves, the slice by slice analysis does not a perfect match between the calculated curve and the one extracted from the 3D analysis, however, both global responses show good agreement.

Finally, the global lateral response of the pile obtained from PLAXIS 3D and (when available) from the pile load tests match within a certain level of deformation the response of the pile obtained by using the proposed CPT-based method. After a certain level of deformation, the proposed method seems to be stiffer than the actual response, however, within the serviceability state limit, all the responses show a high degree of agreement.

Table of Contents

1. Introduction

Currently, the lateral response of the monopiles on which the offshore wind turbines are founded is predicted and calculated according to horizontal load and displacement along the pile by means of $p - y$ curves. However, this approach seems to underestimate the capacity when rigid monopiles, with a small length over diameter ratio, are used. The PISA project evidenced that, in addition to this reaction, other 3 components should be included in order to predict the response correctly: base moment, base horizontal force and a moment along the shaft. In this chapter, the current industry approach and the new promising developments are discussed together with the goals and the methodology of this research.

1.1. Offshore wind industry

To meet the need for future energy supplies that are both sustainable and secure, there is currently significant worldwide growth in the installation of renewable energy systems. European Wind Energy Association (EWEA) anticipates 320 GW of wind energy capacity to be installed in the EU in 2030, of which 254 GW correspond to onshore wind and 66 GW correspond to offshore wind (Corbetta et al., (2015)) There is substantial pressure to increase the installation of offshore wind turbines to more remote locations and a with a greater power output. However, in order to safely meet the demand for larger wind turbines, it must be ensured that the whole structure, and hence the foundation part, is designed according to the highest design standards. The foundation is a critical part of the design and must be able to transfer the loads from the structure to the underlying soil. The most common foundation solution for offshore wind turbines is a single pile, termed the monopile. The efficiency of offshore wind power is related to the rotor diameter of a wind turbine and as the rotor diameters increase in size, the required monopile diameters do as well. Figure 1-1 shows the expected rotor diameter (Reuters, 2017).

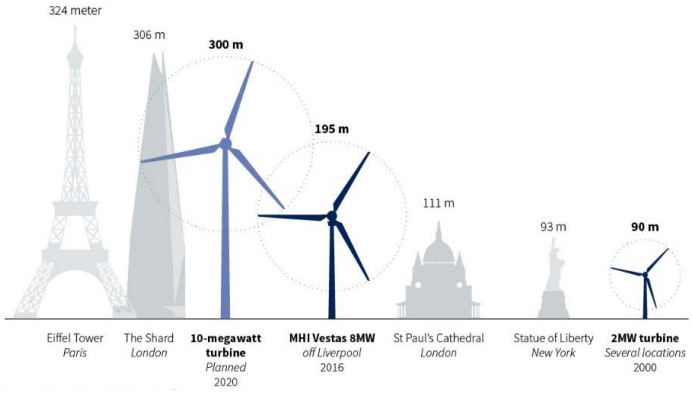

Figure 1-1 Expected size wind turbines (Reuters, 2017)

This means that the typical L/D ratio (slenderness ratio) tends to decrease, where L is the embedded length of the foundation and D is the diameter of the monopile. A wide range of pile dimensions can be found in the oil and gas industry. In the Gulf of Mexico, typical offshore piles have an L/D ratio in the order of 45 to 105 for piles installed prior to 1980 and 20 to 70 for piles installed after 1980. The stronger glacial deposits of the North Sea typically required shorter piles, with L/D ratios in the order of 20 to 60 (Schneider, 2010). In the future, the expected slenderness ratio of monopile foundations for the 10 MW+ next-generation wind turbines is between 2 and 6 (Panagoulias et al., (2018)). In Table 1-1 the typical pile dimensions in both the oil and gas industry and the wind offshore industry are shown. As mentioned above, the monopile foundation is the preferred type of foundations for offshore wind turbines in shallow waters and, since the costs of fabricating, transporting and installing the foundations for offshore wind turbine structures contribute significantly to the overall project costs, financial incentives dictate that foundation systems with minimal (as much as feasible) costs need to be employed, whilst ensuring safe operation of the turbine support structure during its lifetime. In contrast to typical oil and gas structures used offshore, the foundation for an offshore wind turbine generator may account for up to 35% of the installed costs (Byrne & Houlsby, 2004).

Table 1-1 Typical pile dimensions (Foursoff, 2018)

Foundation type	Diameter [m]	Industry
Jacket pile foundation	2	Oil and gas
Monopile foundation	4 – 6	Offshore wind (5W wind turbines)
Monopile foundation (expected)	10	Offshore wind (10W wind turbines)

1.2. Current Situation

The traditional industry approach for the geotechnical design of laterally loaded piles is to follow the *p – y* method as recommended by Det Norske Veritas – Germanischer Lloyd (DNV-GL-AS, 2016) based on American Petroleum Institute (API, 2011) guidelines, which are intended for piles with an L/D ratios > 15. The *p – y* method is on the Winkler assumption according to which the soil surrounding the pile is modelled as a set of uncoupled, non-linear, elastoplastic springs which define the lateral pressure (*p*) applied to the pile at a given depth, as a function of the lateral displacement (*y*). (Figure 1-2). The *p – y* method calibrated using a limited number of pile tests performed on slender jacket piles with diameters of less than 1.0 m. For larger diameter piles, DNV (2016) recommends validating the design through a Finite Element (FE) analysis, although there is no consensus on how this is the best achieved in practice. Piles can be classified according to their geometry as it is shown in Table 1-2.

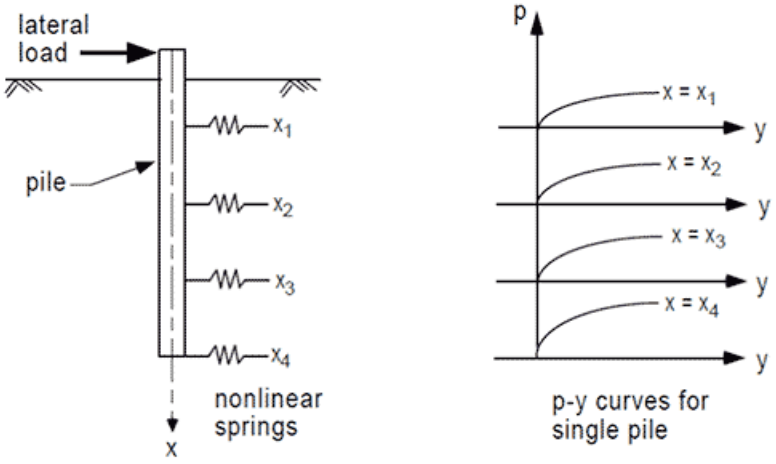

Figure 1-2 P-y curves (Lemnitzer & Favaretti, 2013)

Table 1-2 Pile definition (Foursoff, 2018)

L/D	Pile type
< 3	Short
3 – 6	Intermediate
8 – 10	Long
> 10	Very long

1.3. Latest developments: PISA Project

In 2013, the Pile Soil Analysis (PISA) project was launched in order to investigate and develop improved design methods for laterally loaded piles, specifically tailored to the offshore wind sector. It is a joint industry-academy project that consists of three main streams of work: state-of-the-art numerical analyses, development of new lateral pile design methodology and the execution and interpretation of medium-scale field tests (PISA Academic & PISA DONG, Field Test Factual Report, 2015). Two onshore test sites were chosen for the field testing: a) a clayey site in Cowden in north-east England and b) a sandy site in Dunkirk in northern France.

The PISA project included the three following steps:

(i) *Numerical Finite Element Modelling (FEM) and laboratory testing*
With a 3D numerical FEM model, pile deformation under monotonic lateral loading was investigated and it showed that apart from the lateral soil pressure ($p - y$), also the base moment (M_b), base shear (H_b) and vertical shear stresses along the pile shaft (τ) contribute to the pile lateral behaviour for short piles as it is shown in Figure 1-3. Because the FEM model requires information about soil characteristics as input, laboratory and field tests were performed prior to the numerical analyses.

(ii) *Development of a new method*
In the second phase of the project, a relation for each contributing soil reaction term has been developed.

(iii) *On-site Pile Load Testing (PLT)*

In the third phase of the project, several pile load tests (PLTs) were performed on a range of pile geometries on both field test sites. The piles and areas around the pile were instrumented to measure the response of the soil and the deflection of the piles.

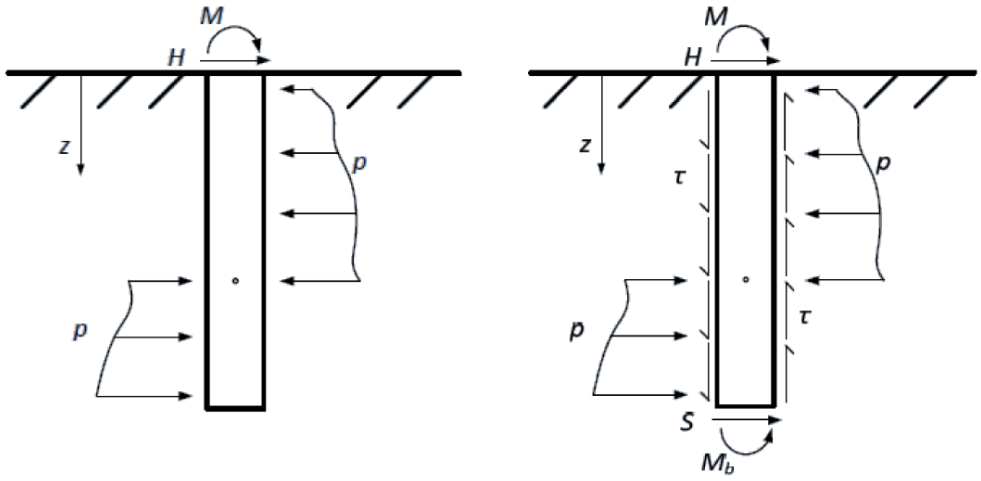

Figure 1-3 Current and new method with additional soil reactions acting on short piles (Foursoff, 2018)

This report is focused on the study of piles embedded in sand and consequently, the data extracted from Dunkirk will be relevant for this investigation. This site has been extensively characterised not only during the PISA project but also in the past which make this specific sand an ideal reference for this study. Earlier studies by Jardine (1985), Lehane (1992), Chow (1997) and Kuwano (1999) provide substantial information related to this site. In total, fourteen piles were tested on-site, mostly instrumented above the ground level although some of them included measurements below ground level, as well.

Together with laboratory testing, several in-situ field tests such as the cone penetration test (CPT) were performed as part of the PISA project. During a CPT, a cone is vertically pushed into the soil while the resistance at the tip (q_c) is continuously measured. Additional parameters may also be measured such as the sleeve friction (f_s), the excess of pore water pressure at different positions along the cone (u), and soil temperature (T).

Due to the wide usability of the CPT to determine the soil profile of sites, several authors developed relations between the tip resistance of the cone and the behaviour of a pile subjected to lateral loads in terms of the $p - y$ curves, based on the fact that the CPT cone resistance q_c is primarily dependent on the horizontal effective stress, mobilised friction angle and soil stiffness characteristics ((Houlsby & Hitchman, 1988) and (Schnaid & Houlsby, 1991)) and hence a direct correlation between the lateral pile response and q_c seems to be convenient. Novello (1999) and Dyson & Randolph (2001) derived a method by means of regression analysis and PLT results of small scale centrifuge model piles in calcareous sands. Later methods have been developed from Finite Element Method (FEM) analysis and PLTs in siliceous sand (Li et al. (2014) and Suryasentana & Lehane (2016)).

1.4. Aims and objective

The *p – y* method, which is the industry standard approach for assessing pile lateral response, was initially developed and empirically validated for long slender piles and thus its applicability to large diameter monopiles is doubtful. New CPT-based approaches have been developed and have been shown good predictions for the laterally loaded piles where the *p – y* response dominates. If large diameter monopiles need to be designed, the soil reactions in terms of springs can be derived from FEM analyses but the process is expensive and highly time-consuming. The aim of this thesis is to propose a CPT-based method to determine the additional components of the soil reaction curves for rigid monopiles, namely the side and base shear and base moment, within the monopile working loads. The results are compared to 3D FEM models and to field tests on monopiles in sand.

1.4.1. Objective

The main objective is to propose a CPT-based method to determine the additional three components of the soil reaction (besides the lateral pressure) for rigid piles and utterly the global lateral response of such piles.

1.4.2. Scope

This research is focused on the lateral response of large diameter rigid monopiles subject to static monotonic loading and embedded in marine Pleistocene sands.

The thesis is based mainly on the geotechnical information of the Dunkirk site derived from CPTs, field tests and laboratory tests in order to define the soil profile and the soil geotechnical properties. Additionally, from the PLTs, information about loads, deformations and rotations was extracted and later compared to the 3D FE models performed in PLAXIS 3D. Finally, all the new theoretical derivations obtained from the PISA group in terms of soil reaction curves when a rigid pile is laterally loaded were also used to develop this research.

1.4.3. Research structure

A summary of the structure of this document is presented in the following Table 1-3. This thesis starts with an extensive literature review which includes the design principles of the offshore structures, the characterisation of the soil model that describes properly the sand identified at the Dunkirk site, the geotechnical modelling of the Dunkirk site, the performance of existing CPT-based *p – y* methods and the analysis of the latest developments reported in the PISA research.

The second part of this document contains the finite element analyses by means of PLAXIS 3D together with PLAXIS MoDeTo (Monopile Tool Design). Within this section, the

validation of the soil model is proved by comparing the results between the pile load tests performed during the PISA project and the model. Furthermore, the four soil reaction curves which are to be considered in the case of the lateral response of large diameter monopiles are extracted from the 3D FEM analyses.

In the third part, simple CPT-based formulations are proposed in order to determine the four soil reactions curves by avoiding the expensive, time-consuming process of the 3D FEM analyses. First, the base horizontal force is analysed by checking the results with different pile geometries and soil properties. Then, the base moment is obtained as a function of the base horizontal force. Secondly, a CPT-based $p - y$ method is chosen and from it, the moment along the shaft is calculated. Finally, the soil reaction curves are entered in MATLAB, modelling the monopile, and the results of the monopile behaviour under lateral loading are compared against results from the 3D FEM analysis and the PLTs.

Table 1-3 Thesis structure

Part I: Introduction and literature study
- Chapter 1: Introduction
- Chapter 2: Literature study
Part II: Soil model and finite element analysis
- Chapter 3: Soil properties and finite elements model
Part III: Soil reaction curves formulation
- Chapter 4: Soil reaction curves
- Chapter 5: General lateral response
Part IV: Conclusions, future work and recommendations
- Chapter 6: Conclusions
- Chapter 7: Recommendations and future work

2. Literature study

Flexible and rigid piles react differently to the lateral loads by developing a hinge in the first case or by acting as a rigid body in the second case. The type of failure in each case is different and therefore the analysis by means of $p - y$ curves through the classic model and CPT-based formulations proved to be insufficient for rigid monopiles. The PISA team, in which several piles were instrumented and then loaded in a sandy site in Dunkirk, France, developed a new theory to predict the behaviour of rigid piles subjected to lateral loads. In this chapter, the difference between flexible and rigid pile behaviours, the theory behind the $p - y$ curves and a summary of the PISA project are included.

2.1. Design principles of offshore structures and soil lateral behaviour

Currently, most of the methods are meant to predict the lateral response of the soil when a load is applied to long and flexible piles. Both API guidelines and CPT-based methods were calibrated and tested by considering this pile type which has been extensively used within the oil & gas industry. However, due to the increasing demand of renewable energies that rules the current stream of development, offshore wind turbines have become particularly popular due to higher wind exposure, bigger turbines and reduced visual impact on this environment. Figure 2-1 and Figure 2-2 show an offshore platform and offshore wind turbines founded on various foundation types, respectively.

Figure 2-1 Offshore platforms (Pisano, 2018)

Figure 2-2 Various foundation types for offshore wind turbines (Pisano, 2018)

Foundations of both structures have to sustain vertical and horizontal loads. However, in the case of the wind turbines, the weight of each structure is relatively low, so the applied vertical load on the foundation is small compared with the overturning load from wind

and waves (Byrne & Houlsby, 2004). Figure 2-3 shows the differences in magnitudes of the vertical and horizontal loads depending on the type of offshore structure.

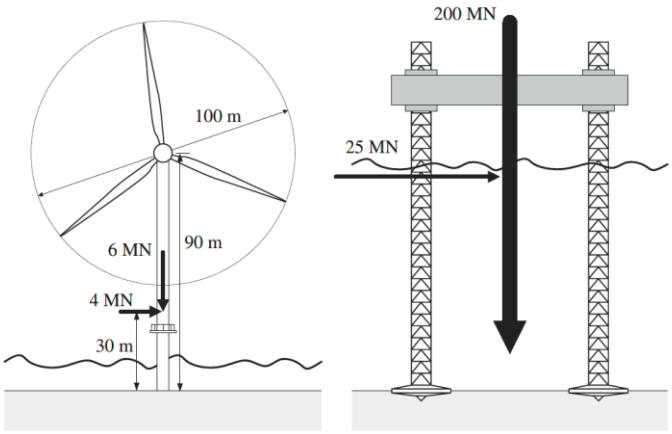

Figure 2-3 Offshore wind turbine and a jack-up rig (Byrne & Houlsby, 2004)

Besides the static loads, a wind turbine undergoes cyclic loads produced by the rotor blades (operational loading) and the environmental conditions (waves and wind). The design of the structure must avoid the resonance of the wind turbine by keeping the frequency of the cyclic loads away from the natural frequency of the structure. The natural frequency of the turbine is highly dependent on the material properties of the monopile and the stiffness of the soil surrounding the foundation, hence the determination of the soil properties where the monopile is embedded is crucial to assure the correct functioning of the structure. Figure 2-4 shows the typical frequency diagram of offshore structures and loads.

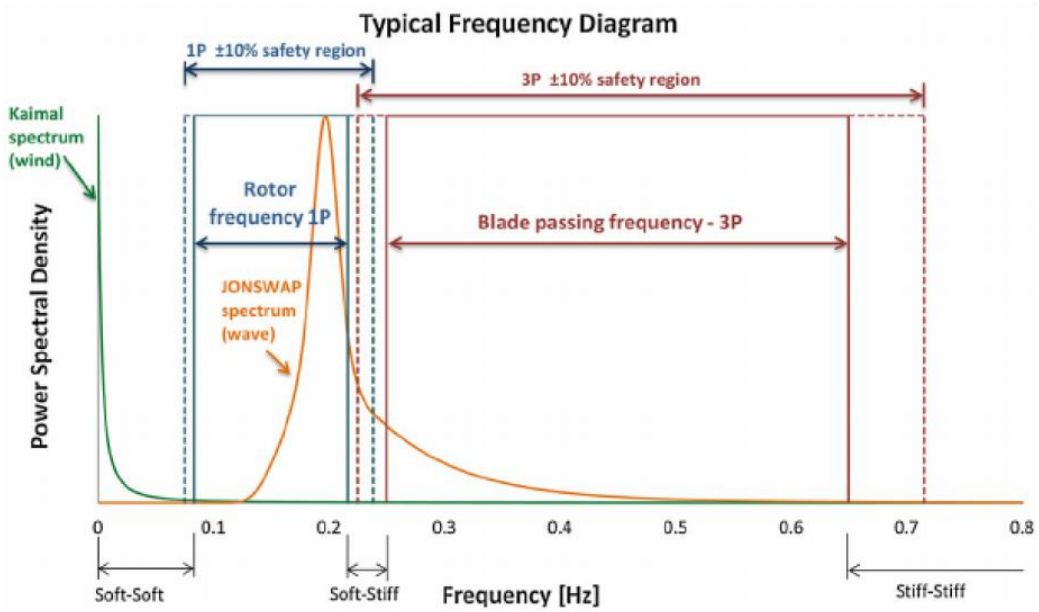

Figure 2-4 Typical frequency ranges present in offshore conditions (Arany, Bhattacharya, MacDonald, & Hogan, 2014)

Offshore wind turbines need to satisfy the design requirements regarding safety and performance as stated in the 'Design of offshore wind turbines structures' (DNV, 2014). A design limit state describes specific criteria, about, for example, maximum loads or

displacements, that are dependent on the structure's function, foundation type and load situations. The most significant limit states are described in Table 2-1.

Table 2-1 Significant limit states (after Foursoff, 2018)

Ultimate limit state (ULS)
The ultimate limit state corresponds to the maximum load capacity that a structure foundation can withstand before failure occurs.
Serviceability limit state (SLS)
The serviceability limit state corresponds to the usability of the structure and usually is related to maximum displacements or rotations of the foundation. Normally for a monopile, the pile head displacement y_0 must not exceed a value that is 10% of the diameter and the pile head rotation, θ_0, must not exceed 2°.
Fatigue limit state (FLS)
The fatigue limit state corresponds to the cumulative damage from repeated loading of the offshore structure. It is not related to the maximum load capacity, because repetitive loading can cause the structure to fail long before the maximum load capacity is reached. The maximum fatigue limit stress depends on the magnitude and frequency of the load (load cycles).

The $p - y$ method focuses mainly on the avoidance of the ultimate failure of the offshore platform. Since the wind turbines are subjected to cyclic loading and lateral displacements, the SLS and FLS have also high importance.

This research focuses on monotonic loading only and therefore the cyclic behaviour of the soil is not discussed.

When a pile is laterally loaded, the soil in front of the pile reacts with a force in the opposite direction called passive reaction of the soil. On the other side, the space created due to the separation of the soil and the pile produces a force in the same direction with the load but smaller in magnitude than the original force called active reaction of the soil. Figure 2-5 shows the soil stresses before and after the application of a horizontal load.

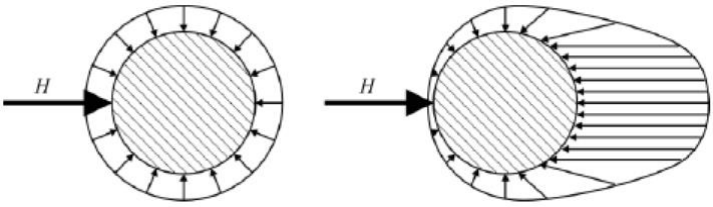

Figure 2-5 Soil stresses before and after the application of a horizontal load (Janoyan & Whelan, 2004)

The failure mechanism of the soil when is laterally loaded depends on the stiffnesses of both, the soil and the pile. In the case of a short (rigid) pile, a rigid rotation point can be identified (see Figure 2-6). In the case of the long piles, a plastic hinge is formed and the soil resistance profile is idealised as null below this point (see Figure 2-7).

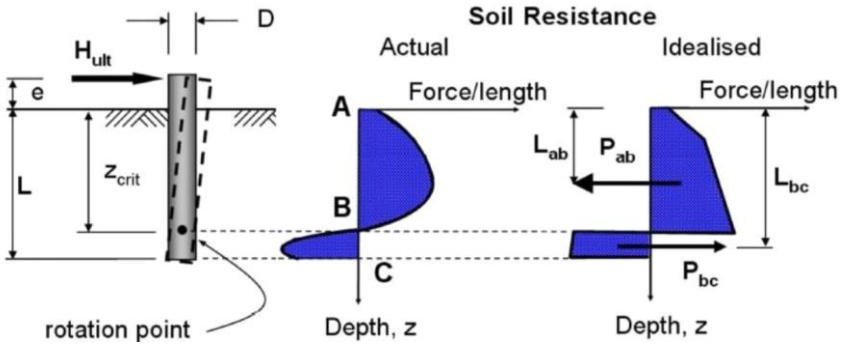

Figure 2-6 Failure mechanism in short piles (Pisano, 2018)

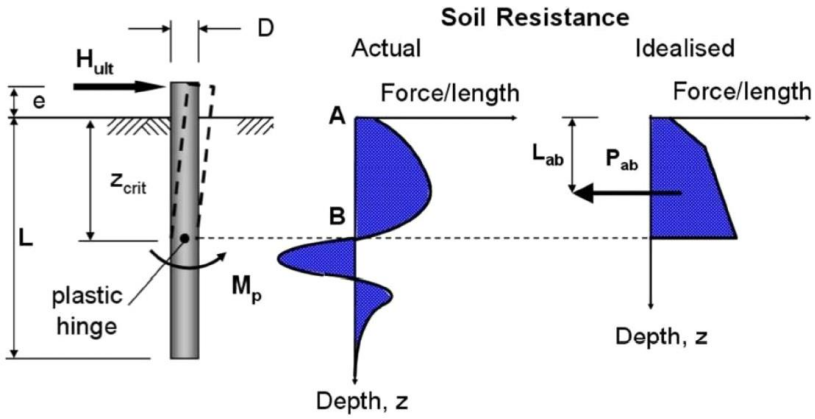

Figure 2-7 Failure mechanism in long piles (Pisano, 2018)

2.2. P-y method

2.2.1. Traditional approach

In a pile response model, the behaviour of the soil can be assessed by relating the pile displacement under a certain load. A well-known method to simulate the soil reaction is the Winkler method, developed in 1867. Winkler's idealisation represents the soil medium as a system of identical but mutually independent, closely spaced, discrete, linearly elastic springs. According to this idealisation, the deformation of the foundation due to the applied load is confined to loaded regions only and, since it considers the relation between load and deformation as elastic, the spring stiffness can be easily calculated as $K_{py} = p/y$ in which p represents the load and y represents the horizontal deformation. Figure 2-8 shows the idealised Winkler method.

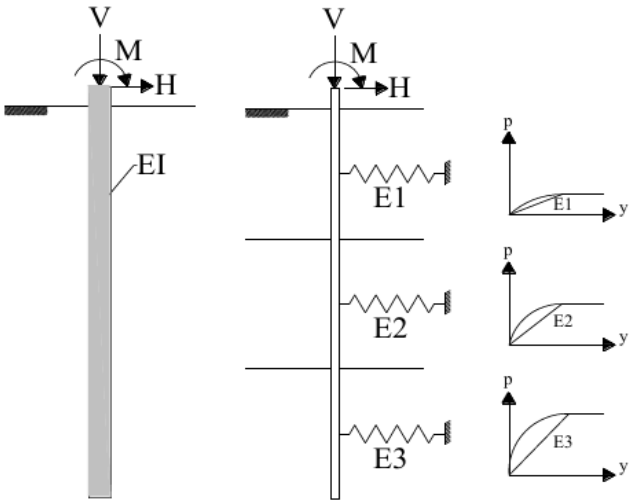

Figure 2-8 Beam by a series of uncoupled springs. Load and displacement relation (Prendergast, 2018)

Several authors have improved the original Winkler's model by proposing different, more-realistic, non-linear, load-deformation relations for different soil types, such as Matlock et al. (1970), Reese et al. (1974) and O'Neill & Murchinson (1983).

The American Petroleum Institute (API, 2011) proposes a simplified method for sands in which non-linear springs are considered and in the absence of more definitive information, the load p can be calculated by the following expression:

$$P = A_{cs} \cdot p_u \cdot tanh\left(\frac{k \cdot H_z}{A_{cs} \cdot p_u} y\right) \qquad \textit{Equation 1}$$

where A_{cs} is a factor to account for cyclic or static loading conditions, p_u the ultimate bearing capacity at depth H_z and k is the initial modulus of subgrade reaction as a function of the soil's internal friction angle.

The pile itself is usually modelled as a beam by means of the Euler-Bernoulli beam theory. According to this theory, the lateral load induces lateral pressures and internal bending moments and do not include vertical shear forces in the model. Nevertheless, for short-rigid piles (L/D < 10), the aforementioned shear forces cannot be neglected (Byrne et al., (2015)). For this reason, a new approach can be used to incorporate these shear forces: the Timoshenko beam theory. The differences between these two approaches are shown in Figure 2-9 and Figure 2-10.

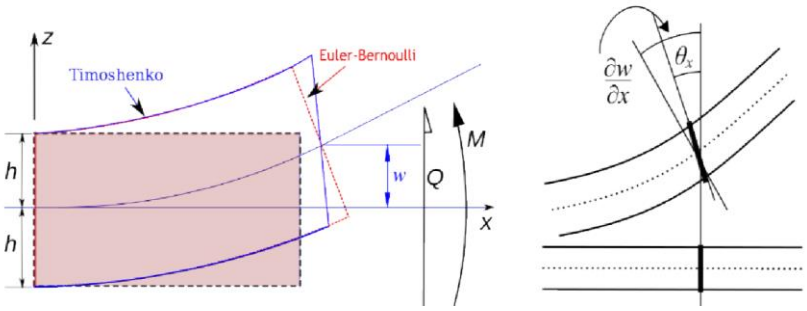

Figure 2-9 Differences between Euler-Bernoulli and Timoshenko beams (after Foursoff, 2018)

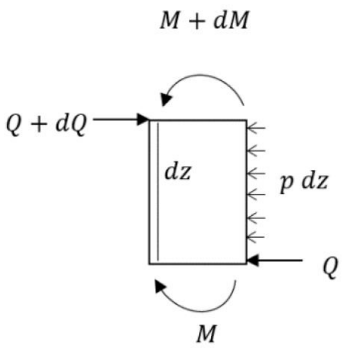

1. $EI\frac{d^4y}{dz^4} = -K_{py}\,y = -p$
2. $EI\frac{d^3y}{dz^3} = -Q$
3. $EI\frac{d^2y}{dz^2} = -M$
4. B: $\frac{dy}{dz} = \theta$

   T: $\frac{dy}{dz} = \theta - \frac{1}{\kappa AG}\frac{d^3y}{dz^3}$

y: pile displacement;
z: depth;
p: soil resistance per unit length;
Q: shear force;
M: bending moment;
θ: rotational slope;
κ: Timoshenko shear coefficient;
G = shear modulus;
A = cross sectional area

Figure 2-10 Beam equation for a small beam element with length dz (after Foursoff, 2018)

2.2.2. CPT-based p-y methods

The cone penetration test (CPT) is one of the most known in-situ methods to determine the soil layering of a site and the geotechnical properties of the identified stratums. The test consists of pushing an instrumented cone-shaped apparatus into the soil while the forces on the tip and along the sleeve are measured. Additional parameters can also be obtained from this test, such as pore pressure, temperature and even dynamic/small strain properties of the soil. The cone resistance is related to the in-situ horizontal effective stress and therefore it can be convenient to express $p - y$ curves in terms of q_c (Houlsby & Hitchman, 1988). Figure 2-11 shows the cone.

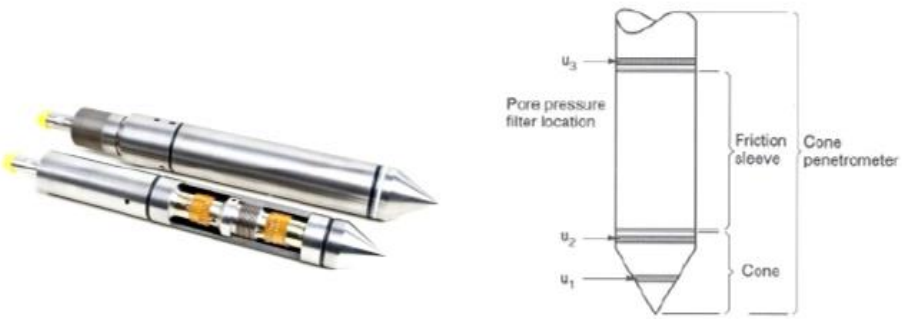

Figure 2-11 Cone penetrometer (Lunne et al., (1997))

The cone can be considered as a small-scale pile foundation since the mean effective stress, compressibility and rigidity of the soil medium have a comparable influence on both a pile and a cone (Wrana, 2015). The q_c provides, therefore, reasonably good assumptions for effective stress values and can be used to normalise site-specific soil parameters (Novello, 1999).

Foursoff (2018) includes a summarised list of 5 CPT-based methods to predict the $p - y$ curves. Different assumptions and methods were used in order to develop these relationships, such us, centrifuge tests, comparison with FEM models and cavity expansion tests. This research is focused on the determination of all four soil reaction curves based on CPT results. However, the component related to the lateral displacement, the $p - y$ component, is taken directly from one of the formulations detailed in Foursoff's research. After testing the methods proposed by Novello (1999), Li et al. (2014), Suryasentana & Lehane (2016) and Dyson & Randolph (2001), the latter provides the best general lateral pile response in comparison to the results obtained from the pile load tests.

The formulation is the following:

$$p = 2.84 \cdot D \cdot (\gamma' \cdot D) \left(\frac{q_c}{\gamma' \cdot D}\right)^{0.72} \left(\frac{y}{D}\right)^{0.64} \qquad \textit{Equation 2}$$

where:

p	=	lateral load per length unit
D	=	pile diameter
γ'	=	soil effective unit weight
q_c	=	CPT cone tip resistance
y	=	lateral displacement

Table 2-2 shows an overview of the Dyson and Randolph method.

Table 2-2 Overview of CPT-based p-y method by Dyson and Randolph (after Foursoff, 2018)

Dyson and Randolph CPT-based *p-y* method	
Date	2001
Based on	CPT, centrifuge tests (N=160), small scale PLT
Soil	Calcareous sands recovered from the seabed on North-West Shelf of Australia
Pile	Driven piles, free headed
Geometry	D = 13 mm, L/D = 26.15

2.3. PISA Project

The joint academia-industry project, Pile Soil Analysis (PISA) project resulted in an improved understanding of the lateral loading response of large diameter monopiles. Based on PLTs data and numerical modelling, a method was developed to derive all soil reaction components from advanced FEM calculations to be used in a one-dimensional (1D) design framework.

Recently, the lateral response of the soil was predicted mainly by means of the relation between the lateral load and lateral displacements. However, the standard *p – y curves* are found to become increasingly unreliable as the pile diameter (D) increases or the embedded length (L) reduces. Figure 2-12 shows the four components (distributed lateral load, vertical shear tractions, base moment and shear force) to be addressed when lateral loading of a monopile is analysed. Figure 2-13 shows the cumulative influence of the components for short piles in sand. The distributed load *p* acts along the pile shaft and it is consistent with the approach adopted by the conventional *p – y method.* The additional components of the distributed moment *m* along the pile results from the vertical shear tractions induced at the soil-pile interface, due to local pile rotation. Besides, if the pile is loaded close to failure, considerable shear tractions are likely to be developed on the passive side of the pile due to the induced wedge-type failure mechanism (Burd, et al., 2017). Two separate soil reaction components are acting on the base (toe) of the pile, the shear force H_B and the base moment M_B.

By only considering the distributed load, lateral pile capacity is highly underestimated in piles with a slenderness ratio (L/D) of less than 6 and therefore several studies have been carried out in order to include those extra components in the analysis.

Current analyses have been mostly developed by means of finite elements which proved to be accurate enough but time-consuming, a factor that becomes relevant when a large area needs to be investigated and the soil conditions can widely vary. Finally, the disturbance of sand samples when extracted may add extra uncertainties to the soil modelling process.

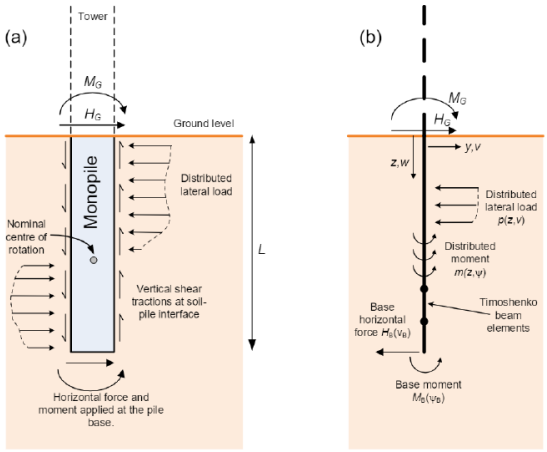

Figure 2-12 Assumed soil reaction components acting on a laterally loaded pile (Burd, et al., 2018)

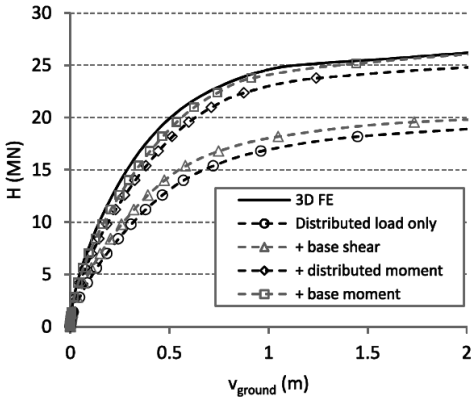

Figure 2-13 Cumulative soil reaction component breakdown in the sand (Byrne et al., (2015))

As part of the site investigation (SI) campaign for the PISA project, individual CPTU profiles were determined at each pile location and some other key points around the site. This exploration together with the analyses performed in earlier stages by several authors provided a complete description of the site. The location of the Dunkirk site is shown in

Figure 2-14. Figure 2-15 shows the pile distribution at the Dunkirk site. The stratigraphy at Dunkirk is shown in Table 2-3.

Figure 2-14 Dunkirk test site

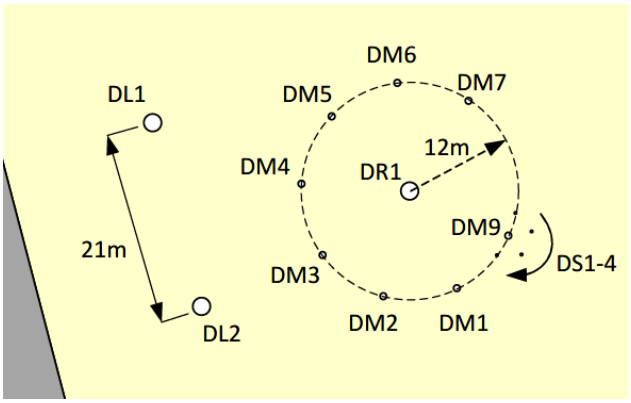

Figure 2-15 Pile set up at Dunkirk site

Table 2-3 Stratigraphy at Dunkirk (PISA Academic & PISA DONG, Field Test Factual Report, 2015)

Depth [m]	Material	Description
0 – 3	Hydraulic Fill	Sand fill that was dredged from the offshore Flandrian deposits and placed to raise the ground level. No compaction or surcharging has taken place.
3 – 30	Flandrian Sand	Marine sand deposited during the three local marine transgressions. These sands are often separated by organic layers which accumulated between transgressions. A 600 mm thick organic layer is found at around 8 m depth, separating the Flandrian sand into upper and middle units.
30 +	Ypresienne Clay	An Eocene marine clay (also known as London Clay and Argile de Flandres) which extends beneath the southern North Sea.

Figure 2-16 shows the maximum, minimum and mean CPT profiles from the PISA site investigation.

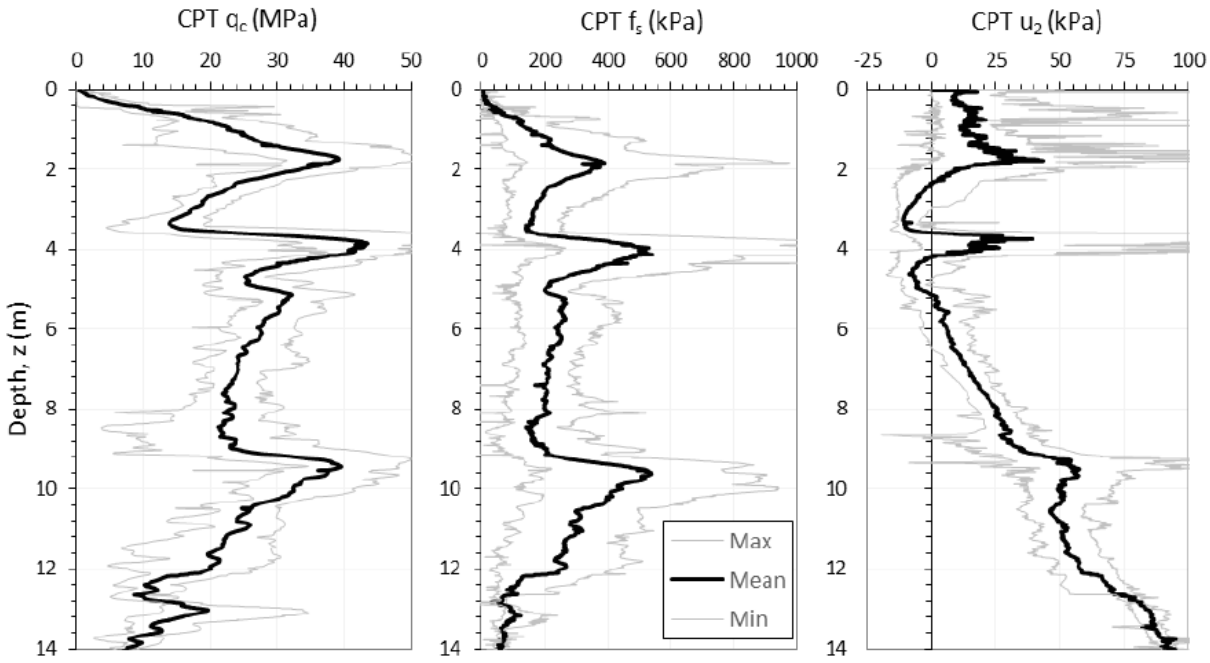

Figure 2-16 CPT profiles at the Dunkirk site (PISA Academic & PISA DONG, Field Test Factual Report, 2015)

Figure 2-17 shows the water depth below ground level, calculated from borehole pressure sensors in the period between June 2014 and April 2015. It can be seen that, on average, the water level is about 4.8 m below the surface. However, from the CPTU data, the water level seems to be about 5.4 m below the surface and, according to Chow (1997), the level was found at 4.0 m below surface.

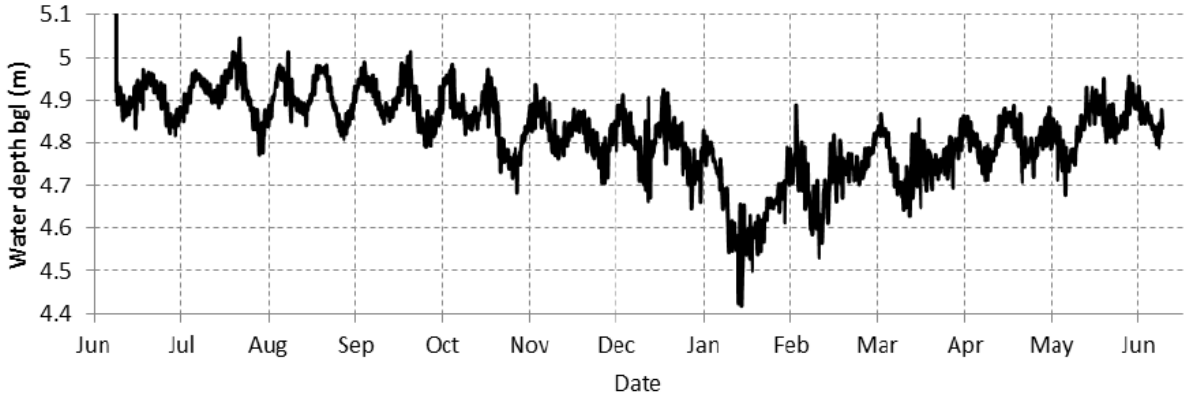

Figure 2-17 Water level b.g.l. 06/2014 - 04/2015 (PISA Academic & PISA DONG, Field Test Factual Report, 2015)

By taking into consideration the interpretation of the CPTs and the information provided by authors in previous investigations (Zdravkovic, et al., 2018), some soil properties were defined as shown in Table 2-4.

Table 2-4 Soil properties (Zdravkovic, et al., 2018)

Soil Property	Unit	Value
Mean particle size, D_{50}	[mm]	0.25
Relative density, $D_{R,FILL}$	[%]	100
Relative density, $D_{R,NAT}$	[%]	75
Bulk unit weight (above water table), $\gamma_{a.w.t}$	[kN/m^3]	17.1
Bulk unit weight (below water table), $\gamma_{b.w.t}$	[kN/m^3]	19.9
Earth pressure coefficient, K_0	[-]	0.4
Minimum void ratio, e_{min}	[-]	0.506 – 0.541
Maximum void ratio, e_{max}	[-]	0.881 – 0.942
Initial void ratio at D_R = 75%, $e_{0,75}$	[-]	0.64
Initial void ratio at D_R = 100%, $e_{0,100}$	[-]	0.57
Small strain shear modulus, G_0	[MPa]	Figures 1-8 & 1-9
Poisson ratio, ν	[-]	0.17
Triaxial compression friction angle, ϕ'_{TXC}	[deg]	32
Triaxial extension friction angle, ϕ'_{TXE}	[deg]	33

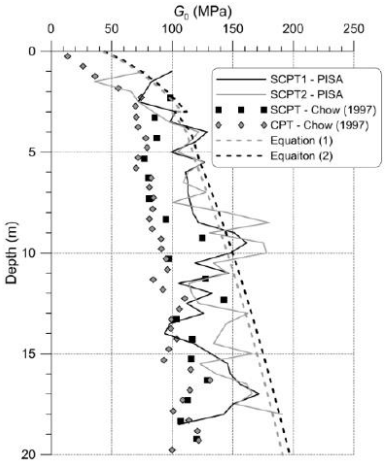

Figure 2-18 G0 all data (Zdravkovic, et al., 2018)

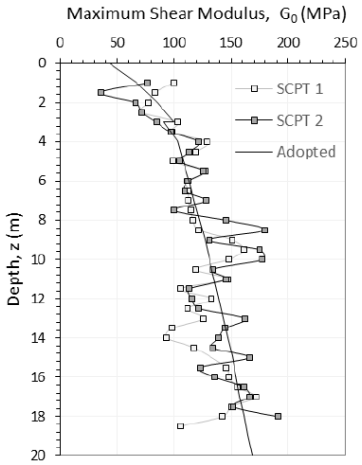

Figure 2-19 G0 PISA data (PISA Academic & PISA DONG, Field Test Factual Report, 2015)

These parameters can, however, be modified since the new investigation indicated geotechnical profiles for PISA profiles that differed significantly from those established in earlier studies (PISA #1: Ground characterisation for PISA pile testing and analysis, 2018). The new Dunkirk profile indicated higher CPT resistances and shear stiffnesses, along with a lower groundwater table. Foursoff (2018) proposed new values for some soil properties that seem to fit better the site investigation performed during the PISA project with internal friction angles, relative densities and unit weights slightly higher than the ones proposed by the PISA group. It should also be noted that due to confidentiality issues, it was not possible to get all the information related to the laboratory tests

2.3.1. Project set-up

Table 2-5 shows the geometry and instrumentation types at Dunkirk. As it was mentioned above, all piles are monitored above the ground level while some of them also below ground level.

Table 2-5 Pile geometry and instrumentation

Pile	D [m]	L [m]	L/D [-]	t [mm]	D/t [-]	Below ground data	Description
DS1	0.273	1.43	5.25	7	39	NO	Small diameter, mid-length
DS2	0.273	1.43	5.25	7	39	NO	Small diameter, mid-length repeat
DS3	0.273	2.18	8	7	39	NO	Small diameter, long
DS4	0.273	2.73	10	7	39	NO	Small diameter, very long
DM5	0.762	2.29	3	10	79	NO	Mid-diameter, short repeat
DM7	0.762	2.29	3	10	79	YES	Mid-diameter, short
DM2	0.762	4.00	5.25	14	54	YES	Mid-diameter, one-way cyclic test
DM4	0.762	4.00	5.25	14	54	YES	Mid-diameter, control geometry
DM9	0.762	4.00	5.25	14	54	NO	Mid-diameter, control geometry repeat
DM1	0.762	4.00	5.25	14	54	YES	Mid-diameter, two-way cyclic test
DM6	0.762	4.00	5.25	19	40	YES	Mid-diameter, thick
DM3	0.762	6.1	8	25	30	YES	Mid-diameter, long
DR1	2.000	8.00	4	25	80	NO	Mid-diameter, reaction pile
DL1	2.000	10.5	5.25	38	53	YES	Large-diameter
DL2	2.000	10.5	5.25	38	53	YES	Large-diameter

The load eccentricity, *h*, was 5 m for small diameter piles and 10 m for the remaining piles. Figure 2-20 to Figure 2-22 show the testing configuration of the medium diameter pile, the set-up of a fully instrumented medium diameter pile and a section featuring the below-ground instrumentation, respectively.

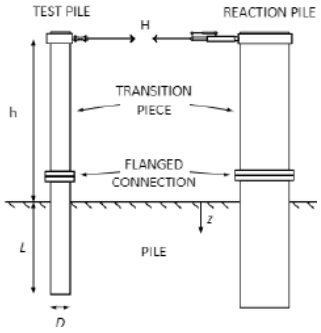

Figure 2-20 Testing configuration (Zdravkovic, et al., 2018)

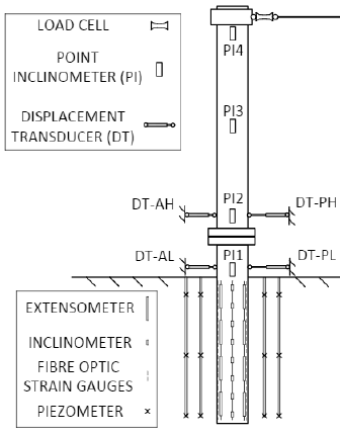

Figure 2-21 Fully instrumented pile (Zdravkovic, et al., 2018)

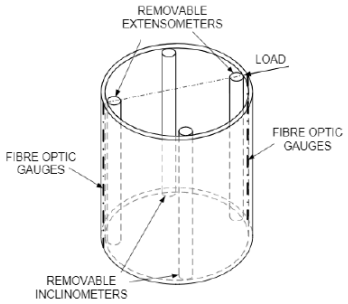

Figure 2-22 Below ground instrumentation (Zdravkovic, et al., 2018)

Test piles were instrumented with inclinometers, strain gauges, displacement transducers and a load cell. Separate specifications were developed for the above and below ground instrumentation. The above-ground instrumentation consisted of:

(i) A full-bridge aluminium body load cell to record the applied lateral load H;
(ii) Microelectromechanical sensor (MEMS) inclinometers;
(iii) Potentiometer displacement transducer attached to the active and passive pile faces;
(iv) Displacement transducer mounted on the loading ram to record the ram movement.

The below-ground instrumentation is:

(i) Fibre Bragg grating sensors used to measure the strains in the pile wall;
(ii) A separate strain measurement system, based on retrievable MEMS extensometers to provide redundancy in the case of optical fibres failure. Those were also used to deduce below-ground pile inclination.

2.3.2. Pile installation

The medium and large diameter piles were installed in a two-stage process, with an initial vibration stage that was used to embed piles to a stable depth (1.0 m to 1.5 m), followed by a pile driving with a hydraulic hammer until reaching the target embedment. In contrast, small diameter piles were simply vibrated to the target embedment (Pisa #2: New analysis methods for instrumented monopile field tests, 2018).

2.3.3. Piles displacements and rotations

Included in PISA #2 (2018) is the derivation of the ground displacement and rotation. Three different approaches were separately analysed in order to get the closest-to reality behaviour of the piles when a lateral load is applied to them, according to the following:

(i) *Approach A*
Simplistically assume that $v_G = v_{DT\text{-}PL}$ (where $v_{DT\text{-}PL}$ is the displacement recorded by DT-PL) and $\theta_G = \theta_{PI1}$ (where θ_{PI1} is the rotation recorded by the inclinometer PI1) (See Figure 2-21).

(ii) *Approach B*
Assume that v_G and θ_G are determined from the displacement transducer readings, assuming that the portion of the pile between the ground and the upper transducer is rigid.

(iii) *Approach C*
Adopt a more detailed approach in which data from above-ground instrumentation is used to determine a structural model for the above-ground structure. This model is then used to infer v_G and θ_G.

Approach C showed good agreement between the structural model and the inclinometer data and therefore provided further confidence in predicting the pile behaviour. The above-ground structure is modelled as three separate Timoshenko beam sections (pile, flanged connection and transition piece, see Figure 2-20). According to Timoshenko, the bending moment, *M*, is:

$$M = -EI\frac{d\psi_r}{dz} \qquad \textit{Equation 3}$$

where *EI* is the local flexural stiffness and ψ_r is the (clockwise) rotation of the column cross-section. The (clockwise positive) rotation of the structure, $\theta = -\frac{dv}{dz}$ where *v* is the lateral displacement, is:

$$\theta = \psi_r + \gamma_{xz} \quad \textit{Equation 4}$$

where γ_{xz} is the shear strain, assumed in Timoshenko theory to be uniform across the cross-section and given by:

$$\gamma_{xz} = \frac{S}{\kappa AG} \quad \textit{Equation 5}$$

where S is the shear force and κAG is the local shear stiffness. It is assumed that *E* = 210 GPa and *G* = 80.77 GPa. The bending moment, *M* and shear force, *S* induced in the above-ground structure are:

$$M = H(h + z) \quad \textit{Equation 6}$$

$$S = \frac{dM}{dz} = H \quad \textit{Equation 7}$$

For uniform section, these equations are integrated to give:

$$\theta = -\frac{H}{EI}\left(hz + \frac{z^2}{2}\right) + \frac{H}{\kappa AG} + a \quad \textit{Equation 8}$$

$$v = \frac{H}{EI}\left(\frac{hz^2}{2} + \frac{z^3}{6}\right) - \left(\frac{H}{\kappa AG} + a\right)z + b \quad \textit{Equation 9}$$

where *a* and *b* are parameters to be determined.

Since the above-ground structure is modelled as three separate beams, six parameters must be determined. The following conditions have to be applied:

(i) The lateral displacement and cross-section rotation at the flanged connection/pile and flanged connection/transition piece are assumed to be continuous;
(ii) The measured inclination at location PI1 and lateral displacement (average of DT-AH and DT-PH, and an average of DT-AL and DT-PL) at the two displacement transducer elevations are equated to the corresponding values from the structural model.

This method is regarded to provide the most robust approach since it includes redundant above-ground measurements. Figure 2-23 shows measured pile rotation data from the embedded and above-ground inclinometers. Figure 2-24 shows the inferred bending moments for 2 selected values of the load, *H*. Both plots show good consistency between the instruments below and

above ground level. It can also be inferred that the fibre Bragg sensors were more reliable than the extensometers although those give extra values that provide redundancy to the system to be solved.

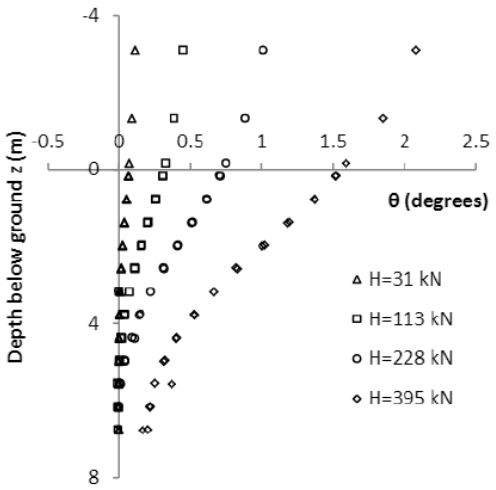

Figure 2-23 Depthwise rotation from inclinometer measurements PISA #2 (Burd, et al., 2018)

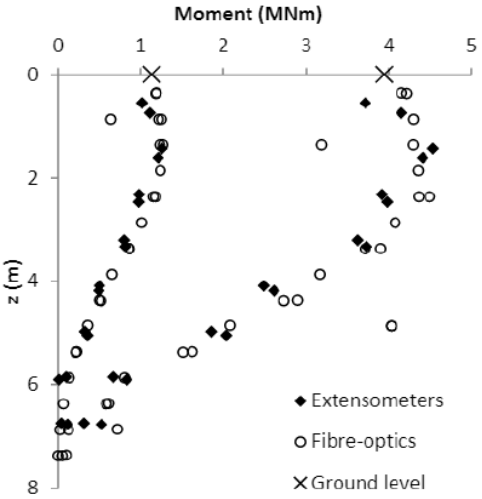

Figure 2-24 Depthwise bending moment at the different load stages. PISA #2 (Burd, et al., 2018)

2.4. Soil Models

Prior to the analyses to be performed on FE software, a suitable soil model must be chosen in order to represent the behaviour of dense sand in offshore conditions. This model should be both: representative of the soil behaviour and simple enough to decrease the uncertainty derived from the correlation between CPT results and soil parameters, considering the limited number of laboratory tests available.

2.4.1. Hardening soil small-strain (*HSsmall* model)

By considering the soil type and the expected behaviour of the sand subjected to a monotonic load offshore conditions, Brinkgreve (2018) recommends a few of the most-known soil models to be utilised when sands are analysed and PLAXIS is used: Mohr-Coulomb (*MC*), with a first-order crude approximation, Hardening Soil (*HS*), which provides reasonable modelling and Hardening Soil small (*HSsmall*), which is deemed as the best standard PLAXIS constitutive models for this type of application. By taking into account the type of loading, both Hardening Soil models are suitable for the cases of primary compression, compression and shear, extension and shear and loading/reloading behaviour even though extension and unloading/reloading cases are not included in the current investigation. Some basic characteristics of the HS model are:

(i) Stress-dependent stiffness behaviour according to a power law;
(ii) A hyperbolic stress-strain relationship in axial compression;
(iii) Plastic strain by mobilising friction (shear hardening);

(iv) Plastic strain by primary compression (compaction hardening);
(v) Elastic unloading / reloading;
(vi) Failure behaviour according to the MC criterion;
(vii) Small-strain stiffness (HSsmall model only).

The parameters for the *HSsmall* model are shown in Table 2-6 after Brinkgreve et al. (2018).

Table 2-6 Parameters for HSsmall model

Component	Parameters
Failure as in Mohr-Coulomb	c = effective cohesion; Φ' = effective angle of internal friction ψ = angle of dilatancy σ_t = tensile cut-off tensile strength
Stiffness	E_{50}^{ref} = secant stiffness in standard drained triaxial test E_{oed}^{ref} = tangent stiffness for primary oedometer test E_{ur}^{ref} = unloading/reloading stiffness m = power of stress-level dependency of stiffness
Advanced	ν_{ur} = Poisson's ratio for unloading-reloading p^{ref} = reference stress for stiffness K_0^{nc} = K_0-value for normal consolidation R_f = failure ratio q_f / q_a $\sigma_{tension}$ = tensile strength c_{inc} = depth-dependant cohesion
Small-strain	G_0^{ref} = reference shear stiffness at small strains $\gamma_{0.7}$ = shear strain at which G has reduced to 72.2% of G_0

The parameter q_f corresponds to the ultimate deviatoric stress and is derived from the Mohr-Coulomb failure criterion, which involves the strength parameters c and φ (Schanz et al., (2000)). Figure 2-25 shows the stress-strain relation for a standard triaxial test and Figure 2-26 shows the hardening process in a q vs p' plot.

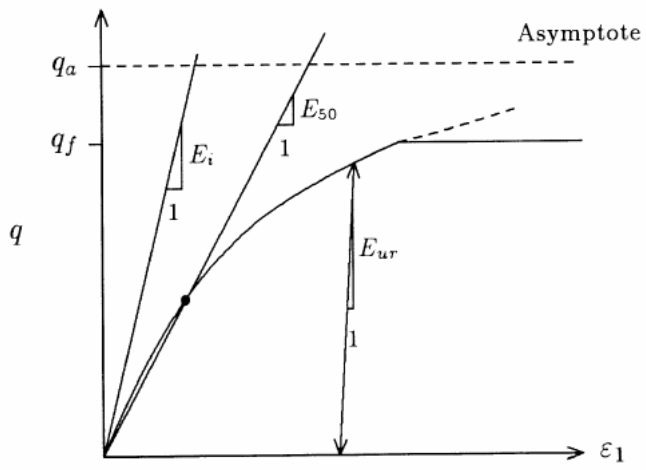

Figure 2-25 Hyperbolic stress-strain relation for a standard drained test (after Schanz et al, 2000)

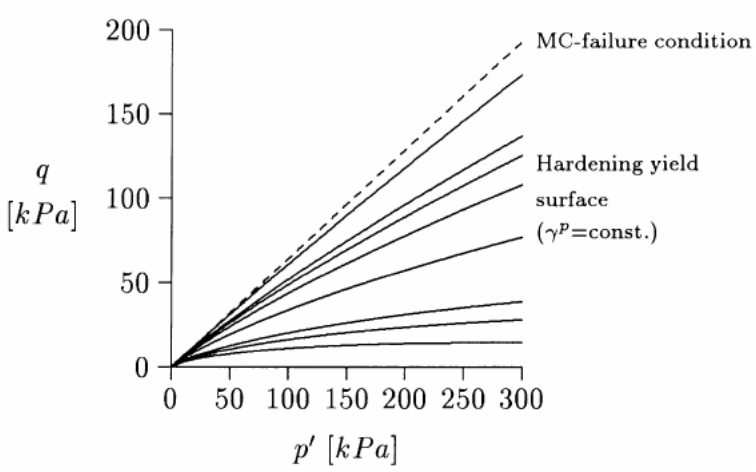

Figure 2-26 Successive yield loci and failure surface (after Schanz et al, 2000)

2.4.2. General Dunkirk Sand Model (GDSM)

In PISA #8 (2018) a new soil model specifically focused on the sand found at the Dunkirk site is defined. The formulations are applicable to monopiles at offshore homogeneous sand sites when drained loads are applied. The 'General Dunkirk Sand Model' (GDSM) proves to be a good 1D approach to a 3D behaviour by conducting analyses for monopile configurations within the calibration space in terms of relative density, element type with the FE analysis, soil type, loading and stratigraphy. In this modelling approach, the underlying simplicity of the *p – y method* is retained, but additional components of soil reaction are incorporated to improve the model's performance.

A particular feature of the sand modelling is that the model parameters are specific to soil with a specific relative density and therefore predict accurately pile-soil system response within the calibration space which took relative densities of 45%, 60%, 75% and 90%.

Since the GDSM includes the four components previously identified when a pile is subjected to lateral loading, the monopile is represented by the Timoshenko beam theory in order to allow the shear strains in the pile to be incorporated in the analysis in an approximate way.

The soil reactions are applied to the embedded beam using a generalised form of the Winkler assumption, in which assumes that the force and the moment reactions are related only to the local displacement and rotation and neglects the coupling that inevitably occurs within the soil. Due to this, the soil reaction curves based on Winkler are unlikely to be unique and depend on the relative magnitude of the translational and rotational movements of the pile. By considering this, the PISA model is calibrated within a design space that is carefully selected to represent realistic loading conditions.

The soil reaction curves used in the GDSM are based on dimensionless forms of both reactions and displacement/rotation variables to ensure the representation of the actual soil reactions at any point of the pile. These dimensionless forms are shown in Table 2-7

Table 2-7 Dimensionless forms for the soil reactions curves (PISA #8: PISA design model for monopiles for offshore wind turbines: application to a marine sand, 2018)

Normalised variable	Dimensionless form
Distributed lateral load, $\bar{p}$	$\frac{p}{\sigma'_{vi}D}$
Lateral displacement, $\bar{v}$	$\frac{vG}{\sigma'_{vi}D}$
Distributed moment, $\bar{m}$	$\frac{m}{pD}$
Pile cross-section rotation, $\bar{\psi}$	$\frac{\psi G}{\sigma'_{vi}}$
Base horizontal load, $\overline{H_B}$	$\frac{H_B}{\sigma'_{vi}D^2}$
Base moment, $\overline{M_B}$	$\frac{M_B}{\sigma'_{vi}D^3}$

σ'_{vi}: local value of initial vertical effective stress in the soil
G: local value of soil small-strain shear modulus
D: pile diameter

It is noticed that *p*, H_B and M_B and their derivatives depend solely on the vertical effective stress and the small-strain shear modulus. However, a connection between the moment *m* and the soil reaction *p* was found since the vertical tractions induced on the pile perimeter are caused by the friction at the soil-pile interface, which can be related to the local distributed lateral load. For this reason, the normalised form of the distributed moment is a function of *p* and therefore a function of both the local displacement *v* and the local pile cross-section rotation, ψ_r.

According to Panagoulias et al. (2018), the term 'soil reaction curves' is employed to represent the functions that relate each one of the non-linear soil reaction components (force or moment) to the local pile deformation (displacement or rotation). The implementation of the model employs the four-parameter conic function:

$$-n\left(\frac{\bar{y}}{\overline{y_u}}-\frac{\bar{x}}{\overline{x_u}}\right)^2+(1-n)\left(\frac{\bar{y}}{\overline{y_u}}-\frac{\bar{x}k}{\overline{y_u}}\right)\left(\frac{\bar{y}}{\overline{y_u}}-1\right)=0 \qquad \textit{Equation 10}$$

where $\bar{x}$ signifies a normalised displacement or rotation variable and $\bar{y}$ signifies each of the four corresponding normalised soil reactions included in the analysis of the lateral response of the soil. The parameter *k* is the initial slope of the curve, $\overline{y_u}$ is the ultimate value of the normalised soil reaction and $\overline{x_u}$ is the normalised displacement (or rotation) at which this ultimate value of the soil is reached. The parameter *n* ($0 < n < 1$) determines the shape of the curve.

Some important features need to be considered regarding the onshore Dunkirk site:

(i) Very dense hydraulic-placed surface layer;
(ii) Water table at about 5.4 m below ground level; presence of partially saturated layers;
(iii) Superficial layers possibly lightly cemented.

Some adjustments were required to develop the model:

(i) The hydraulic fill is not considered;
(ii) A hydrostatic pore pressure distribution is employed.

Most of the soil parameters to be included in the model are taken from the PISA analysis together with the previous investigations made on the site and according to the recommendations by Taborda et al. (2014). The soil constitutive model parameters are included in Table 2-8.

Table 2-8 Parameters for sand constitutive model (Taborda et al., (2014))

Component	Parameters
Critical state line	$p'_{ref} = 101.3\ kPa;\ e_{CS,ref} = 0.910;$ $\lambda = 0.135;\ \xi = 0.179$
Strength	$M_c^c = 1.28;\ M_e^c = 0.92$
Model surfaces	$k_c^b = 2.70;\ k_c^d = 0.88; m = 0.065;$ $p'_{YS} = 1.0\ kPa;\ A_0 = 1.30$
Hardening modulus	$h_0 = 0.4; \alpha = 1.0; \gamma = 0.0;$ $\beta = 0.0; \mu = 1.0$
Non-linear elasticity – small strain stiffness	$B = 875.0; \nu = 0.17$
Non-linear elasticity – shear stiffness degradation	$\alpha_1 = 0.40; \gamma_1 = 1.031x10^{-3}; \kappa = 2.0$
Fabric tensor	$H_0 = 0.0; \zeta = 0.0$

The interface material is represented by an elastoplastic Mohr Coulomb model with a normal and shear stiffness of 1.0 x 10^5 kN/m^3, zero cohesion and friction angle of 32°. The monopile is modelled as an elastic material using thin shell elements, with the following steel properties: Young's modulus, E = 200 GPa and Poisson's ratio, ν = 0.3

In Figure 2-27 and Figure 2-28 the computed response determined from the 1D (GDSM) model and equivalent 3D finite element analyses performed in the software ICFEP (Potts & Zdravkovic, 1999) and (Potts & Zdravkovic, 2001) are compared.

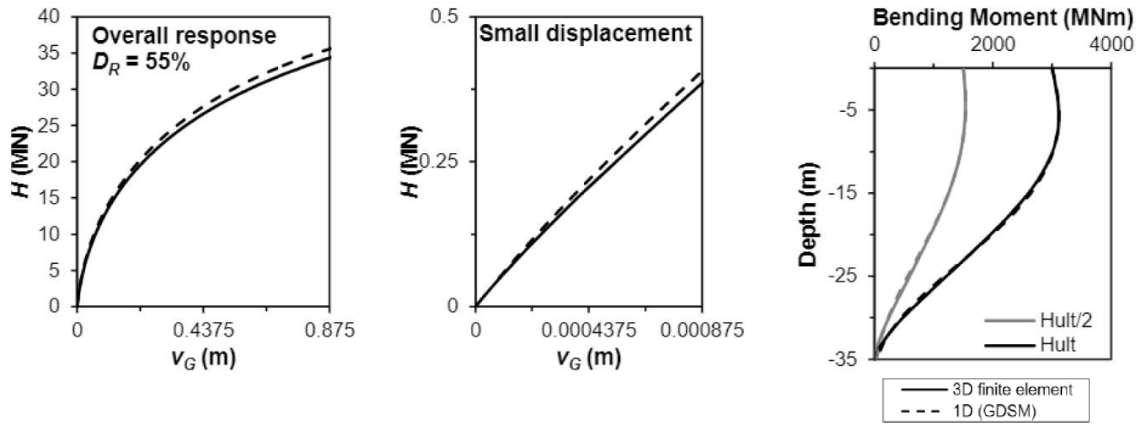

Figure 2-27 Comparison between 1D GDSM and 3D FEM analysis for DR = 55% (Burd, et al., 2018).

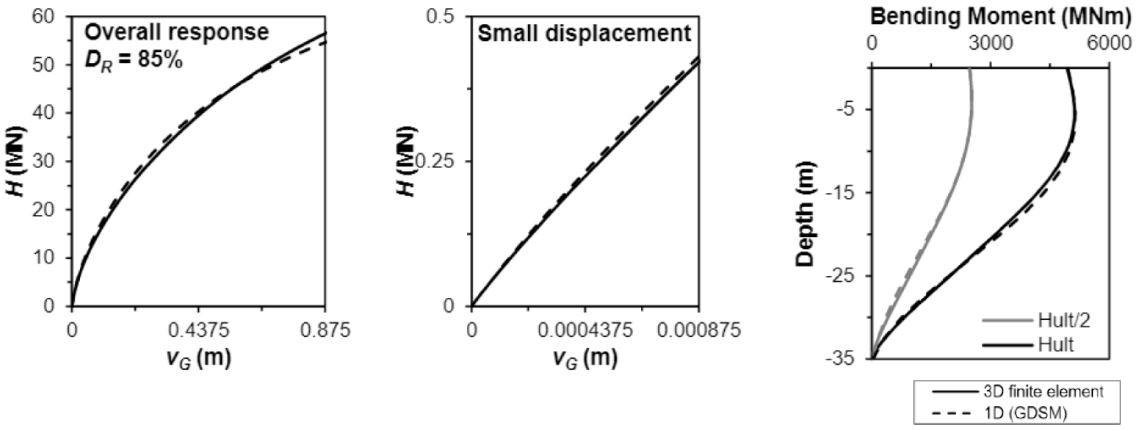

Figure 2-28 Comparison between 1D GDSM and 3D FEM analysis for DR = 85% (Burd, et al., 2018)

3. Finite Elements Model

The definition of the soil properties to characterise the sand in Dunkirk within the serviceability state limit in a 3D FE model is based on, firstly, different formulations obtained from the results of the cone penetration tests and, secondly, relations and limitations proposed by several authors. In order to get an appropriate comparison between the actual data from the pile load tests, the results from the 3D FE analysis and the proposed CPT-based method, a proper characterisation of the soil was defined using the Hardening Soil small-strain model. In this chapter, the definition of the soil layering, the obtention of the soil parameters and the comparison between the 3D FE model and the PLT results are included.

3.1. PLAXIS MoDeTo Analysis

3.1.1. General Features

PLAXIS MoDeTo (Monopile Design Tool) is a software package intended for the design of monopiles as foundation elements for offshore wind turbines under lateral loading conditions. It models the monopile based on the Timoshenko beam theory and non-linear soil reaction curves (PLAXIS, 2018). The monopile design can be performed efficiently by using 1D finite element analyses and the calibration of the soil reactions is based on 3D finite element calculations using PLAXIS 3D (numerical-based design). If for specific site soil conditions and range of monopile geometries, existing (pre-calibrated) soil reactions are available with data that are published in literature, retrieved from existing numerical-based calibrations or provided by consultants, the 3D FE calculations can be omitted and the monopile design can be directly performed using the quick 1D model analyses, (rule-based design).

3.1.2. Sand Model

MoDeTo deals with the calibration of the advanced soil constitutive models employed in PLAXIS 3D and the parameters may either be automatically predefined via correlations or fine-tuned if more information about the soil data is available. By default, MoDeTo is formulated using the Hardening Soil small-strain (*HSsmall*) model with an assumed drained behaviour when the chosen soil type is sand. The following input parameters need to be defined per soil layer:

Table 3-1 Input parameters MoDeTo

Soil parameter	Units
Submerged unit weight, γ'	[kN/m^3]
Small strain shear stiffness modulus in the middle of the soil layer, G_0	[kN/m^2]
Effective angle of internal friction, φ'	[°]
Effective angle of dilatancy, ψ'	[°]
Lateral earth pressure coefficient at rest, K_0	[-]

The rest of the needed parameters to complete de *HSsmall* model can be determined as follows, based on Brinkgreve (2010):

Table 3-2 Hardening soil small-strain model parameters

Soil parameter	Units	Comment/value/formulation
(Un)Saturated unit weight, $\gamma_{(un)sat}$	[kN/m^3]	Same as γ' to be calculated without the need to calculate water pressure and by assuming phreatic level at the bottom of the model.
Initial void ratio, e_{ini}	[-]	0.500
Horizontal effective stress, σ_3'	[kN/m^2]	$K_0 \cdot \sigma_1'$ where $\sigma_1' = \sigma_{v0}'$
Reference effective cohesion, c_{ref}'	[kN/m^2]	0.1
Reference stress level, p_{ref}	[kN/m^2]	100.0
Rate of stress dependency, m	[-]	0.5
Reference small strain shear stiffness, G_0^{ref}	[kN/m^2]	$\frac{G_0}{\left[\left(c_{ref}' \cdot cos\varphi' - \sigma_3' \cdot sin\varphi'\right)/\left(c_{ref}' \cdot cos\varphi' + p_{ref} \cdot sin\varphi'\right)\right]^m}$
Relative density, D_R	[%]	$100 \cdot \left(G_0^{ref} - 60000\right)/68000$
Stiffness modulus at 50% of maximum mobilization at reference stress, E_{50}^{ref}	[kN/m^2]	$60000 \cdot D_R/100$
Oedometric stiffness modulus at reference stress, E_{oed}^{ref}	[kN/m^2]	E_{50}^{ref}
Unloading/reloading stiffness modulus at reference stress, E_{ur}^{ref}	[kN/m^2]	$3 \cdot E_{50}^{ref}$
Shear strain at which G has reduced to 72.2% of G_0, $\gamma_{0.7}$	[-]	$(2 - D_R/100) \cdot 10^{-4}$
Unloading/reloading Poisson's ratio, ν_{ur}	[-]	0.2
Lateral earth pressure at rest in the normally consolidated branch, K_0^{NC}	[-]	$1 - sin\varphi'$
Failure ratio, R_f	[-]	0.9

By using the relations proposed by Brinkgreve (2010), some of the properties are limited by upper values as it is detailed:

- Relative density, D_R, cannot be larger than 100%;
- Consequently, the parameter E_{50}^{ref} and therefore E_{oed}^{ref} are limited to 60000 kPa;
- E_{ur}^{ref} cannot be larger than 180000 kPa;
- Parameter $\gamma_{0.7}$ is always larger than 0.0001.

The constitutive model and the soil material parameters may be modified in PLAXIS 3D despite the MoDeTo input values.

3.1.3. Pile Geometry

Additionally, to the soil properties, five parameters related to the pile geometry and the maximum lateral displacement at the top of the monopile are required to perform the finite element analysis as it is detailed in Table 3-3.

Table 3-3 MoDeTo geometry data set

Parameter	Units
Height above mudline of the application of the resultant horizontal load, h	[m]
Pile embedded length, L	[m]
Pile outer diameter, D_{out}	[m]
Pile thickness, t	[m]
Maximum lateral displacement at the top of the pile, $v_{max,z=h}$	[m]

The maximum lateral displacement at the top of the pile is used as the limit in the calculation phases as is described in the next section. The suggested values of $v_{max,z=h}$ are given in terms of having the monopile rotation point in the ground at a depth of approximately equal to 2L/3, according to the following formulation:

- Minimum target displacement at the ground level is around 0.2D:
  - $v_{max,h=z} = 0.3\frac{D}{L}\left(h + \frac{2L}{3}\right)$ *Equation 11*
- Maximum target displacement at the ground level is around 0.3D:
  - $v_{max,h=z} = 0.45\frac{D}{L}\left(h + \frac{2L}{3}\right)$ *Equation 12*

The by-default and calculated pile structural properties considered for the analyses are shown in Table 3-4:

Table 3-4 Default pile structural properties

Property	Units	Default value
Pile unit weight, w	[kN/m^3]	0 (lateral analysis only)
Young's modulus, E	[kN/m^2]	210E6
Poisson's ratio, v	[-]	0.3
Cross-sectional area, A	[m^2]	$A = \pi(D_{out}^4 - D_{in}^4)/4$
Moment of inertia, I	[m^4]	$I = \pi(D_{out}^4 - D_{in}^4)/64$
Axial stiffness, EA	[kN]	$EA = E \cdot A$
Bending stiffness. EI	[kNm^2]	$EI = E \cdot I$
Shear stiffness, GA	[kN]	$GA = 0.25EA/(1+v)$

3.1.4. FE 3D Model

MoDeTo uses only half of a symmetric model of the monopile, with the vertical plane at y = 0 as the plane of symmetry and the following contours:

- Bottom depth is user-defined;
- The distance from the centre of the pile to the right and left boundaries is 6 times the outer diameter of the pile in the x-direction;
- The model length in the y-direction from the plane of symmetry to the rear model boundary is 4 times the outer diameter;
- Fully saturated soil conditions for offshore application and effective stress approach;

- Linear-elastic isotropic plate elements (shells) for the monopile structure with Young's modulus, Poisson's ratio and wall thickness as input parameters;
- The monopile is weightless and 'wished in place';
- A separate interface material is generated by using the same soil model and properties but with dilatancy angle equal to 0° and friction angle equal to 29°. A different interface is used at the monopile bottom to retrieve soil reactions at the base;
- Finer mesh around the pile: 0.2 outer diameters around the monopile circumference and 0.15 outer diameters below the monopile toe.

Figure 3-1 shows the monopile model generated via MoDeTo in PLAXIS 3D for a monopile embedded in a 5-layers deposit.

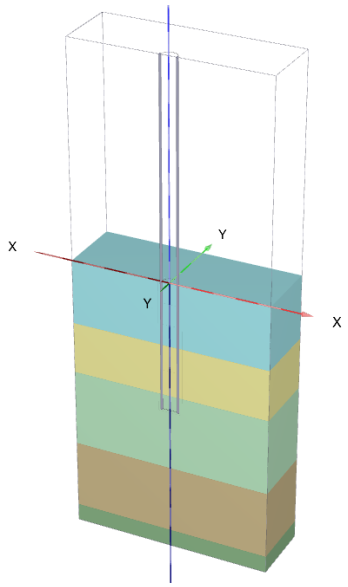

Figure 3-1 Model PLAXIS 3D

By default, when a model is generated in MoDeTo, four different phases are analysed in PLAXIS 3D. The considered calculation phases are:

(i) *Initial Phase:* K_0 – procedure;
(ii) *Phase 1:* Monopile installation (wished-in-place), plastic calculation;
(iii) *Phase 2:* Applying prescribed lateral displacements equal to $v_{max,\, z=h}/1000$, plastic calculation;
(iv) *Phase 3:* Applying prescribed lateral displacements (input value, $v_{max,\, z=h}$), plastic calculation.

Pile installation effects can be considered since they change the stress regime of the soil around and below the pile. This is due to large mesh distortion issues when considering large deformations (Murphy et al., (2018)). Gavin and Lehane (2005) observed that during a single hammer blow the average base stress mobilised is in the range of 10 – 20% of the q_c. Murphy et al (2018) used small vertical displacement increments (0.01D) to approximate the final stages of pile driving. Engin (2013) proposed a technique that involves a step-wise updated geometry, which consists of a straining phase followed by a geometry update. The geometry

update is to model the penetrated part of the pile, which can be achieved by changing the material properties at the beginning of each phase. However, according to Oomen (2017), this method, although advanced, is very time-consuming. Broere and van Tol (2006) proposed a relatively simple horizontal and vertical pre-stressing method both along the shaft and at the tip to mimic the installation process of the pile.

The pile installation effects are analysed in the next chapter of this document.

3.2. Soil Model

The final soil model used in this study is shown in Table 3-5

Table 3-5 Soil model

Depth [m]	γ' [kN/m3]	E_{50}^{ref} [kPa]	E_{oed}^{ref} [kPa]	E_{ur}^{ref} [kPa]	c'ref [kPa]	φ' [deg]	ψ [deg]	$\gamma_{0.7}$ [-]	G_0^{ref} [kPa]	R_f [-]	K_0 [-]
0.0 – 3.0	19.1	250441	250441	464632	0.1	45.9	15	0.0001	321079	0.875	0.5
3.0 – 5.4	20.8	222584	222584	399185	0.1	44.7	9.3	0.000125	285365	0.906	1.0
5.4 – 9.0	11.0	174280	174280	388166	0.1	42.9	9.3	0.000125	223436	0.906	0.8
9.0 – 12.2	11.8	201640	201640	367375	0.1	42.4	9.3	0.000125	258512	0.906	0.65
12.2 – 15.3	9.8	86636	86636	259910	0.1	36.6	9.3	0.000125	111072	0.906	0.65

Note: Soil parameter definitions are included in Table 3-1 and Table 3-2

The soil model was calibrated against available in situ and laboratory soil data from the Dunkirk site. A sensitivity analysis was then carried out in order to compare the monopile response in PLAXIS 3D against the PLT data. Piles DM3 and DM7 were mainly used for the comparison since measurements data is available in both below and above the ground level. Some soil properties were defined as is shown in Appendix I.

Soil properties of the subsoil at the Dunkirk site are derived and presented in several of the PISA reports (see also Section 2.3). In general, numerous sources were consulted in order to describe each of the layers identified through the geotechnical survey, both on this site and in the surroundings. The aforementioned PISA report includes already processed parameters obtained from both old and new in situ and laboratory tests such as 5 triaxial tests performed in the Dunkirk sand which are shown in Figure 3-2 in terms of *q/p'* vs *axial strain* in which *q* is the deviatoric stress and *p'* the mean effective stress. Two extra plots, *axial strain* vs *volumetric strain* and *q* vs *axial strain* (see Figure 3-3), representing the same 5 triaxial tests are included in the PISA Final Report (2016). Four of the tests were performed on samples with a relative density equal to 75% (natural soil) and one of them on a sample with a relative density equal to 100% (hydraulic fill). According to the PISA report, all the samples were taken at the same depth, however, tested at different confining pressures to simulate different overburden stresses. Note that the raw data of the triaxial tests could not be obtained since is currently being used by other researchers. Due to this, the information was obtained by analysing graphically these 3 plots.

Also included in Figure 3-3 is *q* vs *axial strain* curves obtained from the simulation performed by considering the constitutive model developed by the PISA team, the General Dunkirk Sand

Model (dashed lines). Figure 3-4 presents *deviatoric stress (q)* vs *axial strain* plots for 5 triaxial tests and their corresponding simulations with the use of the *HSsmall* soil constitutive model. Simulations are shown as dashed lines and labelled as ST-N(F)-XX in which N or F represents the natural soil or the fill and XX the test confining stress. Simulation soil parameters are detailed in Appendix I.

MoDeTo software requires 5 input soil parameters in order to run the PLAXIS 3D model. From these five parameters, the remaining values are calculated to complete the HSsmall set (PLAXIS, 2018).

According to Brinkgreve (2010) are the formulations to calculate the parameters for the HSsmall model based on the value of the Relative Density.

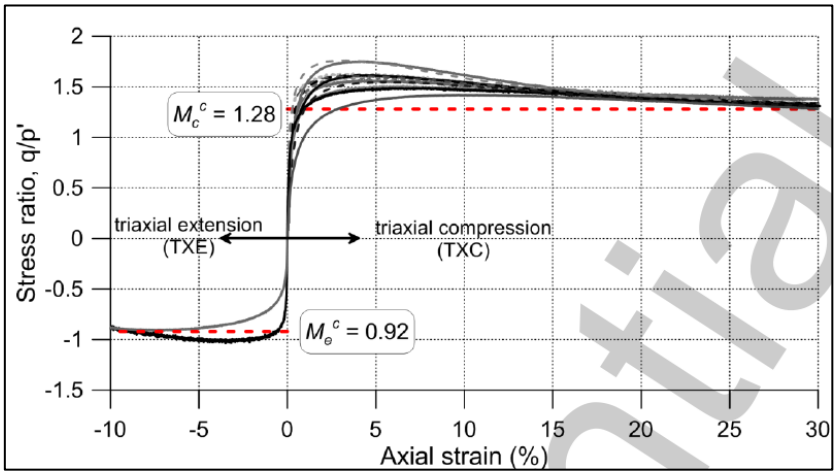

Figure 3-2 PISA triaxial laboratory tests

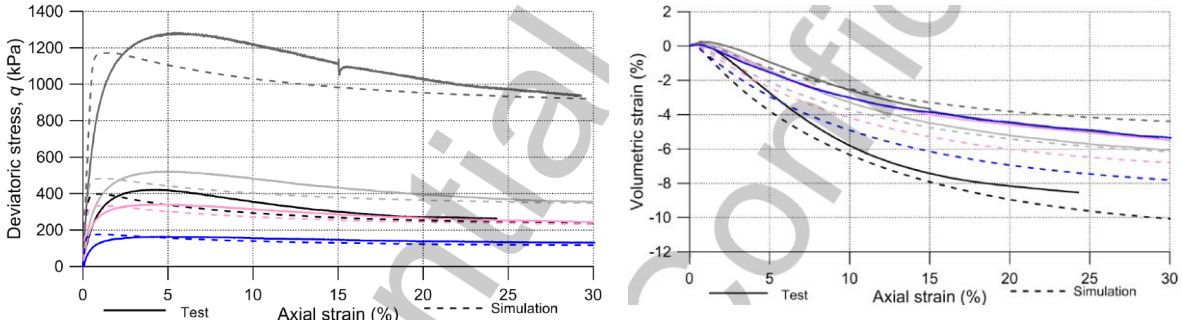

Figure 3-3 PISA triaxial laboratory tests

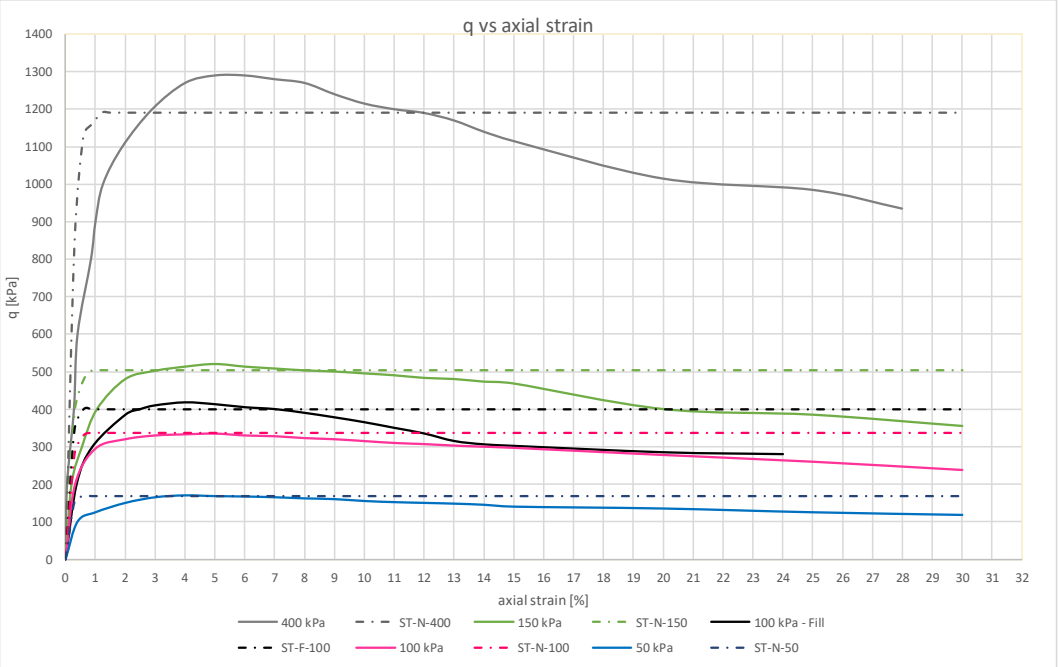

Figure 3-4 PISA triaxial tests (graphically obtained) / Built soil test simulation curves using the HS model

Additionally, some properties were obtained from what it is proposed by Robertson et al. (1986), Robertson (2016), Mayne (2017), Robertson & Cabal (2015) and Lengkeek et al. (2018).

Moreover, different sets of parameters were obtained by following the recommendation proposed by FUGRO and checking several formulations proposed by various authors.

Finally, according to Minga & Burd (2019), a calibration of the parameters of the Dunkirk sand was performed and some properties were determined from these simulations. In this same document, some formulations are included and they were used in order to calculate the soil stiffness. By using the selected G_0 profile included in Figure I-3 of Appendix I, the reference shear stress modulus can be calculated as:

$$G_0 = G_0^{ref}\left(\frac{c'_{ref}cos\varphi' - \sigma'_3 sin\varphi'}{c'_{ref}cos\varphi' - p_{ref}sin\varphi'}\right)^m \qquad \textit{Equation 13}$$

where σ'_3 corresponds to the horizontal effective stress, c'_{ref} corresponds to the reference cohesion and m corresponds to the stiffness decay ratio, in this case, equal to 0.5 for all analyses. The unloading/reloading stiffness E_{ur}^{ref} is calculated, therefore, by using the following formulation:

$$E_{ur}^{ref} = 2 \cdot G_0^{ref}(1+\nu) \qquad \textit{Equation 14}$$

where, ν = 0.17 corresponds to the Dunkirk sand Poisson's ratio. The secant stiffness at the reference stress, E_{50}^{ref}, and the oedometric stiffness, E_{oed}^{ref}, are determined by following the recommendation given by Brinkgreve (2010):

$$E_{50}^{ref} = E_{ur}^{ref}/3 \qquad \textit{Equation 15}$$

$$E_{oed}^{ref} = E_{50}^{ref} \qquad \textit{Equation 16}$$

Also according to Brinkgreve (2010), the remaining parameters used in the *HSsmall* model can be obtained by using the following formulations. The parameter relating the modulus reduction curve to the cyclic shear strain level is $\gamma_{0.7}$ and can be calculated as:

$$\gamma_{0.7} = (2 - RD/100) \cdot 10^{-4} \qquad \textit{Equation 17}$$

where *RD* corresponds to the relative density of the deposit. The failure ratio, R_f, is calculated according to:

$$R_f = 1 - RD/800 \qquad \textit{Equation 18}$$

Table 3-6 to Table 3-11 show a summary of all the different methods that were considered for the derivation of values for every parameter of interest. Due to the fact that some of the methods propose CPT-based correlations, a differentiation is made between the parameter value obtained by using the total averaged CPT value or the value from the CPT performed right next to the piles. For instance, the CPT performed next to pile DM3 is called CPT-DM3, the CPT performed next to pile DM7 is called CPT-DM7, respectively.

Table 3-6 Unit weight

Unit weight, γ [kN/m^3]		
Source	**Value / Equation**	**Comments**
PISA report	17.1	Above the water level
	19.9	Below the water level
Brinkgreve, 2010	$\gamma_{unsat} = 15 + 4.0 \cdot RD/100$	RD = Relative Density
	$\gamma_{sat} = 19 + 1.6 \cdot RD/100$	
Mayne, 2010	$\gamma = 1.95\gamma_w \left(\frac{\sigma'_{v0}}{100}\right)^{0.06} (10 f_s)^{0.06}$	Based on CPT values and vertical effective stress (σ_{vo}')
Robertson, 1986, 2009, 2010	20.0	Related to Robertson classification
Robertson and Cabal, 2010	$\gamma = \gamma_w(0.27 * \log(R_f) + 0.36 * log\left(\frac{q_t}{p_a}\right) + 1.236)$	Based on CPT values
Lengkeek et al, 2018	$\gamma_{sat} = \gamma_{sat,ref} - \beta \frac{log\left(\frac{q_{t,ref}}{q_t}\right)}{log\left(\frac{R_{f,ref}}{R_f}\right)}$	Based on CPT values

Table 3-7 Peak friction angle

Peak friction angle, ϕ [deg]		
Source	**Value / Equation**	**Comments**
PISA report	42.5	Hydraulic fill
	38.8	Natural soil
Brinkgreve, 2010	$\varphi = 28 + 12.5 \cdot RD/100$	RD = Relative Density
Mayne, 2007	$\varphi = 17.6 + 11log\left(\frac{10q_t}{(\sigma'_{v0}/100)^{0.5}}\right)$	Based on CPT values and vertical effective stress
PISA triaxial tests (Figure 3-2, Figure 3-3)	41.8	Hydraulic fill
	38.8	Natural soil
Robertson and Cabal, 2015	$\varphi' = \varphi_{cv} + 15.4log(Q_{tn}) - 26.88$	Based on CPT results and critical state angle (φ_{cv}) from PISA

Table 3-8 Small strain shear modulus

Small strain shear modulus, G_0 [kPa]		
Source	**Value / Equation**	**Comments**
PISA report	See Figures 1-8 and 1-9	Graphically
Rix and Stokoe, 1991	$G_0 = 1.634(1000q_c)^{0.25}(\sigma'_{v0})^{0.375}$	Based on CPT values and vertical effective stress
Robertson and Cabal, 2015	$G_0 = (q_t - \sigma_v) * 0.0188 * 10^{0.55I_c+1.68}$	Based on CPT values

Table 3-9 Secant stiffness at the reference pressure

Secant stiffness from triaxial tests at the reference pressure (100 kPa), E_{50}^{ref} [kPa]		
Source	**Value / Equation**	**Comments**
PISA triaxial tests (Figure 3-2, Figure 3-3)	41308	Hydraulic fill
	46900	Natural soil
Brinkgreve, 2010 Test 18	$E_{50}^{ref} = 60000 * RD/100$	RD = Relative Density
Soil test simulation (Figure 3-4)	250000	Hydraulic fill
	200000	Natural soil
Minga & Burd, 2019	$E_{50}^{ref} = E_{ur}/3$	

Table 3-10 Dilatancy angle

Dilatancy angle, ψ [deg]		
Source	**Value / Equation**	**Comments**
PISA triaxial tests Figure 3-2, Figure 3-3)	15.5	Hydraulic fill
	9.3	Natural soil
Brinkgreve, 2010	$\psi = -2 + 12.5 * \mathrm{RD}/100$	RD = Relative Density
Soil test simulation (Figure 3-4)	15.5	Hydraulic fill
	9.3	Natural soil
PLAXIS manual (2018)	14.5	Hydraulic fill
	9.6	Natural soil

Table 3-11 K_0

Lateral earth pressure coefficient at rest, K_0 [-]		
Source	**Value / Equation**	**Comments**
PISA report	0.4	
Mayne, 1995	$K_0 = \frac{\sigma'^{(1.15sin\varphi')/(1-3.7sin\varphi')}_{v0}(1-sin\varphi')^{1/(1-3.7sin\varphi')}}{2.876^{sin\varphi'/(1-3.7sin\varphi')}q_c^{(0.815sin\varphi')/(1-3.7sin\varphi')}}$	Based on CPT values, friction angle and vertical effective stress
Mayne, 2017	$K_0 = (1-sin\varphi') \cdot OCR^{sin\varphi'}$	Based on friction angle and OCR which is based on CPT values
Robertson, 2016	See Figure 3-5	Based on the Robertson classification chart

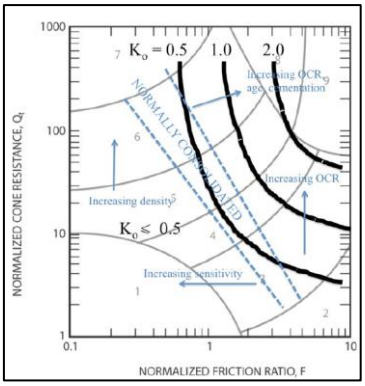

Figure 3-5 K0 according to Robertson chart

Some of the expressions included in the previous tables are detailed as follows:

- γ_w water unit weight;
- q_c CPT tip resistance;
- u_2 CPT excess pore water pressure;
- p_a atmospheric pressure, 100 kPa;
- f_s CPT sleeve friction;
- R_f normalised friction ratio

$$R_f = \frac{100 f_s}{(q_t - \sigma_{v0})}; \quad \text{Equation 19}$$

- q_t corrected tip resistance

$$q_t = q_c + (1 - 0.75)u_2; \quad \text{Equation 20}$$

- $\gamma_{sat,ref}$ reference saturated u.w. $\gamma_{sat,ref}$ = 19.0
- $q_{t,ref}$ reference corrected q_c $q_{t,ref}$ = 5.0
- $R_{f,ref}$ reference normalised R_f $R_{f,ref}$ = 30.0
- β inclination u.w. contour β = 4.12

- Q_{tn} normalised cone resistance

$$Q_{tn} = \frac{\frac{q_t - \sigma_{v0}}{p_a}}{\left(\frac{\sigma'_{v0}}{p_a}\right)^n}; \quad \text{Equation 21}$$

- n exponent n

$$n = 0.381 I_c + 0.05\left(\frac{\sigma'_{v0}}{p_a}\right) - 0.05 \leq 1.0; \quad \text{Equation 22}$$

- I_c CPT material index:

$$I_c = \sqrt{(3.47 - logQ_{tn})^2 + (1.22 + logR_f)^2}; \quad \text{Equation 23}$$

- OCR over-consolidation ratio

$$OCR = \frac{\sigma_{pc}}{\sigma'_{v0}}; \quad \text{Equation 24}$$

- σ_{pc} pre-consolidation stress

$$\sigma_{pc} = 0.33(q_t - \sigma_{v0})^m; \quad \text{Equation 25}$$

- m exponent m

$$m = 1 - \frac{0.28}{1+\left(\frac{I_c}{2.65}\right)^{25}}; \qquad \textit{Equation 26}$$

Figure 3-6 and Figure 3-7 show the tip resistance and the sleeve friction of the average CPT, CPT-DM3 and CPT-DM7.

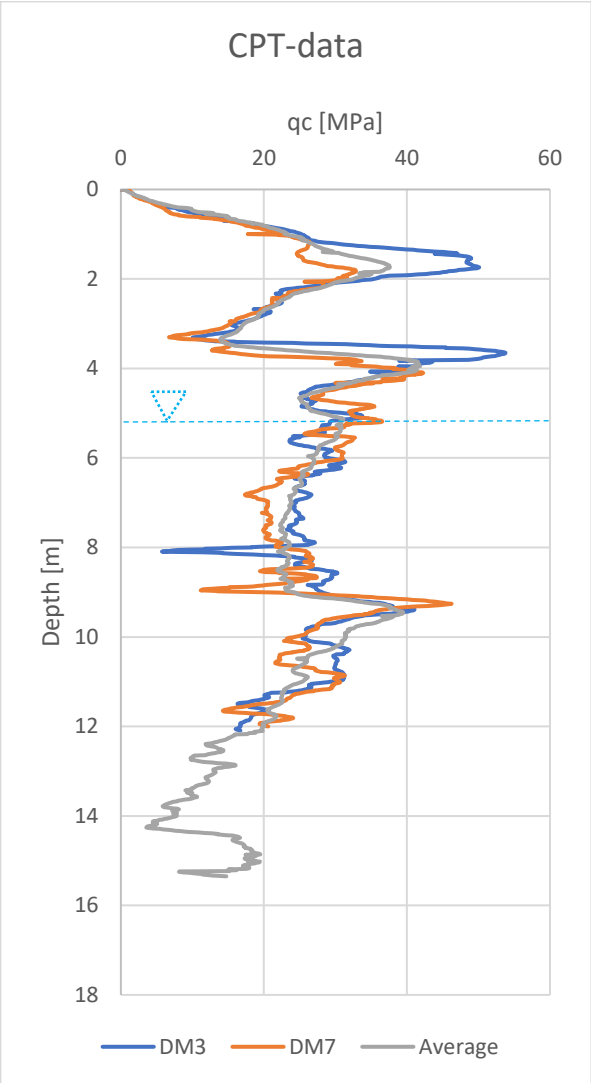

Figure 3-6 CPT tip resistance

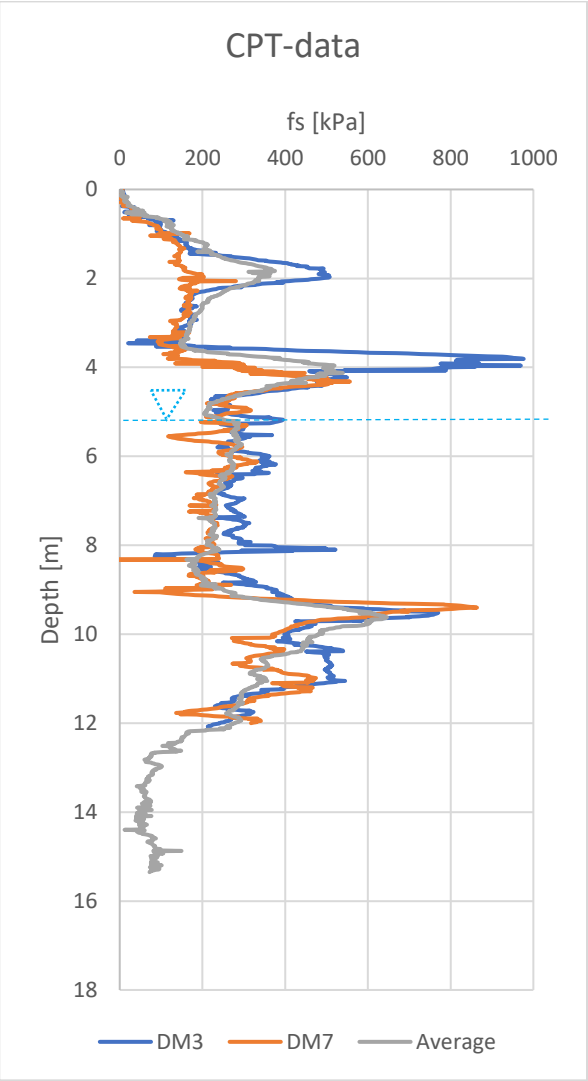

Figure 3-7 CPT sleeve friction

It can be noticed that the CPT performed next to pile DM3 has slightly larger values than the average. On the other hand, the CPT-DM7 presents, in general, smaller values than the average. For all CPT-based correlations for each parameter, the average CPT profile was used.

Plots are included in Appendix I for the unit weight, peak friction angle, shear modulus, secant stiffness, dilatancy angle and lateral earth pressure coefficient at rest. In each plot, all the proposed formulations and methods are identified. The final design value is indicated with a thick red line.

3.3. Sensitivity Analysis

The sensitivity analysis focused on (i) performing 3D FE analyses in PLAXIS with various combinations of soil parameter sets and (ii) checking the monopile responses against the PLT data. The models were created via MoDeTo and analysed in PLAXIS 3D. All the calibration of the site and the sensitivity analyses were based on the results of the DM3 and DM7 PLTs at the Dunkirk site.

Two soil layers were identified during the geotechnical survey:

- From surface to 3.0 m below the ground level: very dense hydraulic fill;
- From 3.0 m to 30.0 m below the ground level: dense natural sand.

Both soils correspond to the same sand deposit.

Every soil model was created via MoDeTo and later modified (regarding soil properties only) via PLAXIS 3D. Mesh, boundaries, stages of analysis and the rest of the default features were not changed.

In order to obtain a characterisation of the sand deposits in Dunkirk for the purposes of this research, several FEM 3D simulations were performed and their results were compared with the real data obtained from the pile load tests (PLTs) in terms of the following:

- Horizontal force vs. mudline displacement;
- Displacement and rotation as a function of the depth at different load steps.

The pile DM3 located in Dunkirk has the geometric properties indicated in Table 2-5 and it is used to perform the first FE analysis since it possesses measurements both above and below ground level. A preliminary analysis with the use of a soil model which combined some parameter values determined in the PISA Field Test Factual Report (2015), friction angle as determined by Foursoff (2018) and the dilatancy angle after Brinkgreve (2010) (see Table 3-12) gave a large offset in both strength and stiffness between the modelled and the actual behaviour of pile DM3, as it is shown in Figure 3-8. The water table is considered to be at 5.4 m deep from the ground level.

Table 3-12 Calibration tests pile DM3

Test	Soil layer	Depth [m]	Soil property				
			γ' [kN/m^3]	G_0 [kN/m^2]	φ' [°]	ψ' [°]	K_0 [-]
1	1	0.0 – 3.0	9.9	75000	42	9	0.4
	2	3.0 – 20.0	9.9	150000	42	9	0.4

Figure 3-8 shows the comparison between the PLT, the 3D analysis performed by means of PLAXIS and the 1D MoDeTo analysis. The test shows a good agreement between the two models. However, both computational analyses show high mismatching respect to the data taken from the pile load test. Same ground displacements are obtained with approximately half

of the load. Both, the stiffness and the strength of the modelled soil seem to be too low to reproduce the behaviour of the pile DM3 tested in Dunkirk. Consequently, a sensitivity analysis is performed in order to get a better fit between the modelled and the real behaviour of the pile DM3. Several of the soil parameters were modified to determine their influence on the behaviour of the model based on what is stated by Schanz et al (2000).

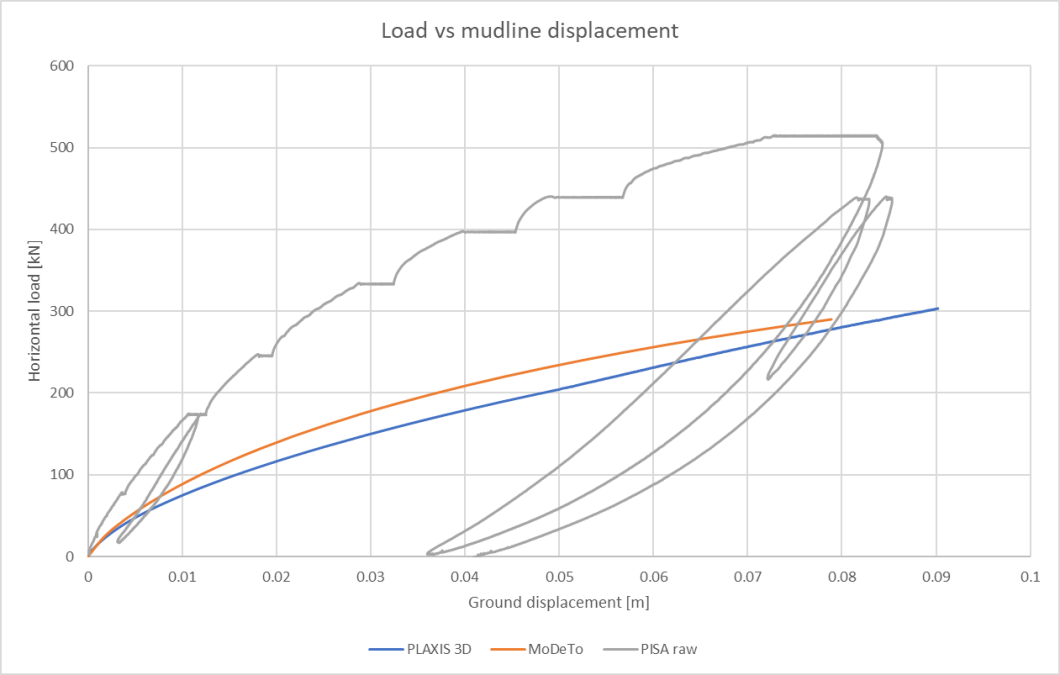

Figure 3-8 Horizontal load vs mudline displacement pile DM3

In total, 28 3D-analyses were performed in order to calibrate the soil model to the measured PLT data. Maximum, minimum and initial void ratio were retrieved directly from the PISA report and were not modified in any of the analysed models: the hydraulic fill with an initial void ratio of 0.571 and the natural soil of 0.628; the minimum and maximum void ratios for this deposit are 0.540 and 0.910, respectively. Also, even though the K_0 values are larger than 0.5 for the hydraulic fill according to the Figure included in Appendix I, this quantity was used as the upper limit of this soil property in this layer.

Besides testing different soil properties obtained from different expressions and sources, the soil layering was also modified. The final layering used is as follows:

- The hydraulic fill is taken as a single layer between 0 and 3.0 m;
- The second layer contains the natural deposit until the water table level, therefore, between 3.0 and 5.4 m;
- CPT results are very similar between 5.4 and 9.0 m, thus, the third layer is defined between these depths;
- Finally, a fourth layer between 9.0 and 12.2 m (two times the DM3 pile embedded length) is defined.

After running the whole set of tests, the results using the final soil model proposed in Table 3-5 are shown in Figure 3-9 to Figure 3-12. In the case of the soil unit weight, the relationships

proposed by Mayne (2010) and Robertson & Cabal, (2015) give a better fit to the desired response. This parameter affects not only the vertical and horizontal stresses but also the calculation of the stiffnesses.

The selection of the friction angle final value was mainly based on the formulations proposed by Mayne (2007) and Robertson & Cabal (2015). In this case, all the formulations give similar results and differences are quite small.

Regarding the small shear strain modulus, by using the profile proposed in the PISA report and the formulation proposed by Rix & Stokoe (1991), the stiffness seems to be too low to represent the pile load test responses accurately. Therefore, a profile with values similar to the ones proposed by Robertson & Cabal (2015) was chosen.

The secant stiffness at the reference stress, E_{50}^{ref}, was obtained by using Equation 13, Equation 14 and Equation 15. These formulations match pretty well the results obtained from the simulated triaxial tests based on the hardening soil model. The stiffnesses extracted directly from the triaxial tests were too low, leading to very soft monopile responses.

Finally, in the determination of the lateral earth pressure coefficient at rest, K_0, a fixed value of 0.5 was defined for the fill. For the rest of the soil profile, a general decreasing trend with depth was adopted based on derived K_0 values from the different methods.

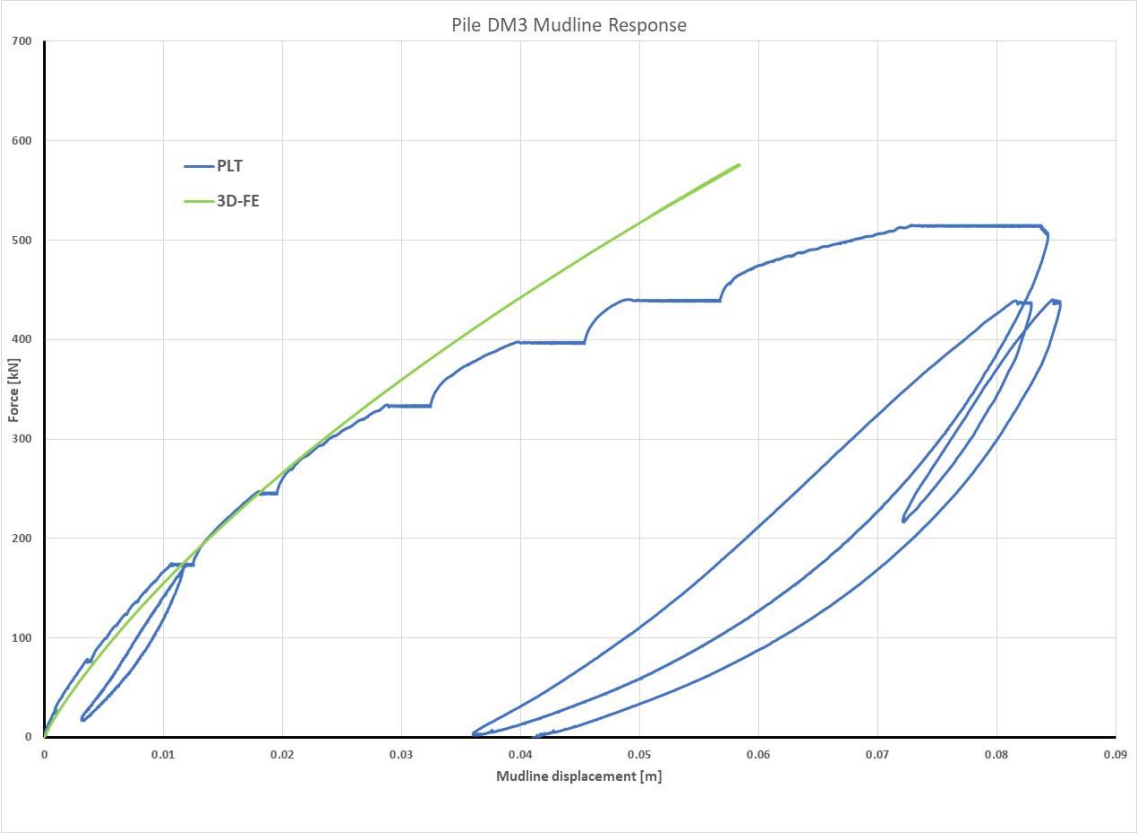

Figure 3-9 Pile DM3 response at mudline

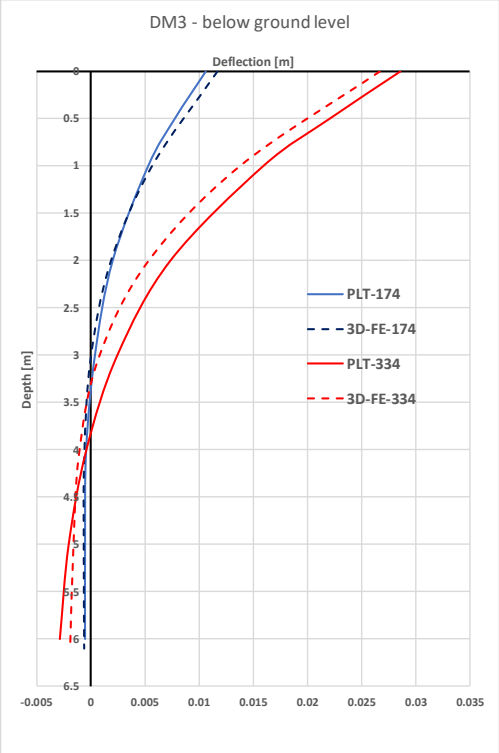

Figure 3-10 Pile DM3 response below ground level

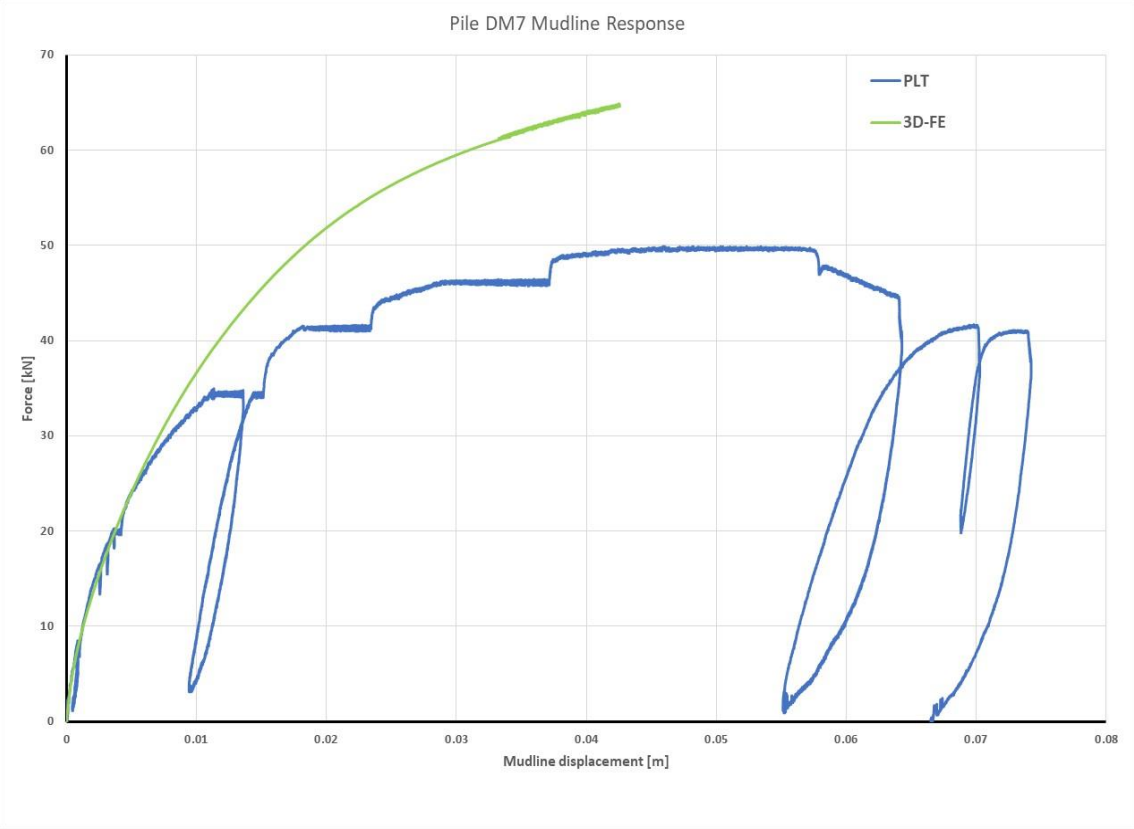

Figure 3-11 Pile DM7 response at mudline

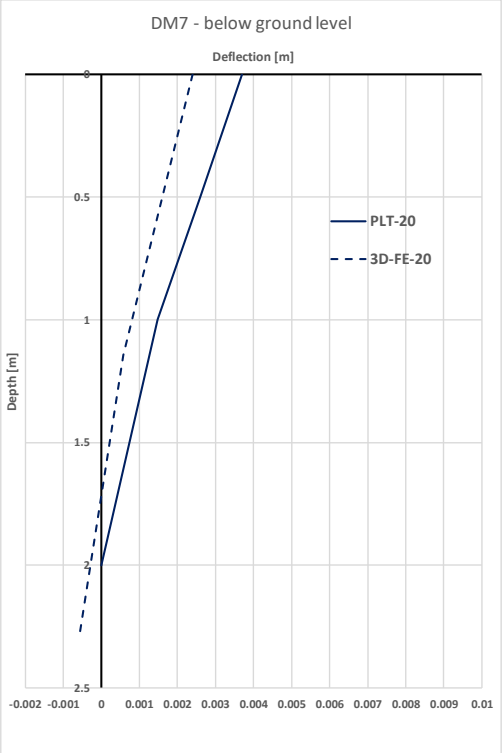

Figure 3-12 Pile DM7 response below ground level

The analyses based on the average properties seem to match both curves. By analysing the monopile response at the mudline, the PLAXIS model gives quite a good fit with the PLT data, especially in terms of the stiffness response during the initial part of the load-deflection curve. This is highly important considering the importance of SLS (and FLS) in the design of wind turbines, as stated earlier in the report. Although, initially the fitting of the load-displacement prediction curve (PLAXIS) with the actual curve (PLT) is very good, at later loading stages more deviation is seen mainly due to the creep steps that were introduced during pile load testing. In later load stages, approximately after the half of the maximum load, the PLAXIS response is stiffer than the actual tests. Figure 3-10 and Figure 3-12 show the deflection below ground level at two load stages which belong to the first half of the maximum load for each of the piles given by the 3D analyses, in which curves are individualised as ‘PLT-load’, ‘3D-FE-load’ and ‘CPT-based-load’ with ‘PLT’ being the data taken from the document PISA #4 (2018), ‘3D-FE’ being the results from the 3D finite element analyses and ‘CPT-based’ being the results from the MATLAB code as it is explained in Chapter 5.

In order to check the pile response at large deformations (ULS), a model was created by including the residual friction angle (32° according to the PISA report) instead of the peak friction angle. The stiffnesses were kept as in the original model. The response of the pile DM3 is shown in Figure 3-13.

Figure 3-13 Pile DM3 response at mudline with residual friction angle

Clearly, the response matches better the later load stages. The initial stiffness is slightly affected by the modification, however, the later stages of the prediction curve are much softer than before. The modelled response matches the response which includes the creep stages. However, the residual friction angle is not represented by any of the CPT-based formulations and therefore a relationship of the soil reaction based on CPT results may generate some inconsistencies.

3.4. Conclusions

Numerous simulations were performed in order to match the modelled behaviour with the actual behaviour obtained from the pile load tests of piles DM3 and DM7 both, at the mudline and below ground level. Soil parameters were modified in order to match the monopile stiffness for working loads (i.e. loads of less than half the failure load), which is the main focus of this research. In order to do that, several formulations given by different authors were used to estimate the soil parameters of the sand at the Dunkirk site and different combinations of them were tested until a good match was obtained.

In general terms, there is a trend in the unit weight values slightly lower than 20 kN/m^3 through the hydraulic fill given mainly for the fixed values reported in PISA, the natural distortion in the CPT values close to the surface and by using the formulation by Brinkgreve. When the natural soil is reached and especially deeper than the water table (5.4 m deep), values increase

up to 23 kN/m^3. There is a decrease beyond 12 meters deep with punctual values of about 17 kN/m^3.

According to the reported by the PISA group, there is a trend related to higher values of the friction angle in the hydraulic fill compared to the ones in the natural soil. This matches the higher relative density of the upper deposit. The first 3.0 meters show peak values of the friction angle up to 51°. Then, punctual high peaks and nadirs can be identified but a clear trend is noticed with friction angles values between 42° and 47°. Deeper than 12.0 m a reduction in the values of the friction angle is identified which follows the tendency of the CPT values. In general, the fixed values obtained from the triaxial tests and from the formulation by Brinkgreve seem to be lower.

The small strain shear modulus obtained from the PISA report shows a close-to-linear increasing trend from the surface to the bottom of the profile. This trend has a good match with the CPT-based correlation given by Rix and Stokoe (1991). The relationship given by Robertson and Cabal (2015), shows larger values of G_0 since the formulation includes a higher value for the exponent of the CPT tip resistance than in the relationship proposed by Rix and Stokoe (1991).

The parameter E_{50}^{ref} shown in Figure I-4 in Appendix I, shows, in general, higher values through the hydraulic fill than through the natural soil. This confirms what is proposed in the PISA report related to the denser deposit at the top. The simulated behaviour via Soil Test gives about 4 times higher values than the rest of the relationships, although the trend is the same.

Figure I-5 shows the values of the dilatancy angle as a function of the depth. Each relationship, but the one given by Brinkgreve (2010), gives values for the hydraulic fill of about 15° and for the natural deposit of about 9.3°. This trend is according to expectations since the density of the upper deposit is higher and therefore a more dilatant behaviour is anticipated. Brinkgreve (2010) gives lower values for both deposits.

Finally, Figure I-6 included in Appendix I, the values of the coefficient of earth pressure at rest, $K_{0.}$ PISA proposed a fixed value equal to 0.4 for the whole deposit. However, other relationships presented in Table 3-VII show larger values at the same depth. A value of 0.5 was selected for the hydraulic fill. For the rest of the soil profile, a general decreasing trend with depth was based on derived K_0 values from the different methods

If later load stages are to be described, the residual friction angle of the sand may be used. Also, some modification to the stiffness may be applied. However, this case is out of the scope of this thesis.

4. Soil Reaction Curves

MoDeTo provides each of the four soil reaction curves from both, directly from the 3D FEM analysis and from the 1D simplification described in the PISA report. By analysing the data, 3 out of 4 of the reactions are characterised by means of CPT-based formulations. The remaining reaction, $p - y$ curves, is assumed as correct and the formulation proposed by Dyson & Randolph is used. In this chapter, soil reactions are extracted from MoDeTo and describe them as CPT-based formulae.

4.1. Introduction

After defining the soil layering and material properties of the Dunkirk site, the soil reaction curves were extracted. By using the interface provided by PLAXIS MoDeTo, the four reactions can be directly obtained from the 3D FEM analysis. Besides the actual piles tested during the PISA project, several fictional piles were modelled and analysed to illustrate the influence of the geometric features in each of the four soil reactions. These fictional piles are in bold text in Table 4-1 and even though some of them have unrealistic geometric features, they were tested to check the influence of the modifications on the diameter and length. Piles DM3 have the same length, but the diameter changes; piles DM7 keep the diameter, but the length is modified. Pile DM4 is also used as data checker since data above and below ground level is available. Each pile was analysed by means of PLAXIS 3D and all the soil reaction curves were extracted in order to be analysed and to define CPT-based formulations that could represent them.

Table 4-1 Pile geometries to determine soil reaction curves

Pile	Diameter, D [m]	Length, L [m]	Slenderness ratio, L/D [-]	Thickness, t [m]
DM3	0.762	6.1	8.0	0.025
DM3A	1.0	6.1	6.1	0.025
DM3B	1.2	6.1	5.1	0.025
DM3C	0.6	6.1	10.2	0.025
DM3D	2.0	6.1	3.05	0.025
DM3E	4.0	6.1	1.53	0.025
DM7	0.762	2.29	3.0	0.010
DM7A	0.762	1.0	1.31	0.010
DM7B	0.762	3.0	3.94	0.010
DM7C	0.762	8.0	10.5	0.010
DM7D	0.762	4.65	6.1	0.010
DM7E	0.762	3.8	4.99	0.010
DM4	0.762	4	5.25	0.014
DL1	2.0	10.5	5.25	0.038

Regarding the values of the soil reaction curves, all of them are based on the soil model detailed in Table 3-5. Since a CPT-based method is proposed to calculate the four soil reaction curves, a value of the tip resistance of each layer must be defined. In order to address this, the CPT tip resistance values are given in terms of the average value of each of the layers proposed in the

soil stratigraphy. By assuming that, the following averaged properties are used, for instance, in the case of the pile DM3 which penetrates the first three soil layers: the first layer corresponds to the hydraulic fill; the second layer corresponds to the natural soil above the water level, and the third layer corresponds to the natural soil below the water level. When the soil reaction curves along the shaft are extracted from the 3D FE analysis, they are discretised, usually, each 1.0 m, although, if they belong to the same soil layer, the properties do not change. Table 4-2 shows the average properties for the top three layers. Soil effective unit weight corresponds to the input value in the 3D model and CPT tip resistance values are the average value of the entire layer, for instance, the average of the first three meters for layer 1. Besides the tip resistance, the layer middle point and the soil unit weight are also presented in the Table since they are used for the calculation of the $p - y$ curves according to the Dyson & Randolph formulation. For longer piles, the same process was performed.

Table 4-2 Layer dependant property values for piles DM3

Pile	Soil Layer	Slice depth [m]	Slice middle point, z [m]	γ' [kN/m^3]	q_c [kPa]
DM3s	1	0.0 to -1.0	-0.5	19.1	22048
		-1.0 to -2.0	-1.5	19.1	22048
		-2.0 to -3.0	-2.5	19.1	22048
	2	-3.0 to -4.2	-3.6	20.8	27930
		-4.2 to -5.4	-4.8	20.8	27930
	3	-5.4 to -6.1	-5.75	11.0	24572

Even though MoDeTo was used to define the finite element model in PLAXIS 3D, the 1D simplification given by the software was finally not used. The reason is that the 1D model proposed by MoDeTo is based on the properties that the user inputs within the software. However, as it was mentioned in previous chapters, the stiffness and strength parameters were limited by predefined values proposed by Brinkgreve (2010). Those values did not match the response obtained from the pile load tests and therefore a modification was done within PLAXIS 3D. For this reason, the soil reaction curves, both at the base and along the shaft, were extracted directly from the 3D analysis and not from the 1D simplification performed internally by MoDeTo.

4.2. Base Horizontal Force

The first reaction to be determined is the horizontal force at the base of the pile, H_B. This force can be considered as a frictional force acting on the base of the pile and it is caused by the translation at the pile toe, as it is shown in Figure 4-1.

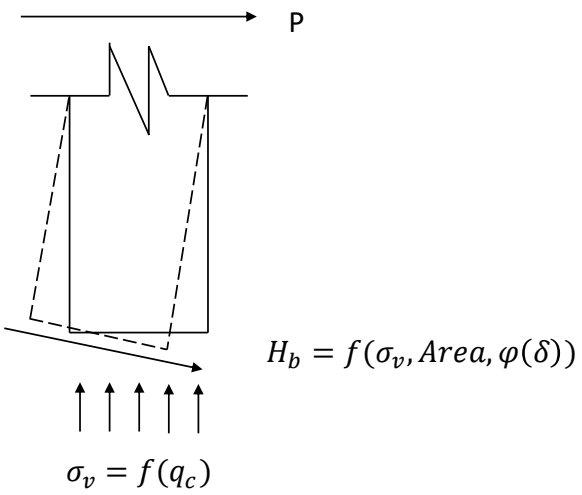

Figure 4-1 Horizontal reaction at the pile base

Due to the applied force at the pile head, the pile tends to move in the opposite direction and therefore a reaction force and a displacement are generated. A simplified approach to determine this force is to consider it as a portion of the vertical force which is a function of the vertical effective stress at the pile base. As it is stated by Murphy et al. (2018), the vertical stress, after driving, is a function of the CPT tip resistance of the soil at the base. Additionally, due to the pile geometries and the installation process, a fully plugged situation can be expected and due to this, the cross-section of the pile is considered as full even though the monopiles are usually open-ended piles. Figure 4-2, Figure 4-3, Figure 4-4 and Figure 4-5 show the predicted base horizontal forces as a function of the base horizontal displacements for piles DM3s, DM7s, DM4 and DL1, respectively. In this case, the base horizontal force for pile DM7C is close to zero and therefore was not included in the analysis.

The linear portion of the curve is limited by the dash lines show in the plot. This limit is defined in the next paragraph.

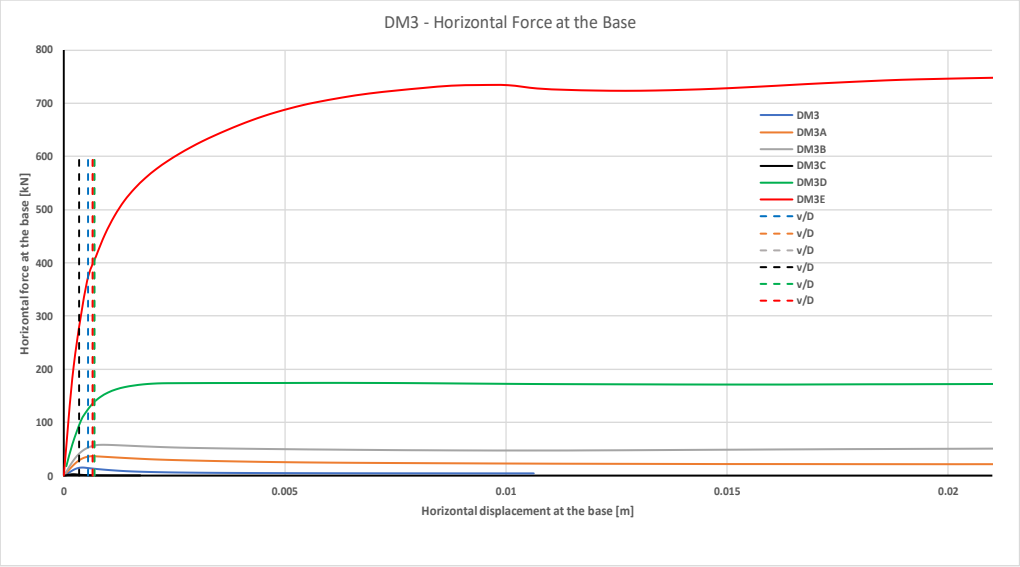

Figure 4-2 Horizontal force versus horizontal displacement at the base - Piles DM3

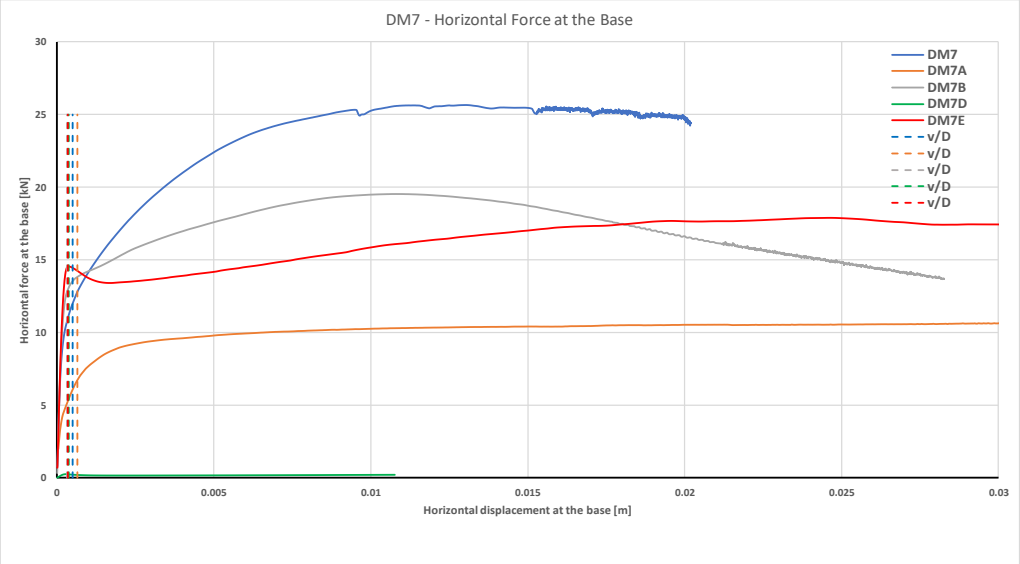

Figure 4-3 Horizontal force versus horizontal displacement at the base - Piles DM7

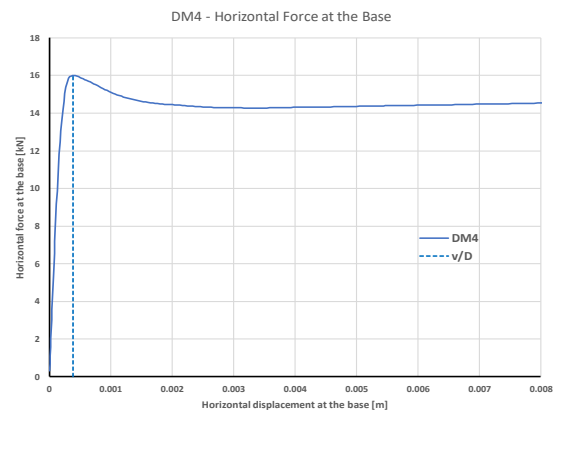

Figure 4-4 Horizontal force versus horizontal displacement at the base - Pile DM4

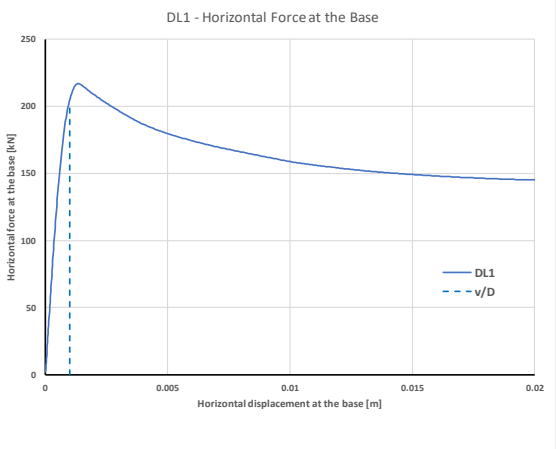

Figure 4-5 Horizontal force versus horizontal displacement at the base - Pile DL1

By looking at the results, some conclusions can be inferred:

- For most piles with L/D ratios greater than approximately 5, a post-peak strain-softening behaviour can be identified;
- The peak H_B is highly influenced by the diameter in a positive correlation;
- A 'linear' relation between force and displacement can be noticed in the first part of the curve. This linear part ends, approximately, at the following point:

$$v_b/D = 0.0005 \text{ [-]} \qquad \textit{Equation 27}$$

  where v_b corresponds to the lateral displacement at the base. The limit of this linear part is indicated with a dashed line in the plots;
- The peak horizontal force increases as the value of L/D decreases.

In order to simplify the calculation of the horizontal force, a bi-linear relation is proposed: the first linear part corresponds to the base displacements between zero and the value given by Equation 27; the horizontal load starts at 0 and reaches the value given by the residual horizontal force of each of the piles. The second part corresponds to a constant value of the horizontal load given by the residual force for every base displacement larger than the one calculated according to Equation 27.

By addressing what it is shown in Figure 4-1, different fitting parameters were tested in order to get a good relation for the horizontal force. Each one of these fitting parameters includes the assumed influencing parameters indicated in the Figure, such as the full area of the cross-section of the pile and the vertical effective stress together with friction angle that are assumed to be correlated with the tip resistance of the CPT. CPT values are detailed in Table 4-2 in the case of piles DM3. Also, a dependency on the slenderness ratio is assumed, since the value of the force increases as the slenderness ratio decreases, as it is shown in the plots. The following parameter, P_{HB}, fits the values of the residual H_B as it is shown in Figure 4-6.

$$P_{HB} = \frac{q_c \cdot D^2}{(L/D)^{0.35}}$$ *Equation 28*

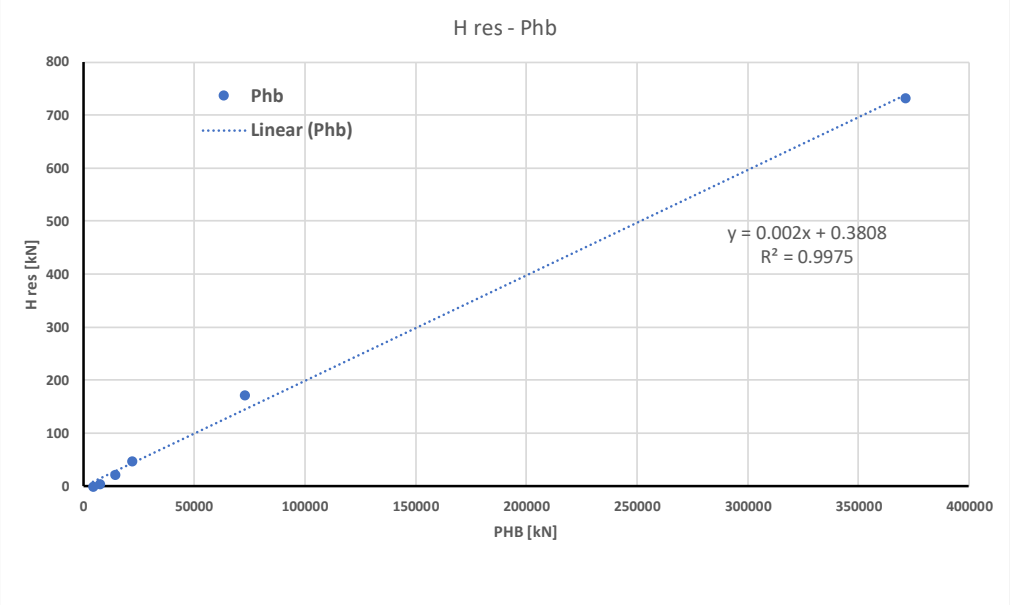

Figure 4-6 Fitting parameter base horizontal force

The linear regression that relates the fitting parameter with the horizontal residual force gives an approximated formulation of $H_{res} = 0.002P_{HB}$. Since this parameter tends to overestimate the residual force in some cases, the residual horizontal load is calculated according to the following formulation:

$$H_B = \frac{0.00185 \cdot q_c \cdot D^2}{(L/D)^{0.36}}$$ *Equation 29*

If the expression for the area is explicit, the formulation can be re-written as:

$$H_B \begin{cases} \dfrac{0.00235 \cdot q_c \cdot \pi D^2}{\left(\frac{L}{D}\right)^{0.36} \cdot 4} v_b & if \quad \dfrac{v_b}{D} \leq 0.0005 \\ \dfrac{0.00235 \cdot q_c \cdot \pi D^2}{\left(\frac{L}{D}\right)^{0.36} \cdot 4} & if \quad \dfrac{v_b}{D} > 0.0005 \end{cases}$$

Equation 30

By considering this maximum value of the horizontal force at the base, plots included in Figure 4-7 to Figure 4-11show the base horizontal forces for various pile geometries, predicted both with 3D FE calculations and the above CPT-based formulation.

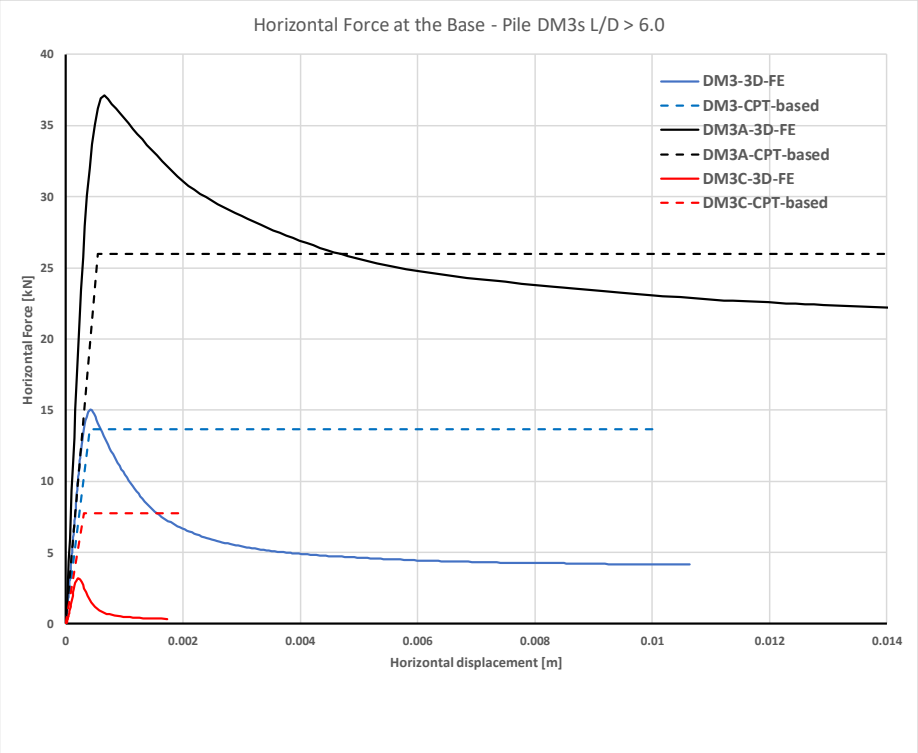

Figure 4-7 Horizontal force at the base - Piles DM3 with L/D > 6.0

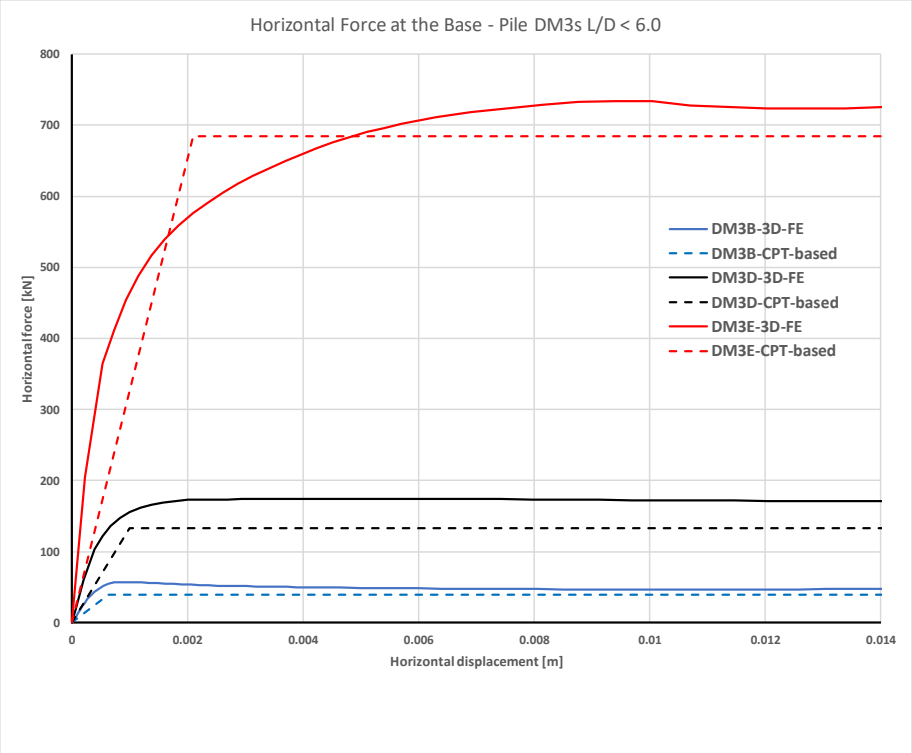

Figure 4-8 Horizontal force at the base - Piles DM3 with L/D < 6.0

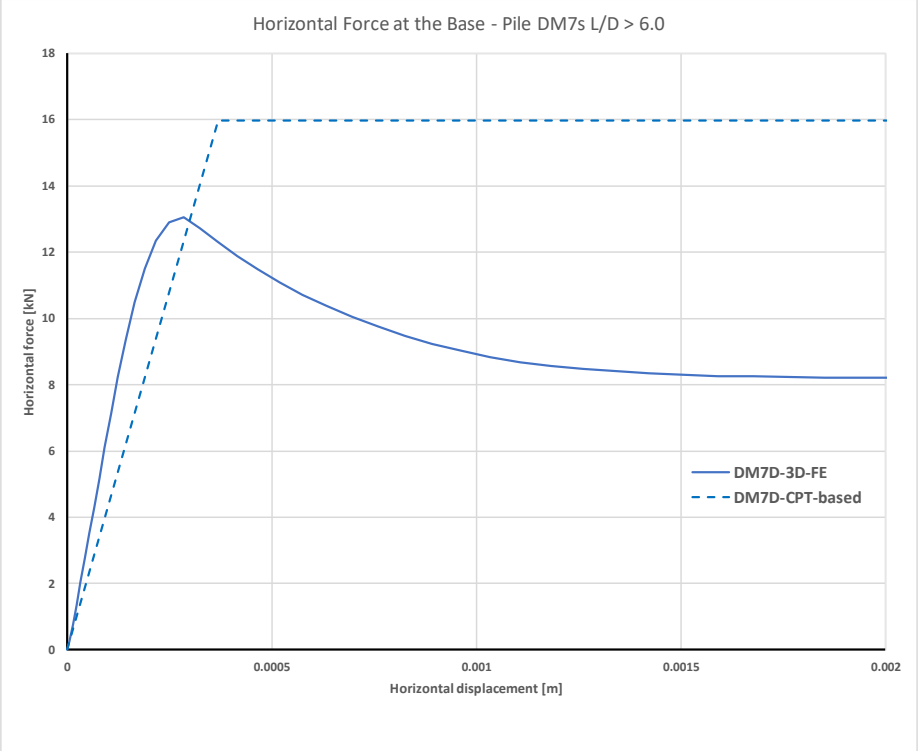

Figure 4-9 Horizontal force at the base - Pile DM7D

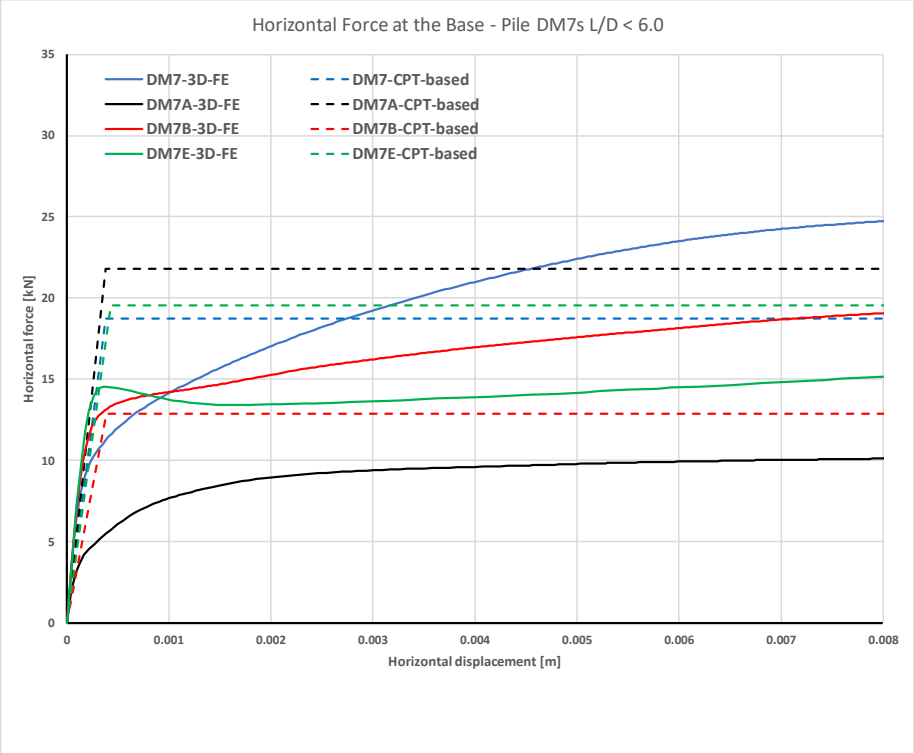

Figure 4-10 Horizontal force at the base - Piles DM7 with L/D < 6.0

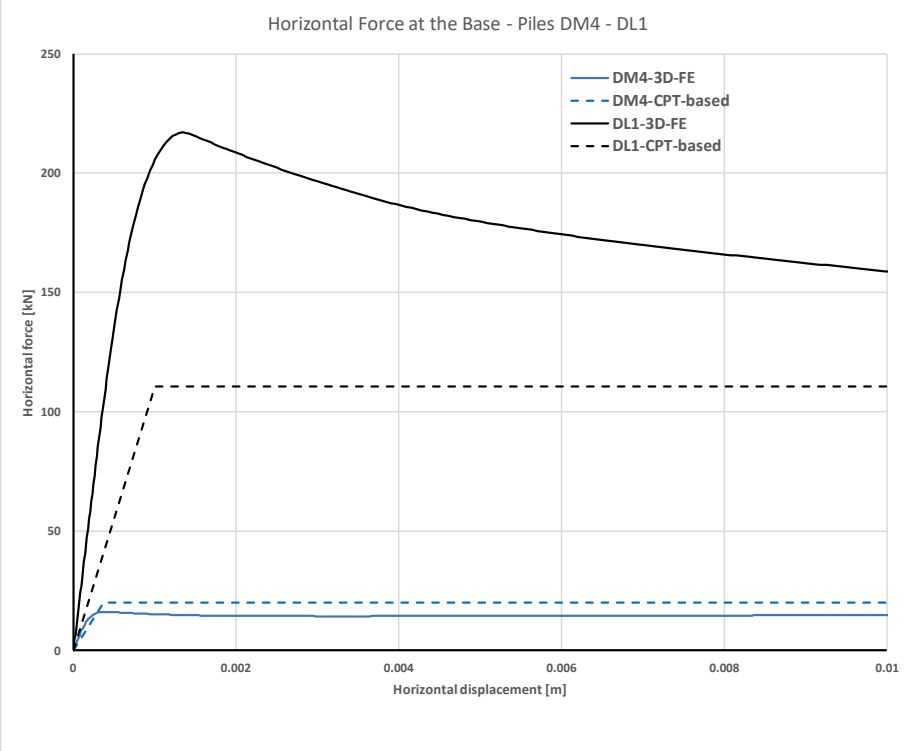

Figure 4-11 Horizontal force at the base - Piles DM4 and DL1

4.3. Base Moment

The base moment is caused by the rotation of the pile toe. It is assumed that the horizontal forces and displacements at the base of the pile are related to the moments and rotations at the same point. According to Table 2-7 taken from the document PISA #8 (2018), the following relationship can be derived for the moment at the base, M_B.

$$M_B = \bar{A} \cdot H_B \cdot D \qquad \textit{Equation 31}$$

where, $\bar{A}$ represents the ratio between the normalised moment and the normalised horizontal force at the base. This factor $\bar{A}$ tends to be constant at large deformations/rotations. A first straightforward approach is to find a trend in the value given by the ratio M_B / H_B. By using the same logic like the one used for the horizontal force at the base, some fitting parameters were tested in order to get a relationship between the moment, the force and some geometric property of the pile. If a pseudo-uniform stress distribution is assumed at the pile base with a pivot located in the middle of the cross-section, the following dimensionless parameter is defined in which the residual moments, M_{Bres}, and forces, H_{Bres}, are included:

$$P_{MB} = \frac{\frac{M_{Bres}}{H_{Bres}}}{\frac{D}{2}} \qquad \textit{Equation 32}$$

This parameter was plotted against the main geometric features, such as the diameter, the length and the slenderness ratio and the latter fits better as it is shown in Figure 4-12:

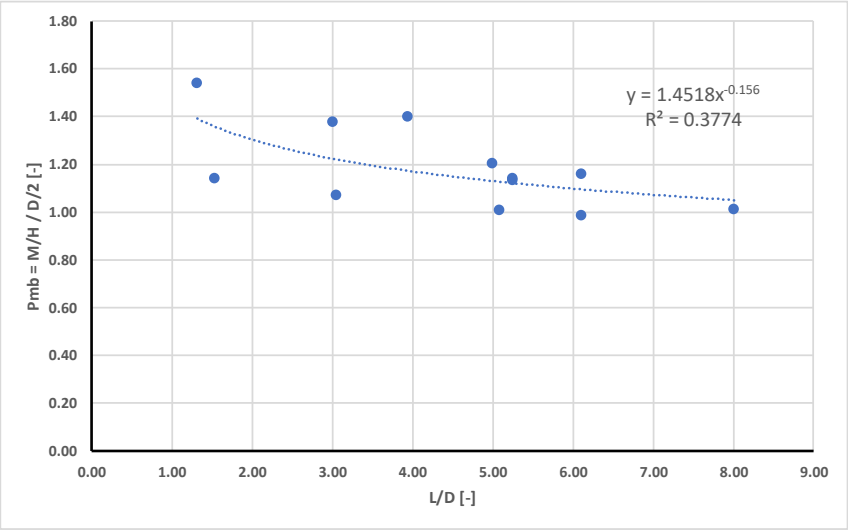

Figure 4-12 Base moment parameter

From the plot, the following relationship can be obtained:

$$\frac{\frac{M_B}{H_B}}{\frac{D}{2}} = 1.4518 \cdot \left(\frac{L}{D}\right)^{-0.156}$$

By looking at the raw data, there is an initial 'linear' portion within the curves and it ends, approximately, at the following point:

$$\psi_b/D = 0.0007 \text{ [rad/m]} \qquad \textit{Equation 33}$$

where ψ_b corresponds to the rotation at the base in radians.

By using Equation 30:

$$M_B \begin{cases} \dfrac{0.00171 \cdot q_c \cdot D \cdot \pi \cdot D^2}{\left(\frac{L}{D}\right)^{0.52} \cdot 4} \psi_b & if \quad \dfrac{\psi_b}{D} \leq 0.0007 \left[\dfrac{rad}{m}\right] \\ \dfrac{0.00171 \cdot q_c \cdot D \cdot \pi \cdot D^2}{\left(\frac{L}{D}\right)^{0.52} \cdot 4} & if \quad \dfrac{\psi_b}{D} > 0.0007 \left[\dfrac{rad}{m}\right] \end{cases} \qquad \textit{Equation 34}$$

The following plots (Figure 4-13 to Figure 4-17) present base moment-rotation curves for various pile geometries, predicted both with 3D FE calculations and the proposed CPT-based correlation.

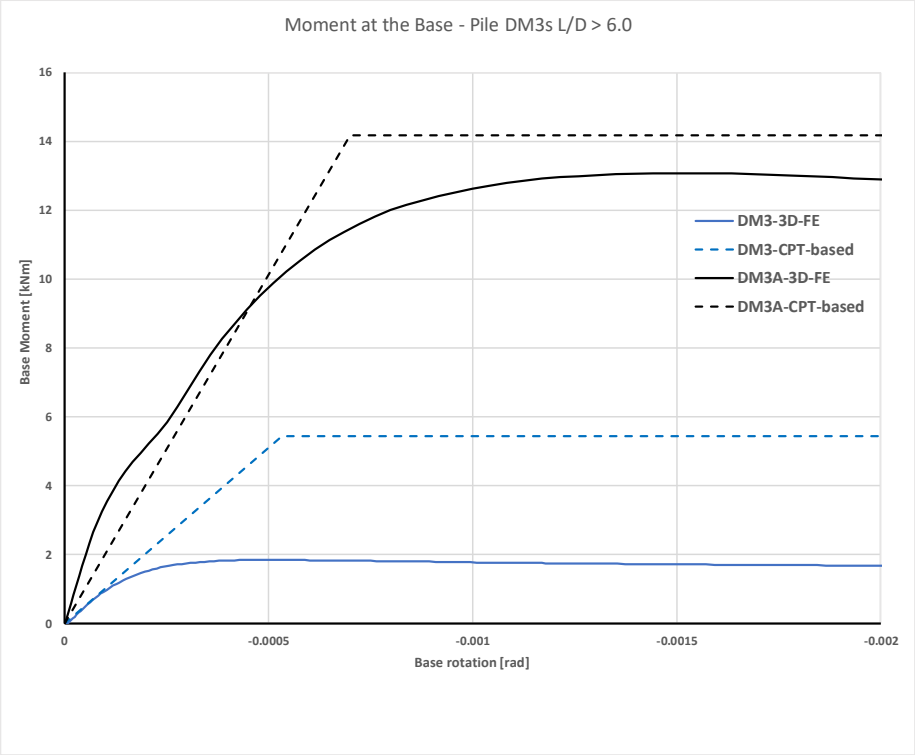

Figure 4-13 Moment at the base – Piles DM3 with L/D > 6.0

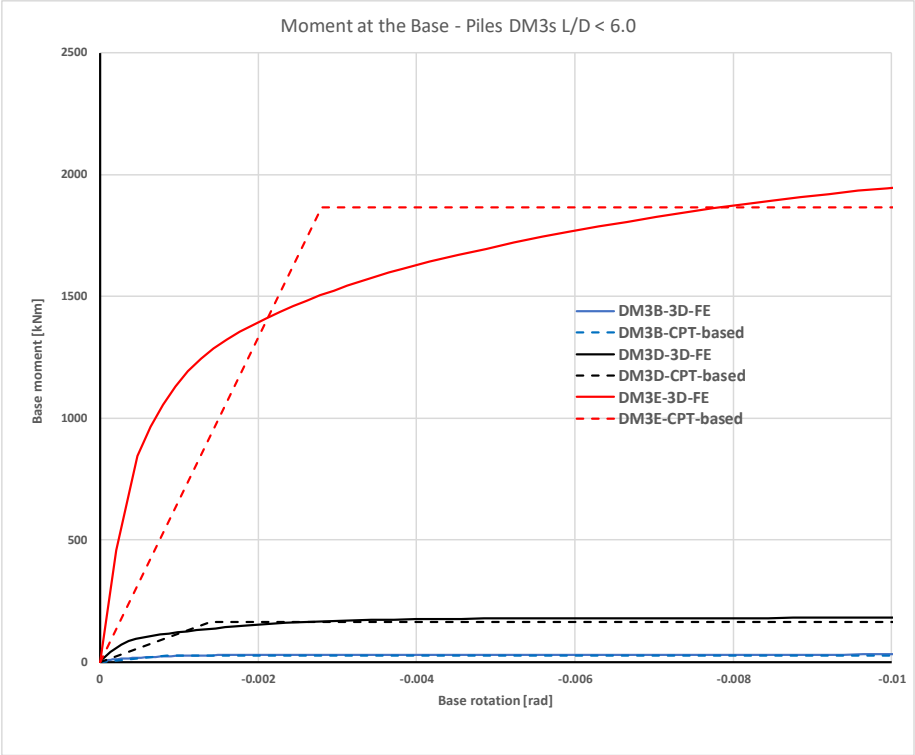

Figure 4-14 Moment at the base - Piles DM3 with L/D < 6.0

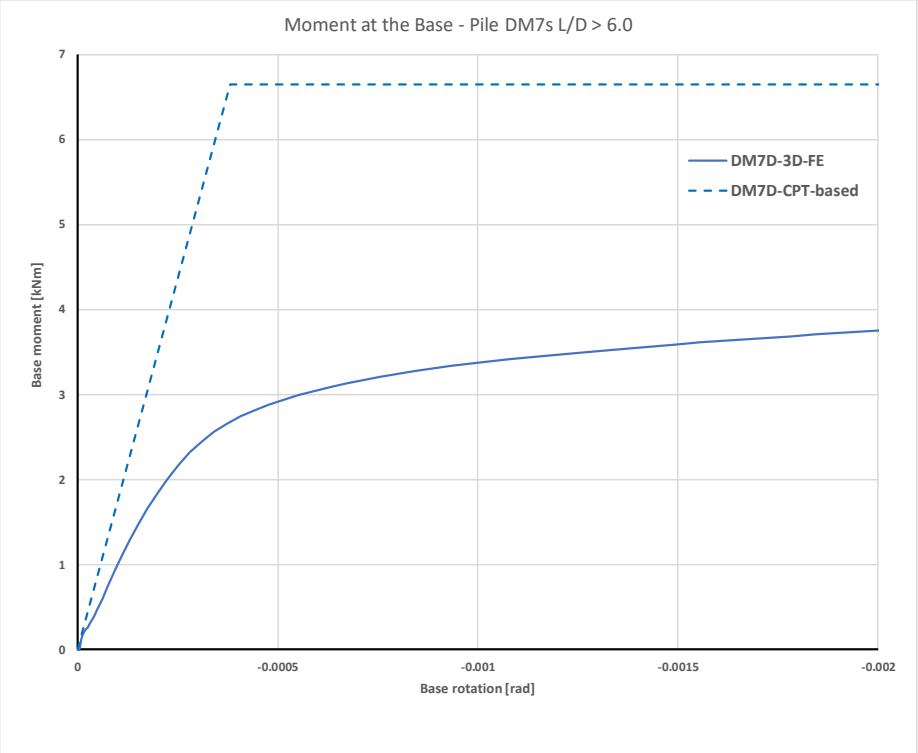

Figure 4-15 Moment at the base - Pile DM7D

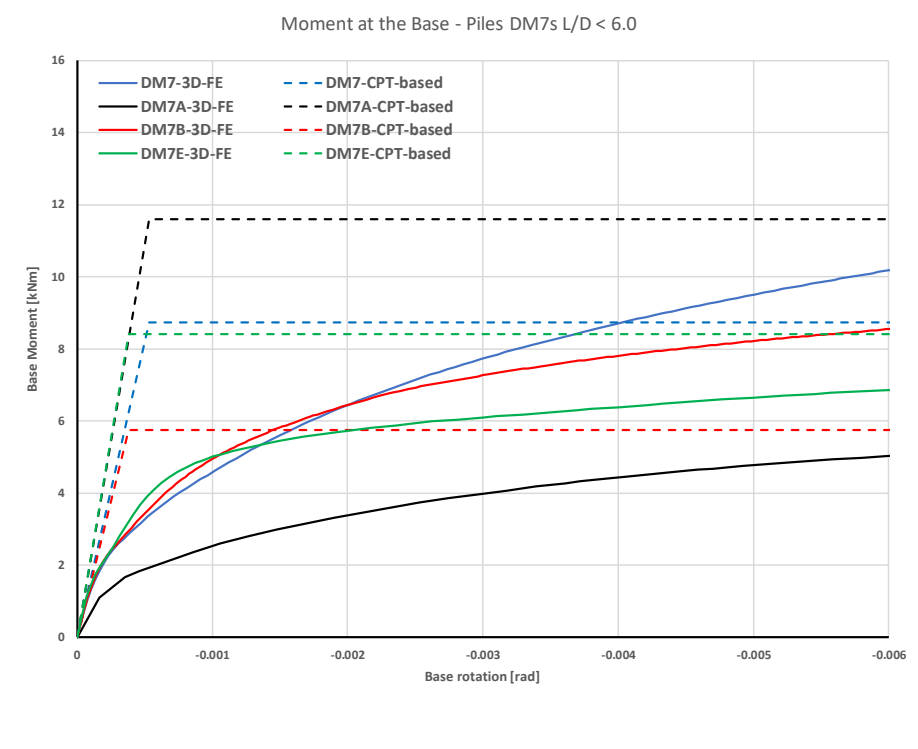

Figure 4-16 Moment at the base - Piles DM7 with L/D < 6.0

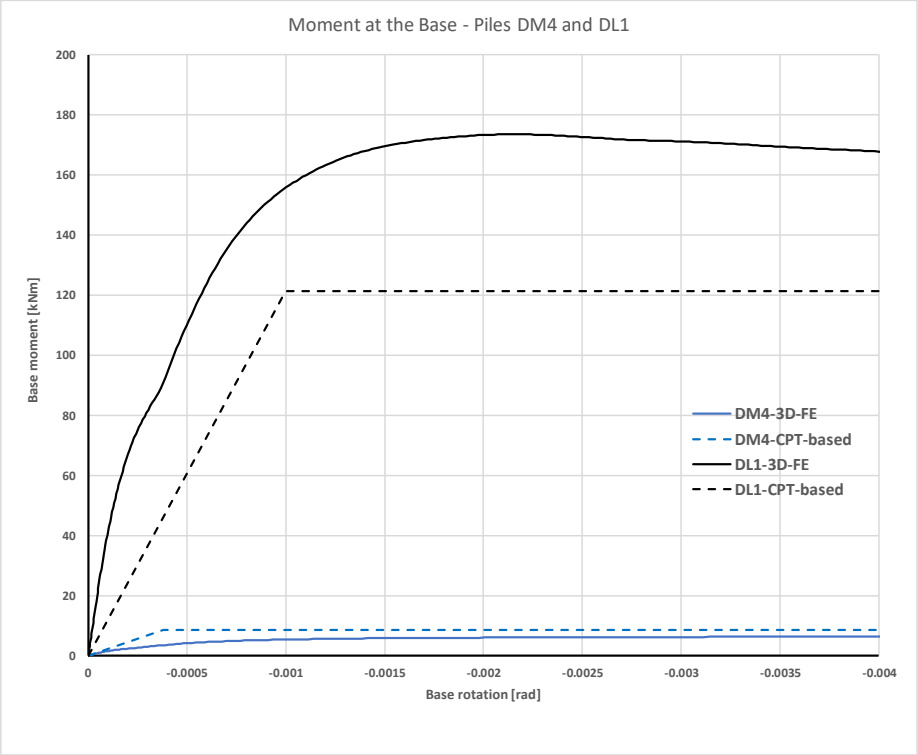

Figure 4-17 Moment at the base - Piles DM4 and DL1

By looking at the results, some conclusions can be inferred:

- There is no distinctive peak moment at the base at any of the analysed rotations.
- The maximum M_B is highly influenced by the diameter in a positive correlation and by the slenderness ratio, L/D, in a negative correlation.
- The 'linear' portion of the curve seems to embrace a smaller part than in the horizontal force versus horizontal displacement relationship. The moment-rotation curve is mostly governed by a non-linear behaviour.

4.4. P-y curves

Additionally to the base force and moments generated by the lateral displacement and rotation at the base of the pile, two reactions act along the pile shaft. The relationship between the lateral displacement and the lateral load along the pile shaft is defined by the $p - y$ method which has been widely investigated. Since the CPT is largely used worldwide, several $p - y$ formulations are based on the results of the tip resistance of the cone. As it was previously mentioned, Foursoff (2018) includes a list of five different CPT-based methods which predict the pile lateral force as a function of the lateral displacement. These methods were proposed by Novello (1999), Dyson & Randolph (2001), Suryasentana & Lehane (2014 and 2016) and Li, Igoe & Gavin (2014). All formulations were obtained by different procedures, such as CPT result analyses, finite element models, cavity expansion tests and centrifuge tests.

The lateral load is calculated by including the tip resistance of the cone, q_c, the effective soil unit weight, γ', the pile diameter, D and the depth, z. Suryasentana & Lehane updated the method proposed in 2014 by including a first linear portion that depends on the maximum shear modulus, G_{max} and a second portion with an exponential form that includes also the effective and total vertical stresses and the water pressure.

All the validation cases are mostly for piles with L/D ratios greater than 5 and therefore out of the scope of this thesis. However, this research considers that the underestimation of the lateral capacity of rigid piles is based on the fact that the other 3 soil reaction components are not considered in the analysis and therefore the CPT-based formulations to determine the $p - y$ component are assumed as correct.

For the purpose of this research, the relationship proposed by Dyson & Randolph (2001) is chosen to be the one to represent the correlation between the lateral load and displacement of the pile. The horizontal load-displacement springs were calculated via the four relationships detailed in subchapter 2.2.2. and used as input in the MATLAB routine (explained in detail in the next chapter) in order to predict the lateral response of the long slender piles (L/D = 20 and L/D = 30) in which the horizontal load-displacement reactions predominate. Later, this response was compared to the response obtained from the 3D FE analyses and the responses obtained by using the Dyson & Randolph (2001) represent better the results obtained from the 3D FE analyses. The CPT-based formulation is:

$$p = 2.84 \cdot D \cdot (\gamma' \cdot D) \left(\frac{q_c}{\gamma' \cdot D}\right)^{0.72} \left(\frac{y}{D}\right)^{0.64}$$

where:

p	=	lateral load per length unit
D	=	pile diameter
γ'	=	soil effective unit weight
q_c	=	CPT cone tip resistance
y	=	lateral displacement

Generally speaking, even though the general lateral response of the pile seems to be close to the behaviour obtained from the 3D FE analysis, a perfect match between the $p - y$ curves given by the 3D analysis and the CPT-based formulations is not expected due to the following reasons:

- $P - y$ curves are not a physical phenomenon, but a useful construction: the stress-deformation curve of an idealised nonlinear spring that substitutes a slice of soil in your model (Lahoz, 2019);
- Springs are defined as independent and therefore there is no 1-to-1 relationship between the shape of the curves and the global behaviour of the monopile, which is seen and assessed at the end (Lahoz, 2019);

- PLAXIS calculates the soil reaction curves, including the $p - y$ curves, by integrating stresses and displacements at the nodes and stress points of each slice along the monopile shell; CPT-based formulations are an idealisation of this equilibrium;
- CPT-based methods are intended to describe the behaviour of medium to long piles and this research is focused on short-rigid piles;
- Close to the rotation point, displacements are close to zero and therefore the CPT-based formulations do not show good agreement with the 3D force equilibrium.

Note that if the comparison is made slide by slide the differences are even larger. Figure 4-18 shows the $p - y$ curves given by the 3D FEM and four of the CPT-based formulations detailed by Foursoff (2018) for the pile DM3. The slices are determined by the FE software and are detailed in Table 4-2.

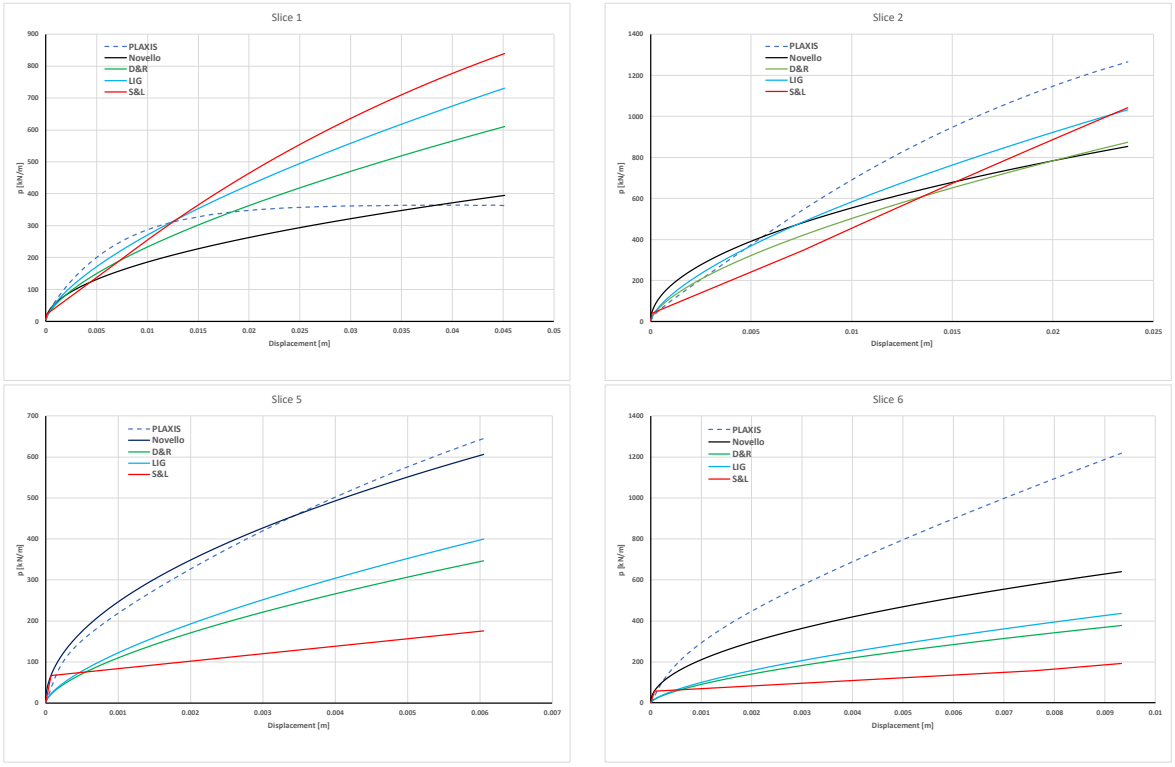

Figure 4-18 p-y curves comparison between 3D FEM and CPT-based methods – pile DM3

For pile DM7, the pile is subdivided into two slices: from 0 m to 1.145 m and from 1.145 m to 2.9 m. The results are shown in Figure 4-19.

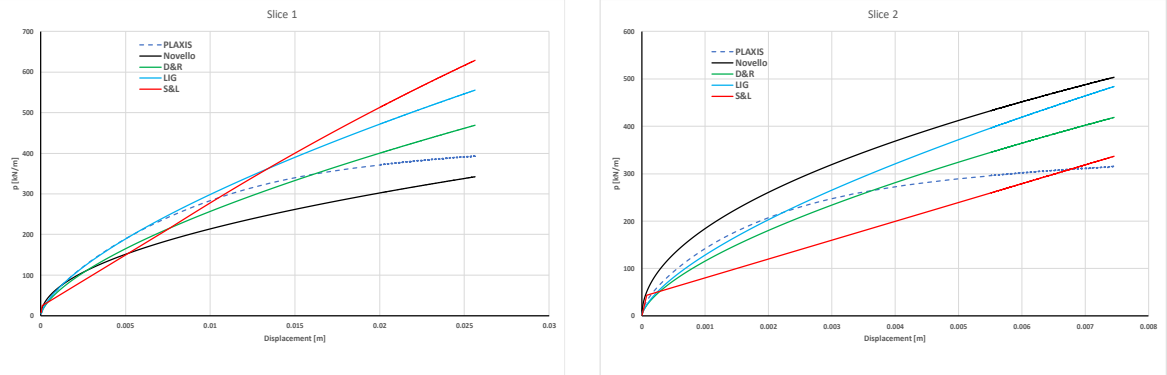

Figure 4-19 p-y curves comparison between 3D FEM and CPT-based methods - pile DM7

The dashed line represents the 3D FEM result. In the case of pile DM3, slices 3 and 4 were not included in the Figure due to the fact that displacements were too small. The formulation proposed by Novello (1999) seems to fit better the curves, however, a mismatch is noticed especially at large deformations for pile DM3. In the case of pile DM7, CPT-based methods fit better the curve given by the FE analysis.

4.5. Moment along the shaft, m – ψ (1st approach)

By using the same approach as defined for the moment at the base, it is intended to find a relation between the $p - y$ curves and the $m - \psi$, which represents the moments produced by the shear stresses at the shaft caused by pile rotation. According to Table 2-7 taken from the document PISA #8 (2018), the following relationship can be derived for the moment m:

$$m = \frac{\bar{B}}{\sigma'_v} p^2 \qquad \textit{Equation 35}$$

where $\bar{B}$ represents the ratio between the normalised moment m and the normalised force p (value that tends to be constant at large deformations), σ'_v is the effective initial vertical stress and p the horizontal load.

A first approach is to find a relation between m and p. Figure 4-20 and Figure 4-21 show the value of m/p at every calculation step of the FE analysis for piles DM3 and DM7 in the case of calculating the horizontal load p with the Dyson and Randolph (DR) formulation.

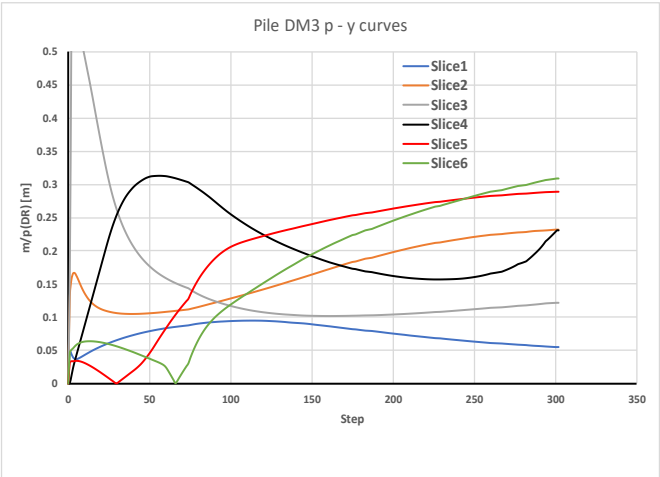

Figure 4-20 m/p - pile DM3

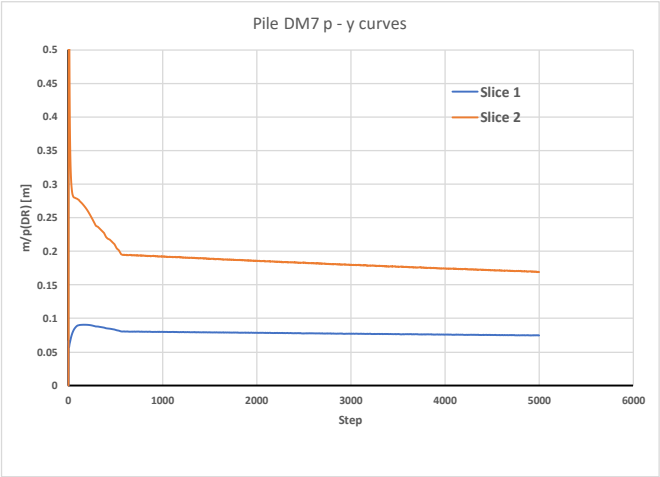

Figure 4-21 m/p - pile DM7

Both plots show the same trend: the deeper the slice (by considering slice 1 the first from the top), the higher *m/p* value. Due to this, normalisation by the effective vertical stress is applied to the *m/p* and the results are shown in Figure 4-22 and Figure 4-23.

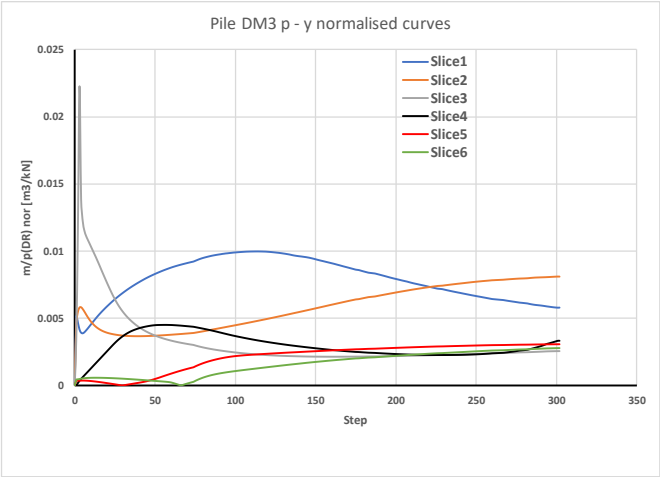

Figure 4-22 m/p normalised - pile DM3

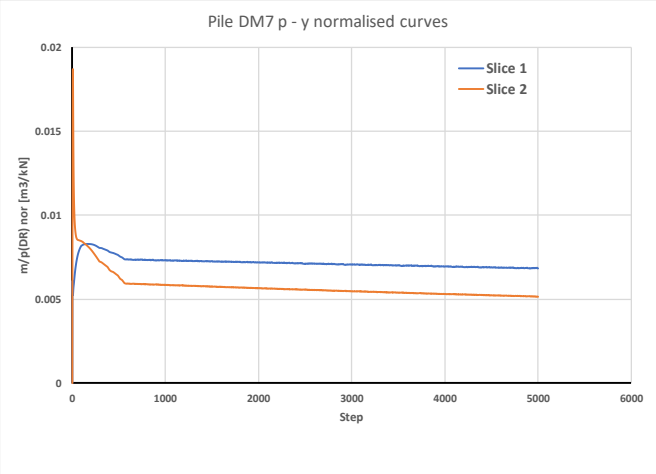

Figure 4-23 m/p normalised - pile DM7

The same process is performed in each of the analysed piles and the following fact can be noticed: at large rotations, all the slices tend to the same value of the parameter $m/(p\sigma'_v)$. By analysing this parameter against different geometric features, a fairly good fit can be found with the slenderness ratio. Figure 4-24 presents this.

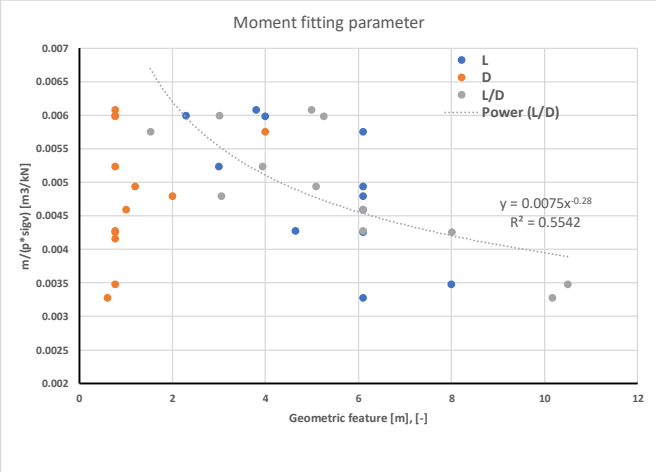

Figure 4-24 Relation between the m parameter and several geometric features

By considering the trendline, the following formulation can be defined in order to calculate the moment m:

$$m = 0.0075 \cdot p \cdot \sigma'_v \cdot \left(\frac{L}{D}\right)^{-0.28}$$ *Equation 36*

In order to keep the formulation dimensionally consistent, the factor 0.0075 has units of [m^3/kN], p of [kN/m], σ'_v of [kN/m^2] and m of [kNm/m]. By applying this formulation, a comparison between the values of m given by the 3D FE analysis and the ones obtained via this formulation for piles DM3 and DM7 is shown in Figure 4-25 and Figure 4-26.

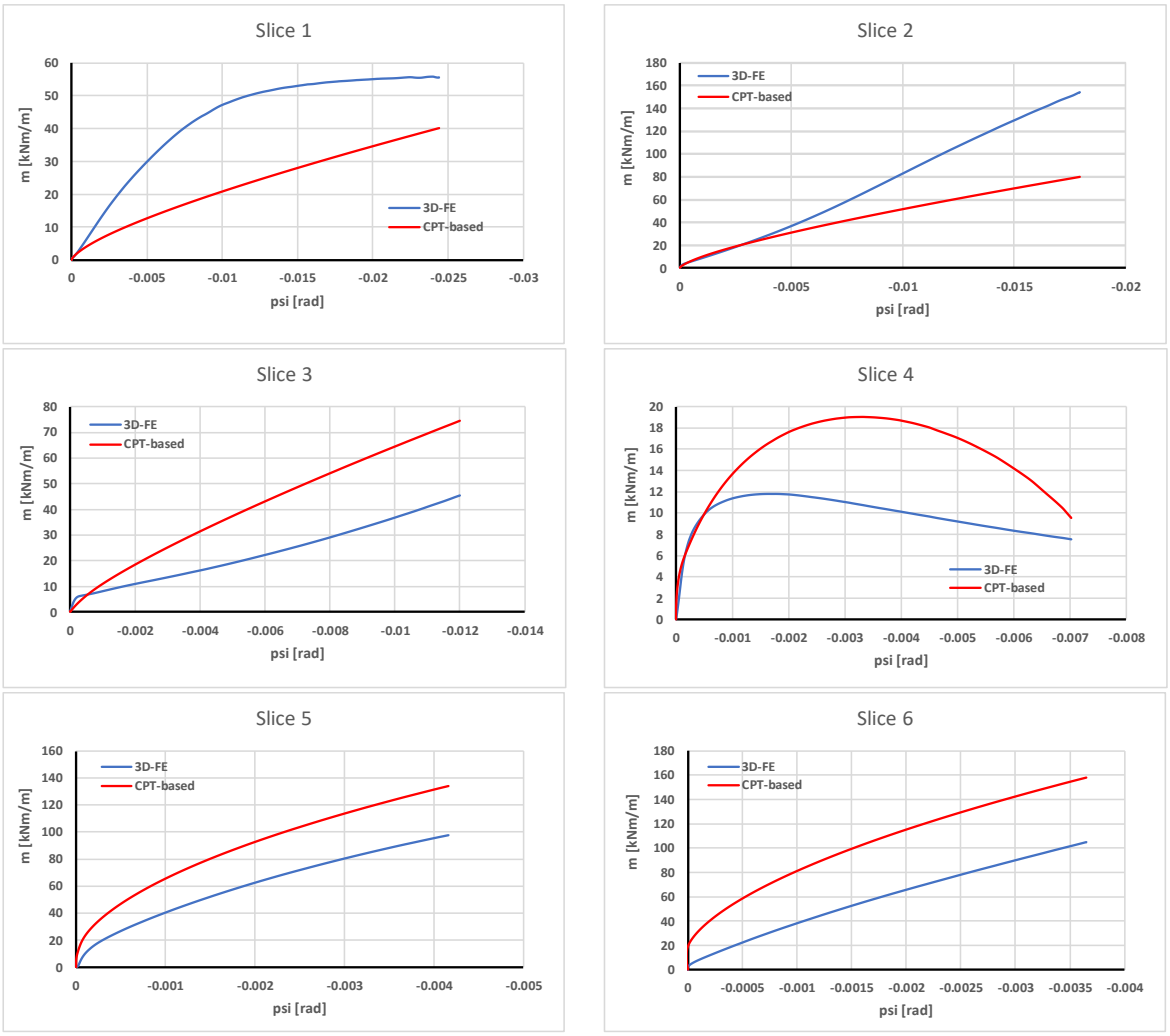

Figure 4-25 Moment-rotation curves along the pile shaft, as predicted from 3D FE analyses and from CPT-based correlation - pile DM3

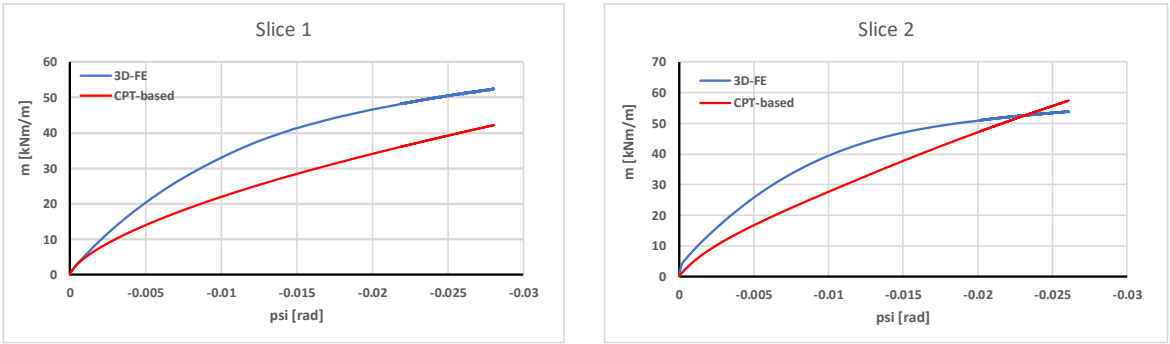

Figure 4-26 Moment-rotation curves along the pile shaft, as predicted from 3D FE analyses and from CPT-based correlation – pile DM7

As in the case of the $p - y$ curves, a mismatch is noticed at every slice in both piles. However, this can be attributed to the same reasons as stated above for the $p - y$ curves.

4.6. Moment along the shaft, m – ψ (2nd approach)

The inclusion of a non-dimensionless constant in the proposed Equation 36 generates some "noise" in the formulation. The formulation detailed in Equation 35 fits quite well in case of having both, *p* and *m* extracted from the same source, in this case, the 3D FE analysis. However, since the horizontal load *p* is obtained by using a CPT-based formulation, some distortion is added to the results. Due to this, an approach, similar to the one utilised for the pile base moment, is also proposed for obtaining the moment along the pile shaft. If it is assumed that the horizontal load *p* acts in a normal direction with respect to the pile shaft and the moment *m* is generated due to the shear stresses along the pile, a frictional relationship can be obtained. Figure 4-27 shows the horizontal displacement and the rotation of the pile shaft together with the horizontal load and the shear forces.

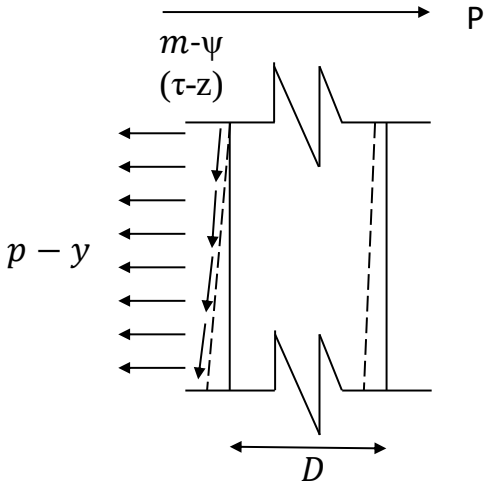

Figure 4-27 Relation between normal and tangential forces along the pile shaft

By assuming a pseudo-uniform distribution of the stresses along the cross-section, it is reasonable to propose that the tangential force, *m (τ)*, depends on the horizontal (normal) force *p*, the interface friction angle, δ (calculated as 2/3 of the soil friction angle) and the pile diameter, *D*. As a first approach the following fitting parameter can be defined:

$$P_{\tau z} = p \cdot D \cdot \tan(\delta) \qquad \textit{Equation 37}$$

Figure 4-28 shows the ratio between the moment, *m*, obtained directly from PLAXIS 3D and the fitting parameter, $P_{\tau z}$. It is noticed that this ratio shows some trend with respect to the slenderness ratio, *L/D* and the length, *L*. By analysing both geometric properties, the best fit is given by the slenderness ratio according to the power trendline included in Figure 4-28. The following formulation is proposed to calculate the moments along the pile shaft:

$$m = 0.07 \cdot p \cdot D \cdot \tan(\delta) \cdot \left(\frac{L}{D}\right)^{0.7} \qquad \textit{Equation 38}$$

Moment-rotation curves along the pile shaft, as predicted from 3D FE analyses and from the above correlation are presented in Figure 4-29 and Figure 4-30.

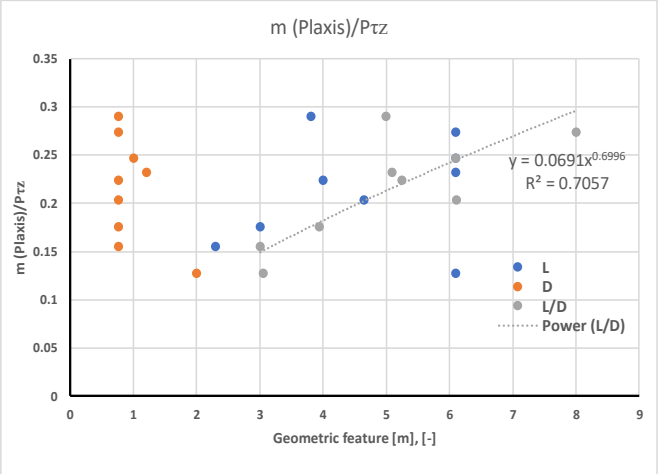

Figure 4-28 Moment m (PLAXIS 3D) and fitting parameter Ptz ratio

The results extracted from the 3D FE analyses include the independent (displacements and rotations) and the dependent (forces and moments) values at every step of the test. To plot the moment versus the rotation of the pile section, the value of *m* was calculated considering the horizontal load *p* with the respective displacement *y* at each step and the rotation was assumed as the one at the same step as *p* and *y*.

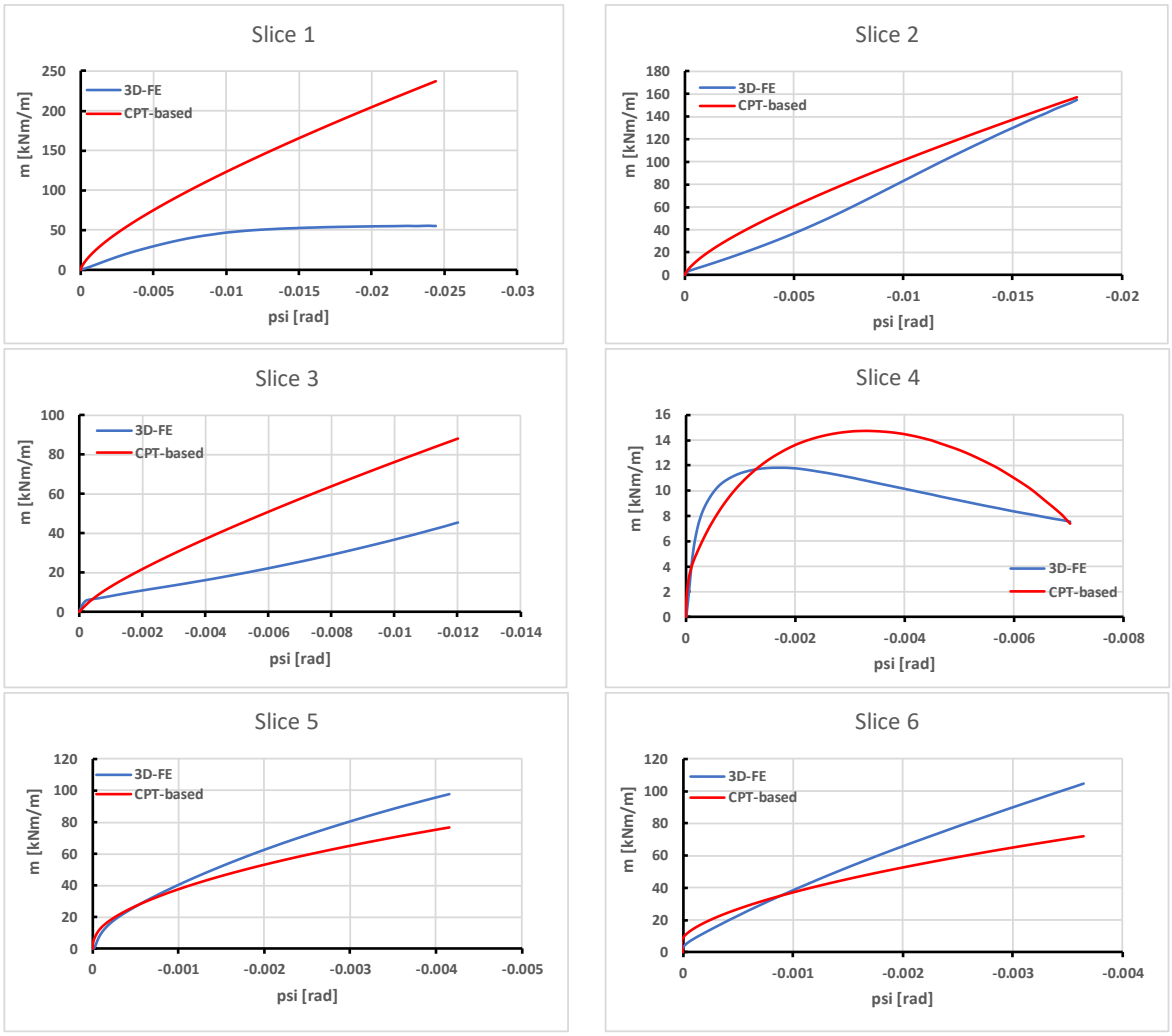

Figure 4-29 Moment along the shaft obtained from 3D-FE analysis and from the CPT-based formulation – Pile DM3

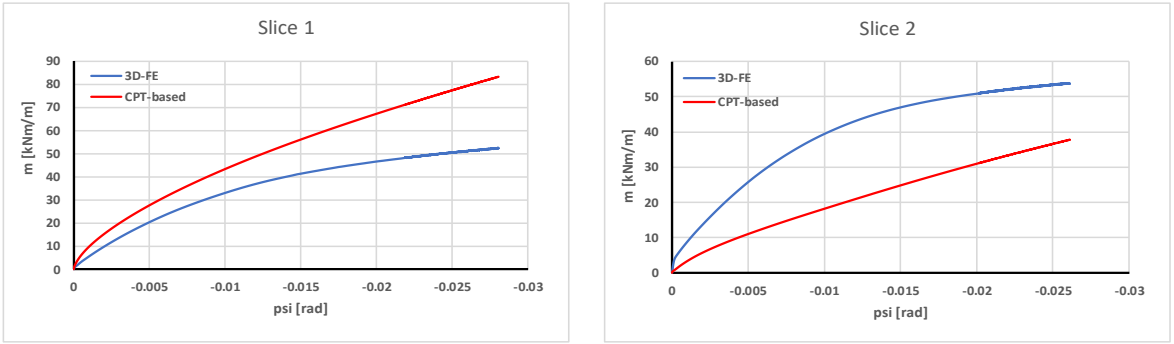

Figure 4-30 Moment along the shaft obtained from the 3D-FE analysis and from the CPT-based formulation - Pile DM7

4.7. Conclusions

Regarding both reactions at the base, horizontal force and moment, a bi-linear relation is proposed due to the simplicity of implementing such type of formulation. Both reactions seem to be hyperbolic shaped curves, however, as a first approach, it is believed that a very complex formulation will not substantially improve the resulting general monopile response. Besides,

the achieved shape of the proposed curves represents both branches of the raw reactions obtained from the 3D analysis: a first linear part and a flat part (plateau). The horizontal force at the base presents a peak in the case of piles with L/D > 5 and then a reduction in the force until a constant value is reached. At small load stages, even flexible piles behave as rigid due to the magnitude of the force. Then, when the load is larger, a flexible behaviour is noticed with a shape as it is shown in Figure 2-7. This first 'rigid behaviour' stage is consistent with the level of deformation until the development of the peak to be followed, later, by the more flexible behaviour which might be the reason to explain the reduction of the maximum capacity to a final constant value.

In general, moments at the base do not show a distinctive peak and the maximum reaction is equal to the residual one noticed at large values of the base rotation.

After testing the performance of the four CPT-based methods to calculate the $p - y$ reaction in two long piles, the formulation proposed by Dyson & Randolph (2001) fits better than the others for this type of soil at the Dunkirk site. Even though the analysis and comparison of results on individual monopile slices showed noticeable differences not only for this but for all the analysed methods, the comparison between the 3D FE and the CPT-based general lateral behaviour showed good agreement for this formulation.

Unlike the reactions at the base, a direct relationship between the normal horizontal load (and displacement) and the shear-vertical load (and rotations) cannot be formulated by manipulating the formula included in Table 2-7. For that reason, by assuming a simple relation between a normal and a frictional force, a relationship can be found in order to relate the CPT-based horizontal load p and the shear moment m that includes a friction factor and the pile diameter. When this formulation is implemented and compared with the moments given by the 3D FE analysis, the results are similar to the ones obtained by the formulation proposed in the first approach (subchapter 4.5).

It was assumed that the horizontal load p already included the effects of the slenderness or the magnitude of the pile diameter and length and the value and therefore dependency on any of the geometric features was not necessary. However, as it is shown Figure 4-28, a slight dependency on the slenderness ratio and on the length is noticed. The proposed formulation infers that for very flexible piles, the moment along the shaft reaches very high values. However, this is countered by the very small values of the horizontal load p. A more detailed analysis of this situation is necessary by, for instance, adding more data to the database.

5. General Lateral Response

By using the CPT-based proposed formulation for each of the four soil reactions (including the $p - y$ curves by Dyson & Randolph), the structural system of the monopile is solved by means of MATLAB in order to obtain the displacement and rotations of the analysed piles. In this chapter, a comparison among the actual data (when available), results from the 3D analysis and from the proposed CPT-based method is shown.

5.1. Introduction

In Chapter 4 the soil reaction curves were obtained by proposing different CPT-based expressions to be used. In this chapter, a MATLAB code is used in order to manually input those formulations and to obtain the lateral response of the monopile in terms of lateral deformation and rotation. Results from the pile load tests, PLAXIS 3D analyses and the MATLAB routine are compared in order to check the suitability of the formulations and to validate the proposed method. In this chapter, plots with the responses are included. The numerical data can be found in Appendix II.

5.2. MATLAB routine

The MATLAB routine was provided by Professor David Igoe who is Assistant Professor at Trinity College Dublin and part of the PISA project. The routine solves the structural system of the pile by adding the four soil reactions as springs inside the total stiffness matrix of the structure. The results are given in terms of displacements and rotations of the pile at different depths. A summary of the routine is explained in the following steps:

- Input of the structural properties of the pile: diameter, thickness, elasticity modulus, unit weight and yield force (only if structural checks are necessary);
- Input of the horizontal force and the moment at the pile head;
- Division of the pile in nodes and sections: by default the length of each section of the pile is 1.0 meter and the number of nodes is the number of sections plus one;
- Calculation of geometric properties of the pile: area and inertia;
- Definition of the number of reactions to include in the calculation: the pile response can be obtained by adding all the for reactions or only some of them;
- Creation of the basic stiffness matrix of the pile elements by adding the terms related to the elastic and geometric properties of the structure. The size of the square matrix is two times the number of nodes;
- Definition of the location of the nodes and reset of the displacements and rotations to zero;
- Definition of each of the soil reaction curves as springs;
- Addition of the springs to the general stiffness matrix: translational and rotational;

- Definition of the force matrix: inclusion of the moment and the force;
- Resolution of the matrix equation: *deflections = total stiffness matrix / force matrix;*
- Rotations calculated as the difference between the deflections divided by the distance between the points;
- Calculation of displacements and rotations along the pile.

In order to assure the match between the results obtained from the PLAXIS 3D analysis and the MATLAB routine, two preliminary checks were performed: i) a different section length was used in order to check the influence of a smaller discretisation of the pile. To do this, a random pile of 4.0 m length and 1.0 m diameter was tested embedded in a simulated sand profile; ii) springs taken directly from MoDeTo and inserted into the routine to check if the 1D model created from the 3D model fits the MATLAB routine which solves the beam. Results from pile DM3 was used to prove this. Figure 5-1 and Figure 5-2 show the result of both tests in terms of the lateral response at the mudline versus the induced load on the pile.

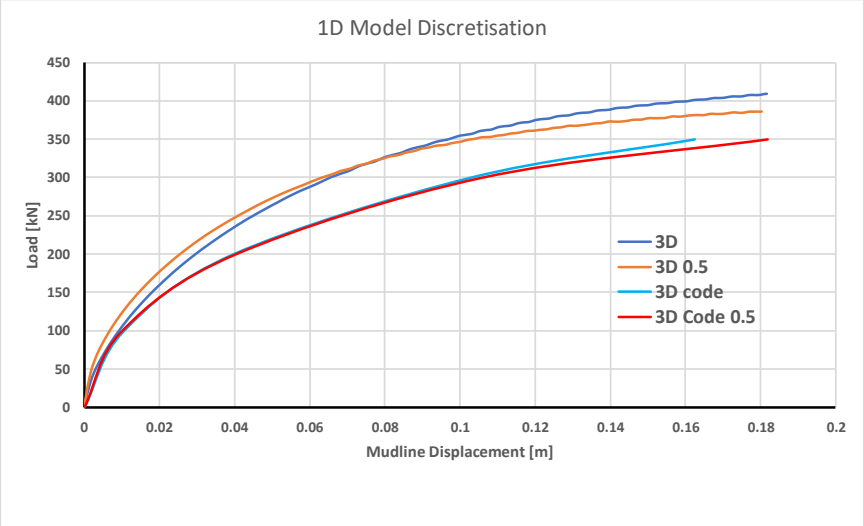

Figure 5-1 Structural discretisation of the pile

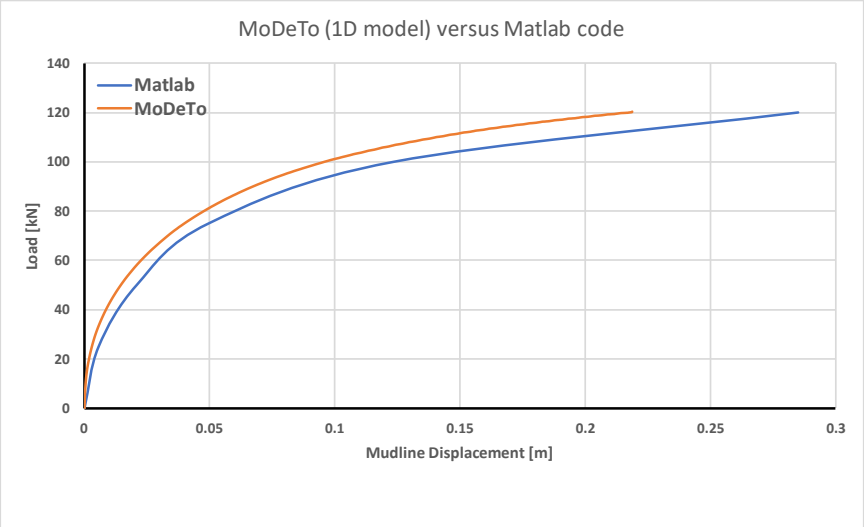

Figure 5-2 MoDeTo - MATLAB comparison

The MATLAB routine provides a fairly good agreement with the results obtained from the 3D FE analysis. Two different discretisations were compared in order to check the validity of the routine. A very small difference between the cases in which the pile is divided into slices of 1.0 m or 0.5 m is noticed. By considering the by-default case of 1.0 m per slice, the code provides good results and the process can be performed faster. A second check was performed in order to check the validity of the code if the springs extracted directly from the MoDeTo 1D simplification were inputted in the code. The MATLAB routine gives a slightly softer response at every step of the analysis, however, at the same displacement, the differences in the applied loads are less than 10%.

5.3. Pile response

5.3.1. Displacement at the mudline

In order to compare the PLT data with the response obtained from the 3D analysis and the one obtained from the MATLAB code with the CPT-based springs, the first variable to check is the displacement at the mudline versus the applied lateral load at the pile head. All the actual and fictional piles (see Table 4-1) were analysed. However, due to the applicability and the scope of this thesis, piles with a slenderness ratio larger than 8.0 (e.g. DM3C, DM7C) were discarded from the results, because they can be defined as flexible piles. Also, results of piles with an *L/D* smaller than 1.6 (DM3E, DM7A) are not shown since such ratios are not realistic for monopiles. To compare the 3D FE analysis with the 1D model provided by the MATLAB routine, the maximum horizontal load applied in the code is similar to the one reached in the 3D model. A third curve is also included in the plots: the response obtained from the MATLAB routine, although by including the springs extracted directly from the 3D analysis. Finally, when available, the results obtained from the pile load tests are also included. Within the plots, results are labelled as: ‘Code’, if the response is obtained from MATLAB with the CPT-based springs; ‘Code+3D’, if the response is obtained from MATLAB with the springs extracted from the 3D analysis; ‘3D’ when the response is extracted from the 3D FE analysis; and ‘PLT’ if the pile load test response is available (in the case of pile DM4, Figure 5-10, the PLT response is simplified to a discrete points). Figure 5-3 to Figure 5-10 show the lateral responses at mudline.

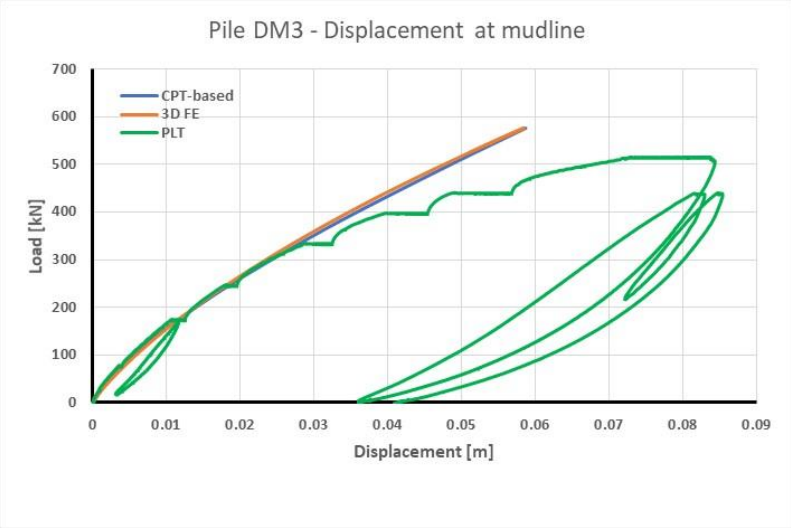

Figure 5-3 Lateral response pile DM3

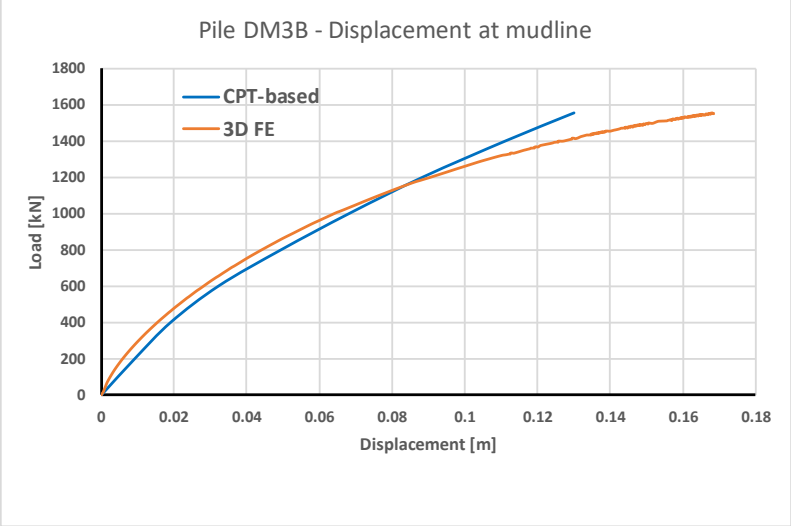

Figure 5-4 Lateral response pile DM3B

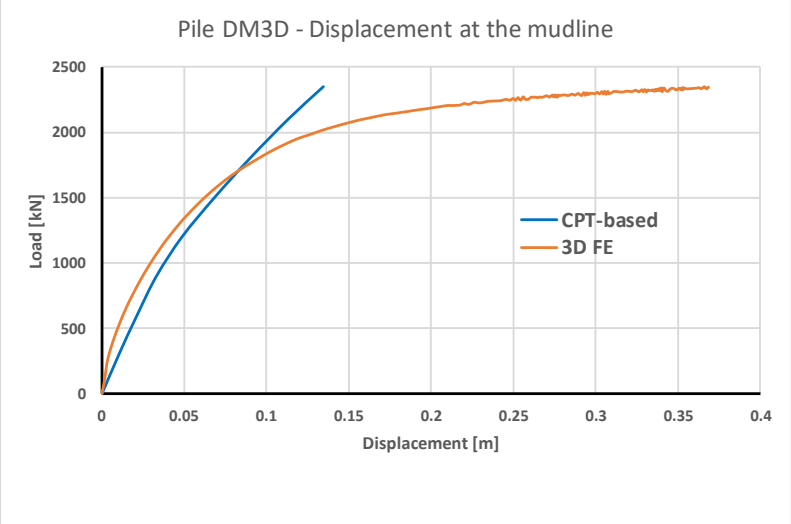

Figure 5-5 Lateral response pile DM3D

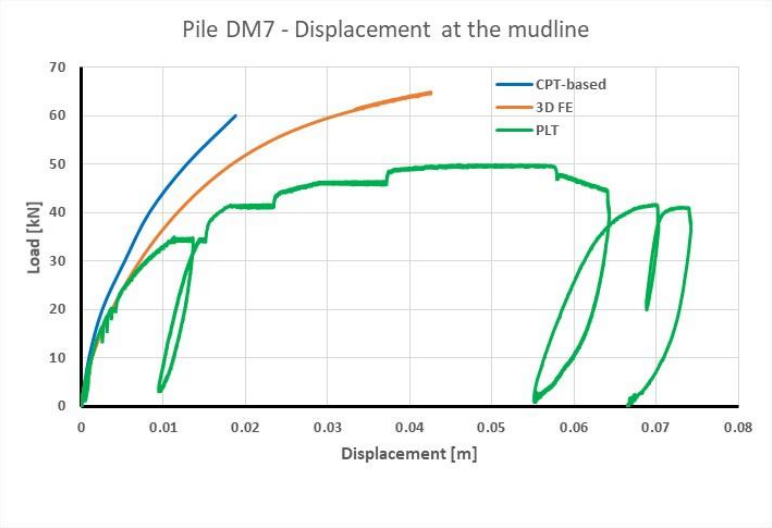

Figure 5-6 Lateral response pile DM7

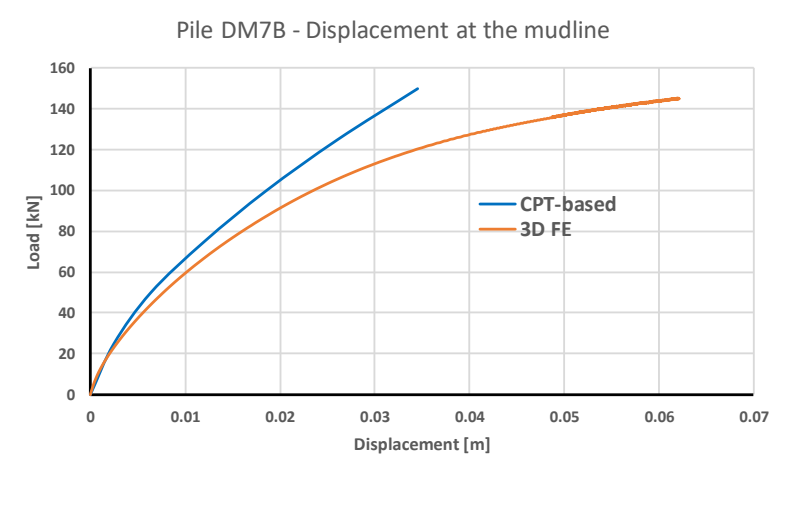

Figure 5-7 Lateral response pile DM7B

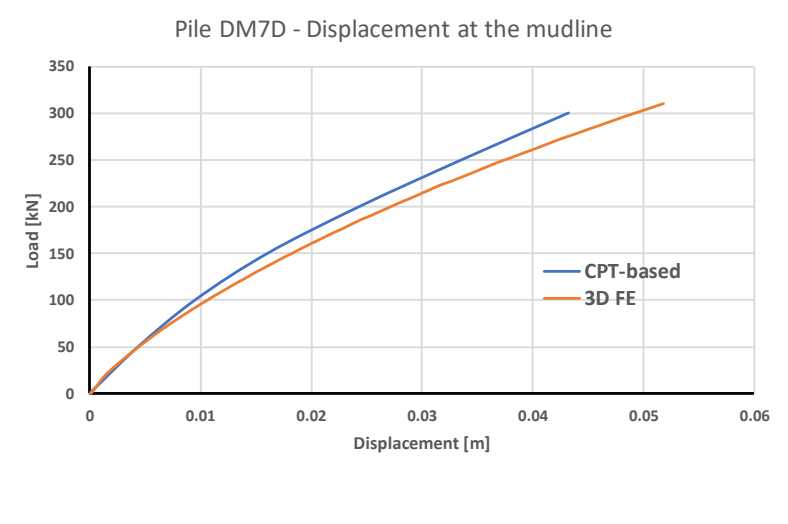

Figure 5-8 Lateral response pile DM7D

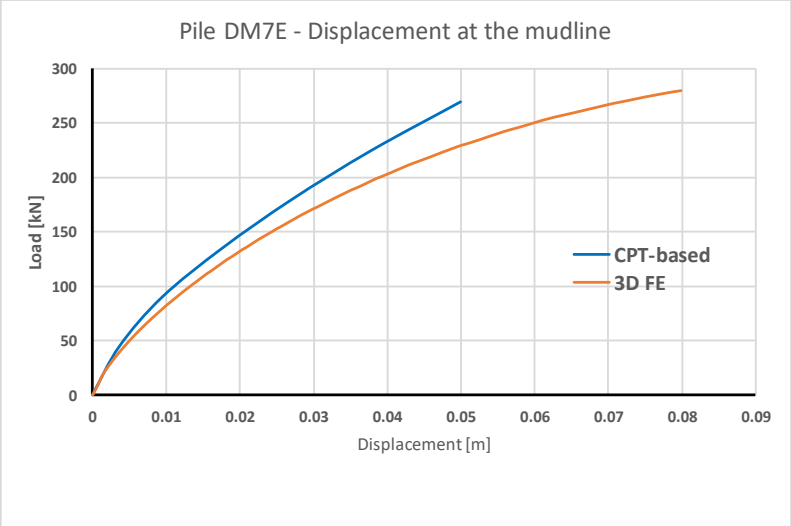

Figure 5-9 Lateral response pile DM7E

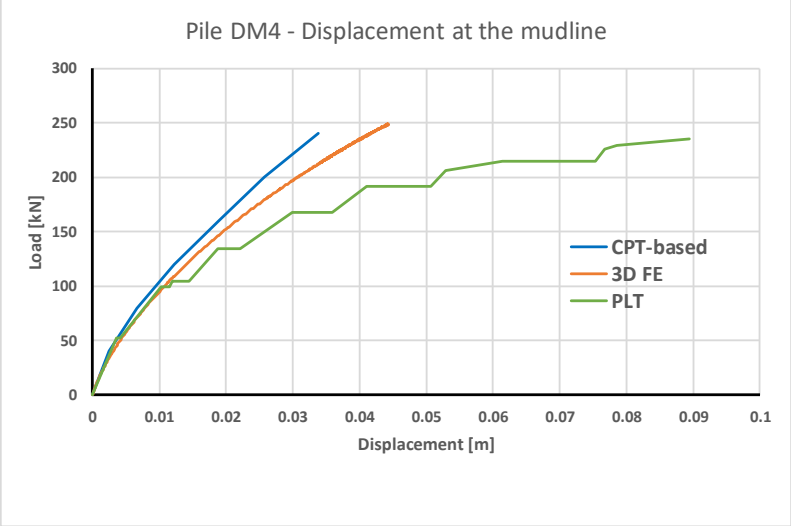

Figure 5-10 Lateral response pile DM4 (simplified PLT response)

In Appendix III the plots with the lateral response at the mudline when only the $p - y$ reaction is included and also when $p - y$ and $m - \psi$ ($\tau - z$) are included together are shown.

5.3.2. Deflection below ground level

Additionally to the displacement at the mudline, the deflection below ground level was also compared. Within the plots, data is labelled as: 'PLT-load' if the deflection is taken directly from the pile load test (when this information is available in one of the PISA reports or papers); '3D-FE-load' if the deflection is calculated from the 3D model; and 'CPT-based-load' if the deflection is taken from the code with the CPT-based springs; the load included is in [kN]. As it was mentioned in previous chapters, this research focuses more on the serviceability limit state and therefore deflections are compared only at the first load stages (until the load is about the half of the maximum load). Figure 5-11 to Figure 5-17 show the deflection below ground level for some of the analysed piles.

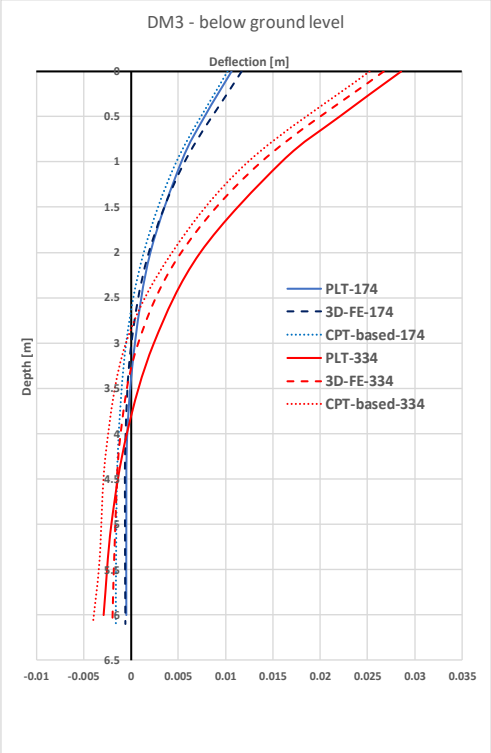

Figure 5-11 Deflection below ground level - Pile DM3

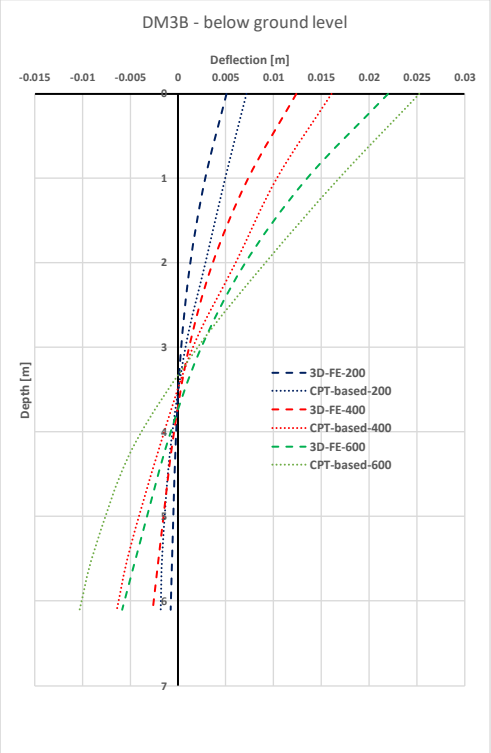

Figure 5-12 Deflection below ground level -Pile DM3B

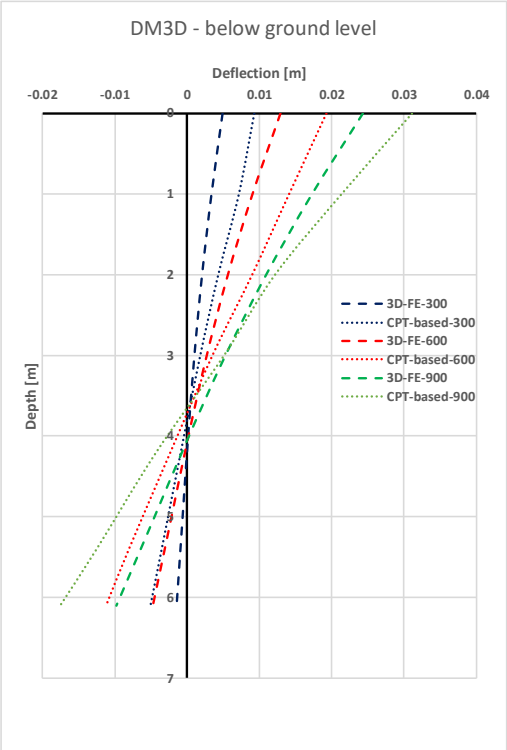

Figure 5-13 Deflection below ground level - Pile DM3D

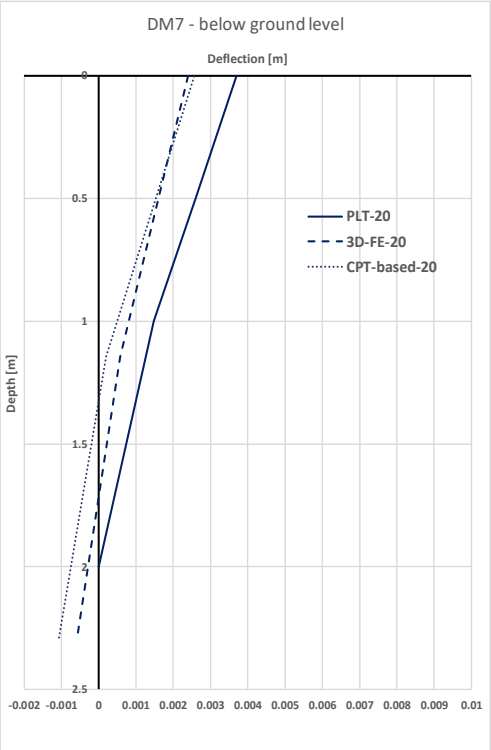

Figure 5-14 Deflection below ground level - Pile DM7

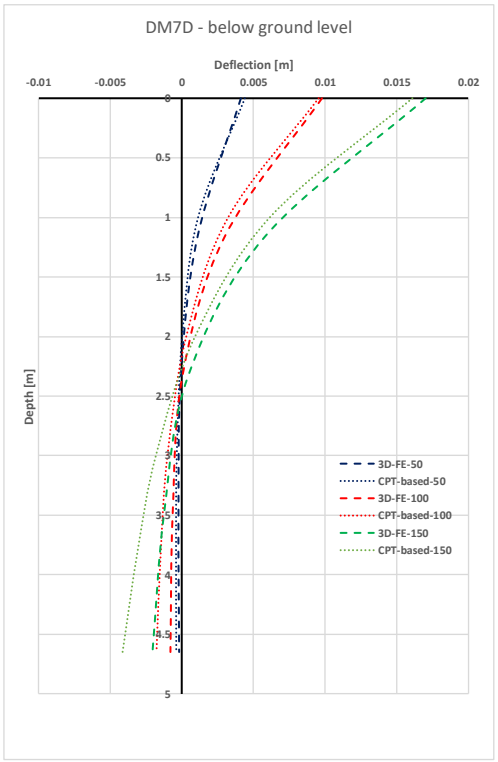

Figure 5-15 Deflection below ground level - Pile DM7D

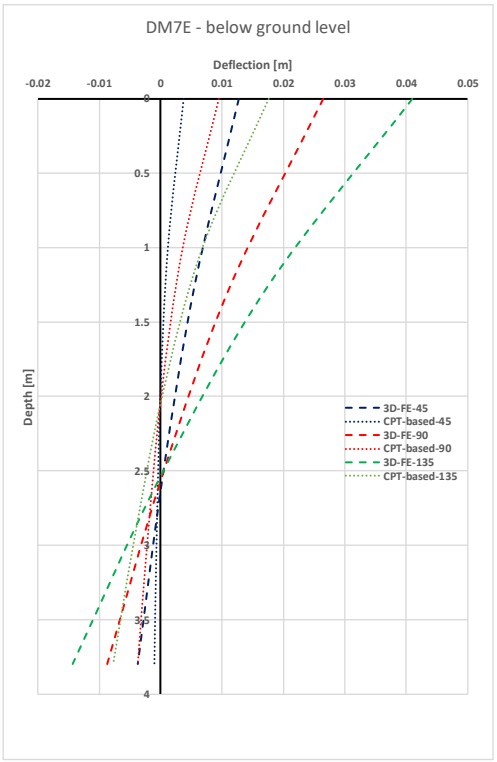

Figure 5-16 Deflection below ground level - Pile DM7E

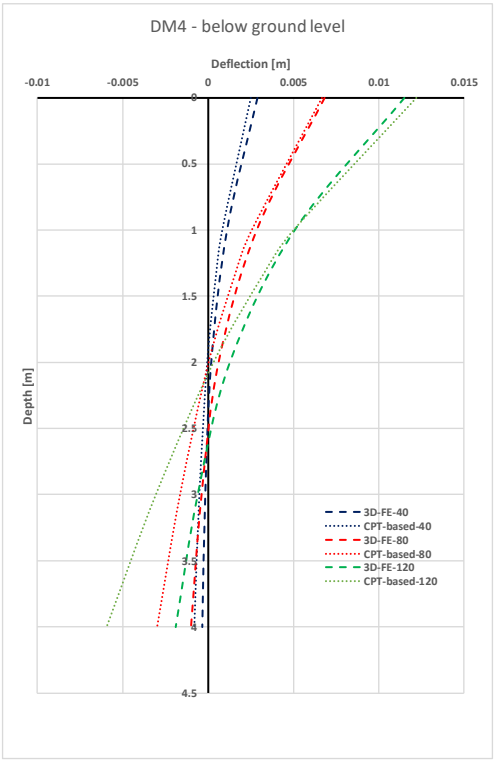

Figure 5-17 Deflection below ground level - Pile DM4

5.3.3. Rotation below ground level

The pile rotation below mudline as predicted from the CPT-based formulations are presented for various pile geometries and compared against 3D FE analyses (Figure 5-18 to Figure 5-21).

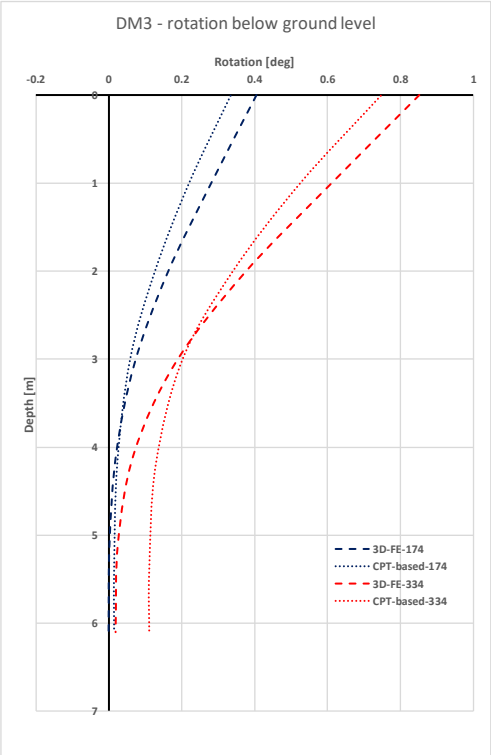

Figure 5-18 Rotation below ground level - Pile DM3

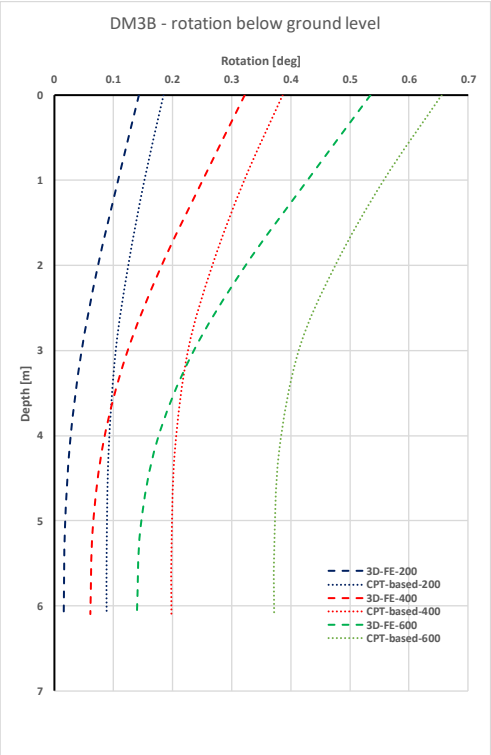

Figure 5-19 Rotation below ground level - DM3B

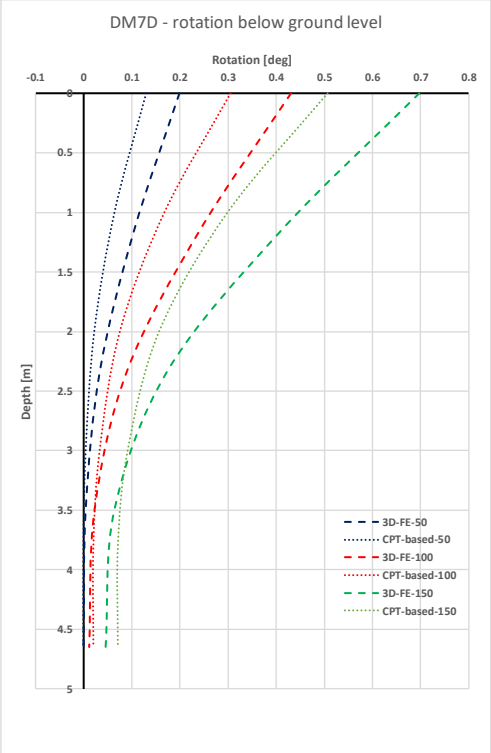

Figure 5-20 Rotation below ground level - Pile DM7D

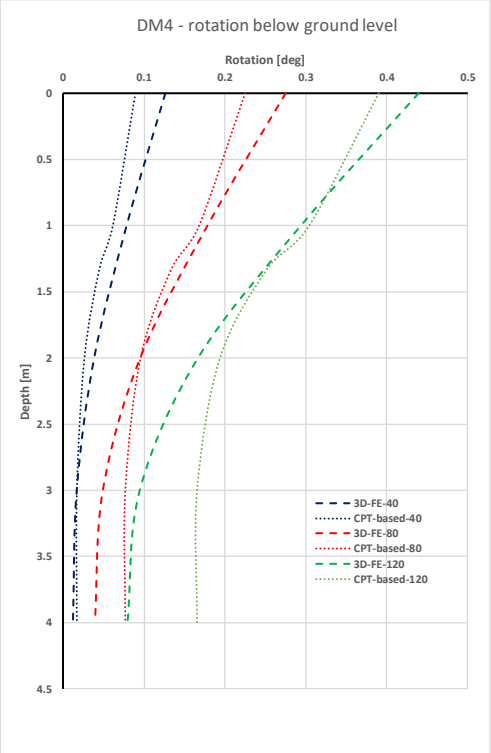

Figure 5-21 Rotation below ground level - Pile DM4

5.4. Applicability of the CPT-based method

Figure 5-3 to Figure 5-10 show the lateral response of the pile in terms of displacement at mudline versus the applied lateral load. However, it is noticeable that the response given by the CPT-based springs combined with the MATLAB routine is not always the same as the one given by the 3D FE analysis or the PLT data, especially at relatively large pile deflections. For this reason, a cut-off point is defined in order to limit the applicability of the CPT-based method to the small pile displacements regime. A point is defined as the limit in which the results of the CPT-based method, as presented in this report, should not be used. This point can be either, the point beyond which the CPT-based method cuts the 3D FE analysis (see example in Figure 5-22) or the point in which the difference between the 3D FE analysis and the CPT-based method is larger than 20% (see example in Figure 5-23).

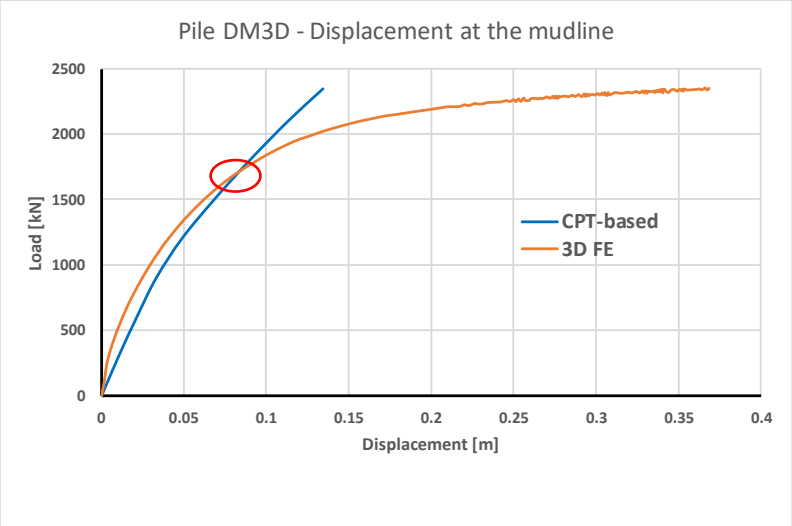

Figure 5-22 Cut-off point - Pile DM3D

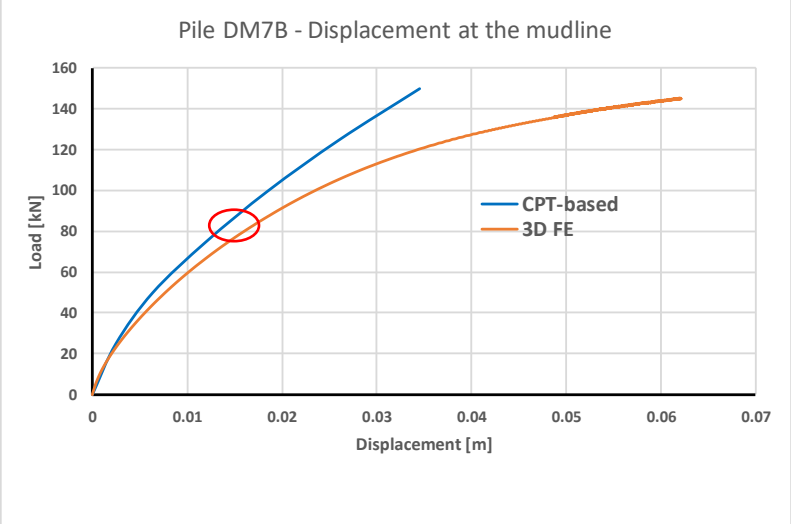

Figure 5-23 Cut-off point - Pile DM7B

Considering this, an approximate relationship between the cut-off point and the diameter of the pile can be determined as it is shown in Figure 5-24. Consequently, it is assessed that the present CPT-based method is applicable for predictions of the monopile lateral response in which the pile displacements at mudline are not larger than 2 – 3% of the pile outer diameter.

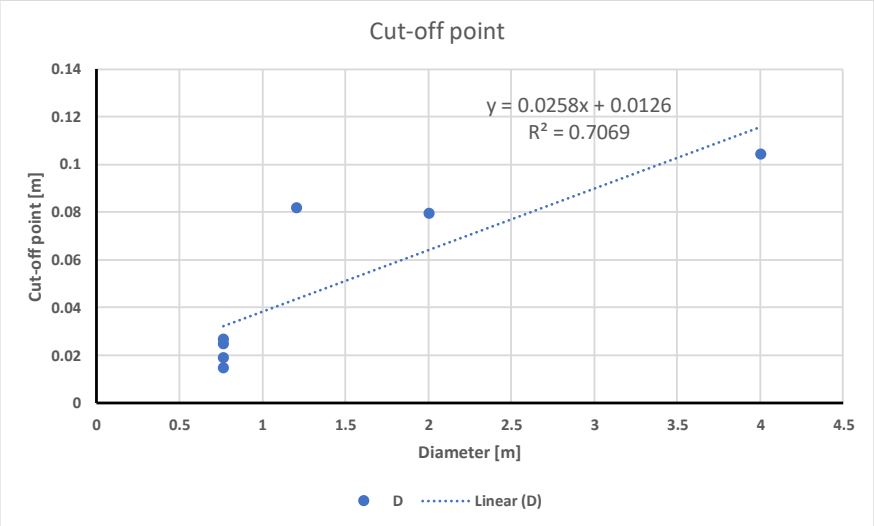

Figure 5-24 Cut-off point versus pile diameter

5.5. Conclusions

The general lateral response in terms of the displacement at the mudline versus the applied load shows a good agreement until the cut-off point which was defined in the range of 2% to 3% of the pile diameter. Some of the pile responses provided by the CPT-based method are softer than the ones given by the 3D FE analysis (and/or the pile load tests) and some of them are stiffer. The coefficients from the proposed formulations can potentially be better estimated and a better general fit may be found if more PLT data is later included and analysed. By modifying those numbers, a better general fit may be found.

In general, the lateral response of the pile is highly influenced by the $p - y$ reaction in both, the magnitude of the load-displacement relationship and the shape of the general response. At large deformations, a plateau-shaped curve is noticed by looking at the results obtained from the 3D FE analyses. On the contrary, the CPT-based $p - y$ relationship proposed by Dyson & Randolph (2001) shows a more consistently increasing load-displacement relation and, therefore, this shape also predominates in the monopile lateral response and the plateau-shaped curve is not noticed.

Similar conclusions can be inferred from the results of the pile deflection and rotation below ground level. Some of the CPT-based pile responses are softer and some are stiffer than the pile responses according to the 3D FE analyses. However, in general, the shape of the CPT-based response curves are similar than the response obtained from the 3D FE analyses.

In Appendix II and III, the pile lateral response is shown in two different cases: i) when only the $p - y$ reaction is included and ii) when the $p - y$ and $m - \psi$ reactions are included together. In the case of piles with L/D > 6.0, the $p - y$ reaction makes the largest contribution to the pile lateral response. In the case of rigid monopiles with L/D $\leq$ 6.0, the other three soil reactions become relevant and the contribution of these reactions is larger, being the moment along the

shaft, $m - \psi$, the most important. The reactions at the base, $H_B - v_b$ and $M_B - \psi_b$, contribute approximately to the 10% of the pile lateral response.

It can be seen that there is some deviation in the pile load-deflection curves between MoDeTo and the MATLAB code. This difference may be attributed to the way that the depth variation functions (which define the soil reaction curves that are used by the 1D model within MoDeTo) are defined and used by the 1D kernel, which is unknown to the author of this thesis.

Moreover, it should be stated that Kaltekis et al. (2019) have shown that the 1D MoDeTo model can, in some occasions, over-predict the monopile stiffness in comparison to the equivalent PLAXIS 3D model.

The PLTs show especially in the case of the short piles, softer response than the response of the 3D FE model and the CPT-based method. This can be partly attributed to soil disturbance effects from the pule installation process, which were not accounted for during this research.

6. Conclusions

6.1. Soil parameters

A sensitivity analysis, including 28 different 3D finite element models, was performed in order to obtain a good match between the model and the results obtained from pile load tests (PLTs). The soil properties were calculated based on different formulations proposed by several authors until a good combination of those was found. To define a good set of parameters, the displacement at the mudline at different load stages was analysed. Since this thesis is focused mostly on the serviceability limit state (SLS), more weight was assigned into having a good match at the first load stages (until around the half of the maximum load). Piles DM3, DM7 and DM4 were used as a reference to calibrate the model. In Chapter 3, it can be seen that the proposed model fulfils the requirements and that the modelled load-deflection curve at mudline shows good agreement with the respective PLT-extracted curve. Also, the deflection below ground level is presented in that chapter. As the displacement at the mudline, the model shows a good agreement with the PLT data. In this case, only a few load stages were analysed (mostly the first ones), since the model response is stiffer in later stages.

The selected soil parameters were checked against different formulations, soil test simulations and data extracted from in-situ and laboratory tests. In general, regarding the properties which have CPT-based formulations, the ones proposed by Robertson & Cabal (2015) fit better the Dunkirk sand. The limitations proposed by Brinkgreve (2010), in general, do not fulfil what it was sought in this thesis and usually predicted a much softer response. Soil test simulations together with the equations that relate the stiffnesses moduli provided good values for those parameters. The coefficient of lateral earth pressure at rest, K_0, showed a high dispersion especially at the first meters from the surface. Since the soil at the top is a fill, a constant value of 0.5 was selected as appropriate to characterise this deposit. Deeper natural layers show some degree of over-consolidation and, therefore, higher values of K_0.

An important amount of time was spent in defining the soil properties and most of the attempts were based on CPT-based formulations. Since the CPT tip resistance was used as the parameter to describe the soil reactions, it was assessed that a soil model derived by a CPT-based parametrisation process was likely to give a good approximation of the modelled pile-soil behaviour.

Some selected soil parameter values tend to be higher than expectations at the first meters. This can be explained by the partial saturation of the soil at this region since the water table was found between 4.0 and 5.4 m below the surface. It was assessed that this partial saturation may have a positive influence on the soil properties.

6.2. Soil reaction curves

Soil reaction curves were extracted directly from the 3D FEM analysis and then, a simple relationship was found in order to describe them. It was assumed that the horizontal force at the base is a frictional force and therefore it should be related to the vertical force (stress) at the base. The vertical stress at the pile base was related to the value of the tip resistance of the cone q_c. A fully plugged pile was assumed and therefore the total cross-section of the pile was considered. A bi-linear relationship was determined for the horizontal force which includes the CPT tip resistance, q_c, the pile cross-sectional area and a dependency on the slenderness ratio (L/D) (negatively correlated).

The horizontal moment at the base was related to the horizontal force and the pile diameter. Uniform stress distribution along the cross-section and a moment lever arm of half the pile diameter were considered. Similar to the horizontal force, a bi-linear relationship was defined to describe the base moment, which depends on q_c, pile cross-sectional area, the pile diameter and on L/D (negatively correlated).

Both CPT-based pile base reactions tend to overestimate the maximum value for flexible piles and slightly underestimate the maximum values for rigid piles. However, the overestimation in long piles can be disregarded since the magnitude of both base reactions is small in comparison to the other two reactions along the shaft.

The horizontal load-displacement relationship along the shaft ($p - y$) was calculated according to the formulation as proposed by Dyson & Randolph (2001). More CPT-based $p - y$ formulations were checked as well but the one by Dyson & Randolph (2001) was giving the best predictions compared to the others. Even though the slice-by-slice analysis showed a high offset between the CPT-based formulation and the 3D FE result analyses, the general response of the pile showed good agreement.

The moment generated by the shear stresses along the shaft was assumed to be related to the horizontal load, p. Similar to the base moment, this reaction was considered to be a frictional force and therefore it is dependent on the normal force, the pile-soil interface and the pile diameter. As with the $p - y$ results, the slice-by-slice comparison between the results obtained by the CPT-based formulation and the 3D analysis showed a high mismatch but the general performance is comparable. Contrary to the physics, the moment m shows a slight tendency to increase as the slenderness ratio (and the pile length) increases, however, statistically this trend is noticeable. This tendency must be checked against more data.

6.3. General and partial lateral response

With the use of MATLAB, the CPT-based springs were included in the pile stiffness matrix to get displacements and rotations of the piles. In general, the CPT- based method shows a good agreement with the PLT data (and the results from the 3D analyses) until a certain level of deformation which was defined as the cut-off point. In some piles, the 3D analysis gave a stiffer

response and in some others softer. By adding new data to this work, a better calibration of the CPT-based proposed formulations can be obtained and therefore a better fit can be found.

In general, in piles with a slenderness ratio larger than 6, the $p - y$ component represents more than 90% of the response, and the other three reactions could be disregarded for simplicity purposes. For rigid piles, the contribution from the $m - \psi$ component becomes more prominent and can represent up to 40% of the total response. In general, even for very rigid piles, the base reactions represent no more than 10% of the total response of the pile.

By analysing the deflections and rotations below ground level, a generally good agreement is noticed. Similar to the case of the displacement at the mudline, some responses are softer and some stiffer, however, with the addition of new data the proposed formulation should be better calibrated and the responses will be better represented. Deflections obtained from the CPT-based method represent in a good way the difference between a flexible and a rigid pile in which the flexible pile deflection shape shows a hinge (see Figure 5-11) and the rigid pile which looks similar to a straight line with no hinge (see Figure 5-13). Rotations follow the same logic and, generally, a good match was observed except in the case of pile DM4 that shows a slight change in the direction of the rotation. This might have been caused by the level of pile discretisation within the MATLAB routine.

6.4. General conclusions

Depending on the geometry of the pile, the soil layering, the type of soil and some numerical control parameters (tolerated error, the maximum number of iteration, etc.), a 3D finite element analysis by means of MoDeTo and PLAXIS, takes several hours. Even considering these testing piles used in the PISA project, which have smaller dimensions than a real monopile acting as a foundation of a wind turbine, the process is highly time-consuming and it can take up to 14 hours for one analysis to finish.

By assuming that the user has a routine to structurally represent the monopile, the complete process of the proposed CPT-based method takes only a few minutes. The calculation of each reaction is simple and a small number of points is enough to characterise the curves in a correct way (in this thesis, each reaction curve was discretised by 21 points), both at the base and at every slice along the shaft. Depending on the level of the detail required, the pile can be divided into more slices and the process would take longer, but as it was shown, slices of 1 m gave already a good result.

Even though the proposed method was tested in a North Sea sand deposit, its results may be used as a preliminary indication for any type of sand. However, caution should be taken when doing so since the PLT results from a single sand deposit (i.e. Dunkirk sand) were only used to calibrate the method.

Since this is a CPT-based method, the soil model was defined mainly based on CPT-based formulations, where applicable. In this case, to represent the serviceability limit state, relations proposed by Robertson & Cabal (2015) represent better this situation.

The validity of the method is limited to a deformation range at mudline between 2% and 3% of the pile diameter. After this threshold, the proposed method tends to overestimate the capacity of the monopile-soil system.

7. Recommendations and Future Work

In the development of the CPT-based method to predict the lateral response of a monopile subjected to a monotonic load, 3 out of 4 new formulations were proposed regarding the soil reactions involved in the lateral behaviour of the pile-soil system, according to what is stated in the research conducted by the PISA group as part of the PISA project.

Even considering that the results shown in this investigation are promising, some recommendations for further research are addressed in order to, both, improve the current investigation and also broaden it to different soil types, limit states, load regimes, etc.

7.1. Soil model

It was defined during the scope of the investigation that the state in which the research would be focused on is the serviceability limit state for monotonic loading of monopiles. In order to compare the deformation and the rotation of the pile with the results obtained from the pile load tests and the 3D FE analyses, a soil model was defined to represent the mentioned load state and the soil parameters were defined according to this specific limit state.

If other limit states (e.g. *ULS*) or the effect of cyclic or creep loads are to be studied, then the soil model need to be re-defined and re-calibrated.

7.2. Pile load tests

Fictional piles modelled in PLAXIS 3D were also used in order to define and validate the soil model. Some of the data obtained from the pile load tests was used in order to compare the deflection of the pile as well as the rotation at different points. Obtaining forces and stresses along the pile and at the base, requires mathematical handling that includes differentiation, integrations and curve-fitting techniques which adds inaccuracies in final values. A useful measure is to include load cells along the piles to obtain the data directly from the instruments.

New data is required to be added to validate the proposed method. Since the method is intended to predict the behaviour in saturated soil, new pile load tests in these soil conditions are useful to prove the accuracy of the formulations. It was noticed that the partial saturation within the 5.4 meters from the surface may improve the soil properties and several changes in the soil properties were made to incorporate this effect and represent the real situation as accurately as possible.

PISA project included several geometric features in order to study a wide range of possible pile sizes. In the case of piles similar to rigid monopiles (for example, DM7), the length was only 2.29 meters and thus shallow effects coming from the installation process or the superficial embedment in not-fully-saturated soil may induce inaccuracies. Fully instrumented longer piles are recommended to be used to validate the proposed formulation.

7.3. Soil reactions

Proposed formulations were obtained by using the available data from the PLTs performed at the Dunkirk site in addition to the fictional piles analysed by means of PLAXIS 3D. To prove the validity of the formulations and to improve them if necessary, more piles actual and simulated should be analysed in order to add more points to the fitting plots. By increasing the data, the numerical coefficients are prone to improve whilst more data is added.

The present investigation proposes a CPT-based method to predict the lateral behaviour of monopiles. Each of the formulations is based on the tip resistance of the CPT and therefore can be later used in any sandy soil in which CPT measurements are available. However, $p - y$ curves were calculated according to Dyson & Randolph (2001) since the lateral response in long piles, in which this reaction is predominant, fits better the response given by the 3D FEM analysis and the MATLAB code for the sand studied in this investigation. For other types of sand, different formulations can potentially predict better the expected behaviour.

The consideration of the slenderness ratio, L/D, in the formulation to calculate the moment along the shaft, m, should be extensively investigated by adding more points to the fitting plots. Moment along the shaft is defined in terms of the horizontal reaction p and physically there is no reason to add the slenderness ratio in the formulation. However, statistically, there is a slight trend as it is shown un subchapter 4.6. More data is needed to conclude about this reaction.

7.4. General lateral response

Besides displacements and rotations, a structural check of the monopile can be performed by obtaining moments and shear forces along the monopile and comparing them with the resistance of the structural element.

References

API. (2011). Geotechnical and foundation design considerations, ANSI/API RP 2GEO. Washington, DC: API Publishing Services.

Arany, L., Bhattacharya, S., MacDonald, J., & Hogan, S. (2014). *Simplified critical mudline bending moment spectra of offshore wind turbine support structures* . Bristol: John Wiley & Sons.

Brinkgreve, R. (2018). *TU Delft Brightspace.* Retrieved from Possibilities & limitations of material models for soil and rocks: https://brightspace.tudelft.nl/

Brinkgreve, R., Engin, E., & Engin, H. (2010). Validation of empirical formulas to derive model parameters for sands. *Research Gate*, 6.

Brinkgreve, R., Kumarswamy, S., & Swolfs, W. (2018). *PLAXIS 3D material model manual.* Delft: PLAXIS B.V.

Broere, W., & van Tol, A. (2006). Modelling the bearing capacity of displacement piles in sand. *Proceedings of the institution of Civil Engineers, Geotechnical Engineering*, 159.

Burd, H., Beuckelaers, W., Byrne, B., Gavin, K., Houlsby, G., Igoe, D., . . . Zdravkovic, L. (2018). *Pisa #2: New analysis methods for instrumented monopile field tests.* Geotechnique.

Burd, H., Byrne, B., McAdam, R., Houlsby, G., Martin, C., Beuckelaers, W., . . . Muir Wood, A. (2017). Foundation design of offshore wind structures. *Proceedings of TC 209 workshop* (pp. 35-44). Seoul : ResearchGate.

Burd, H., Taborda, D., Zdravkovic, L., Abadie, C., Byrne, B., Houlsby, G., . . . Potts, D. (2018). *PISA #8: PISA design model for monopiles for offshore wind turbines: application to a marine sand.* Geotechnique .

Byrne, B., & Houlsby, G. (2004). Foundation for offshore wind turbines. *Philosophical Transactions of the Royal Society*, 2909 - 2930.

Byrne, B., McAdam, R., Burd, H., & Houlsby, G. (2015). New design method for large diameter piles under lateral loading for offshore wind applications. *Third international symposium on frontiers in offshore geotechnics* (p. 7). Oslo: Researchgate.

Chow, F. (1997). *Investigations into the behaviour of displacement piles for offshore foundations.* London: Imperial College, University of London.

Corbetta, G., Ho, A., & Pineda, I. (2015). *Wind energy scenarios for 2030.* The European Wind and Energy Association.

DNV. (2014). *Design of offshore wind turbine structures.* Det Norske Veritas.

DNV-GL-AS. (2016). *DNVGL-ST-0126: Support structures for wind turbines.* DNV-GL-AS.

Dyson, G., & Randolph, M. (2001). Monotonic lateral loading of piles in calcareous sand. *J. Geotech. Geoenviron. Engng*, 346-352.

Engin, H. (2013). *Modelling installation effects - A numerical approach.* Delft: TU Delft.

Foursoff. (2018). *Investigation into a new CPT-based design method for large diameter monopiles in sand.* Delft: TU Delft.

FUGRO. (2018). *Cone Penetration Test Interpretation.* FUGRO.

FUGRO, N. M. (2018). *User Manual CPT Soil Classification Module in program UNIPLOT.* FUGRO Netherlands Marine.

Gavin, K., & Lehane, B. (2005). Estimating the end bearing resistance of pipe piles in sand using the final filling ratio. *Front Offshore Geotech, Perth: Taylor and Francis*, 717-24.

Hardin, B., & Richart, J. F. (1963). Elastic wave velocities in granular soils. *Journal of Soil Mechanics & Foundations Div*, 89.

Houlsby, G., & Hitchman, R. (1988). Calibration chamber tests of a cone penetrometer in sand. *Geotechnique 38*, 39-44.

Janoyan, K., & Whelan, M. (2004). Interface between soil and large diameter piles. In A. Geotechnical, *Drilled shafts, micropiling, deep mixing remedial methods and special foundation systems.* ASCE.

Jardine, R. (1985). *Investigations of pile-soil behaviour, with special reference to the foundations of offshore structures.* London: Imperial College, University of London.

Kaltekis, K., Panagoulias, S., van Dijk, B., Brinkgreve, R., & da Silva, M. (2019). Comparative concept design study of laterally loaded monopiles. *J. Phys.: Conf. Ser. 1222 012027.*

Kuwano, R. (1999). *The stiffness and yielding anisotropy of sand.* London: Imperial College, University of London.

Lahoz, M. (2019, June 12). MoDeTo p-y curves (Personal Communication). Delft.

Lehane, B. (1992). *Experimental investigations of pile behaviour using instrumented field piles.* London: Imperial College, University of London.

Lemnitzer, A., & Favaretti, C. (2013). *Find a Pile.Com*. Retrieved from http://www.findapile.com/p-y-curves/definition

Lengkeek, A., de Greef, J., & Joosten, S. (2018). CPT based unit weight estimation extended to soft organic soils and peat. *Cone Penetration Testing 2018: Proceedings of the 4th International Symposium on Cone Penetration Test (CPT '18)* (p. 8). Delft: London: CRC Press.

Li, W., Igoe, D., & Gavin, K. (2014). Evaluation of CPT based p-y models for laterally loaded piles in siliceous sand. *Geotechnique Letters*, 110-117.

Lunne, T., Robertson, P., & Powell, J. (1997). *Cone penetration testing in geotechnical practice.* New York: Blackie Academic/Routledge Publishing.

Matlock, H. (1970). Correlations for design of laterally loaded piles in soft clays. *Offshore technology conference*, (p. 18). Dallas.

Mayne, P. (2017). Stress History of Soils from Cone Penetration Tests. *Soils and Rocks*, 203-216.

McAdam, R., Byrne, B., Houlsby, G., Beauckelaers, W., Burd, H., Gavin, K., . . . Zdravkovic, L. (2018). *Monotonic lateral loaded pile testing in a dense sand at Dunkirk.* Geotechnique.

Minga, E., & Burd, H. (2019). Validation of the PLAXIS MoDeTo 1D model for dense sand. 1-18.

Murphy, G., Igoe, D., Doherty, P., & Gavin, K. (2018). 3D FEM approach for laterally loaded monopile design. *Computers and Geotechnics*, 76-83.

Novello, E. (1999). From static to cyclic p-y data in calcareous sediments. *Engineering for calcareous sediments* (pp. 17-27). Perth: A.A. Balkema.

O'Neill, M., & Murchinson, J. (1983). *An evaluation of p-y relationships in sands - Research report N GT-DF02-83.* Houston: Department of civil engineering, University of Houston.

Oomen, K. (2017). *Pile foundations NL an analysis of the 4D/8D method through numerical modelling.* Delft: TU Delft.

Panagoulias, S., Brinkgreve, R., & Hosseini, S. (2018). An innovative design methodology for offshore wind monopiles foundations. *Research Gate*, 12.

Panagoulias, S., Brinkgreve, R., Minga, E., Burd, H., & McAdam, R. (2018). Application of the PISA framework to the design of offshore wind turbine monopile foundations. *Research Gate*, 9.

PISA Academic, W. G., & PISA DONG, E. G. (2015). *Field Test Factual Report.* DONG Energy.

PISA Academic, W. G., & PISA DONG, E. G. (2016). *PISA Final Report.* DONG Energy.

Pisano, F. (2018). *TU Delft Brightspace.* Retrieved from Offshore geotechnical engineering - Course introduction: http://brightspace.tudelft.nl

PLAXIS. (2018). *PLAXIS MoDeTo Manual 2018.* Delft: PLAXIS B.V.

Potts, D., & Zdravkovic, L. (1999). Finite element analysis in geotechnical engineering: theory. *Thomas Telfrod*.

Potts, D., & Zdravkovic, L. (2001). Finite element analysis in geotechnical engineering: application. *Thomas Telford*.

Prendergast, L. (2018). *TU Delft Brightspace*. Retrieved from Soil-structure interaction - Lateral loading of piles: http://brightspace.tudelft.bl

Reese, L., Cox, W., & Koop, F. (1974). Analysis of laterally loaded piles in sand. *Offshore technology conference* . Houston.

Reuters. (2017, June 20). *Reuters Graphic*. Retrieved from http://fingfx.thomsonreuters.com/gfx/rngs/GLOBAL-POWER-WIND/010041KT3EP/POWER-WINDTURBINES-01.jpg

Rix, G., & Stokoe, K. (1991). Correlation of initial tangent modulus and cone penetration resistance. *Proceedings of the first international symposium on calibration chamber testing* (pp. 351-362). New York: Elsevier Science Publishing.

Robertson, P. (2016). Estimating K0 in sandy soils using the CPT. *Geotechnical and Geophysical Site Characterisation 5*, 515-519.

Robertson, P., & Cabal, K. (2015). *Guide to Cone Penetration Testing for Geotechnical Engineering* (6th Edition ed.). Signal Hill, California: Gregg Drilling & Testing, Inc.

Robertson, P., Campenella, R., Gillespie, D., & Greig, J. (1986). Use of piezometer cone data. *In-situ '86 Use of in-situ testing in Geotechnical Engineering*.

Schanz, T., Vermeer, P., & Bonnier, P. (2000). The hardening soil model: formulation and verification. *Beyond 2000 om Computational Geotechnics - 10 Years of PLAXIS (c)*, 1-16.

Schnaid, F., & Houlsby, G. (1991). An assessment of chamber size effects in the calibration of in situ tests in sand. *Geotechnique 41*, 437-445.

Schneider, J. A. (2010). Foundation Design: A comparison of oil and gas platforms with offshore wind turbines. *Marine Technology Society Journal*, 32-51.

Suryasentana, S., & Lehane, B. (2016). Updated CPT-based p-y formulation for laterally loaded piles in cohesionless soil under static loading. *Geotechnique 66*, 445-453.

Taborda, D., Zdravkovic, L., Kontoe, S., & Potts, D. (2014). Computational study on the modification of a bounding surface plasticity model for sands. *Computers and geotechnics*, 145-160.

Wrana, B. (2015). Pile load capacity - Calculation methods. *Studia Geotechnia et Mechanica, Vol. 37, N4*, 11.

Zdravkovic, L., Jardine, R., Taborda, D., Burd, H., Byrne, B., Gavin, K., . . . Ushev, E. (2018). *PISA #1: Ground characterisation for PISA pile testing and analysis.* Geotechnique.

I. APPENDIX: Soil Properties

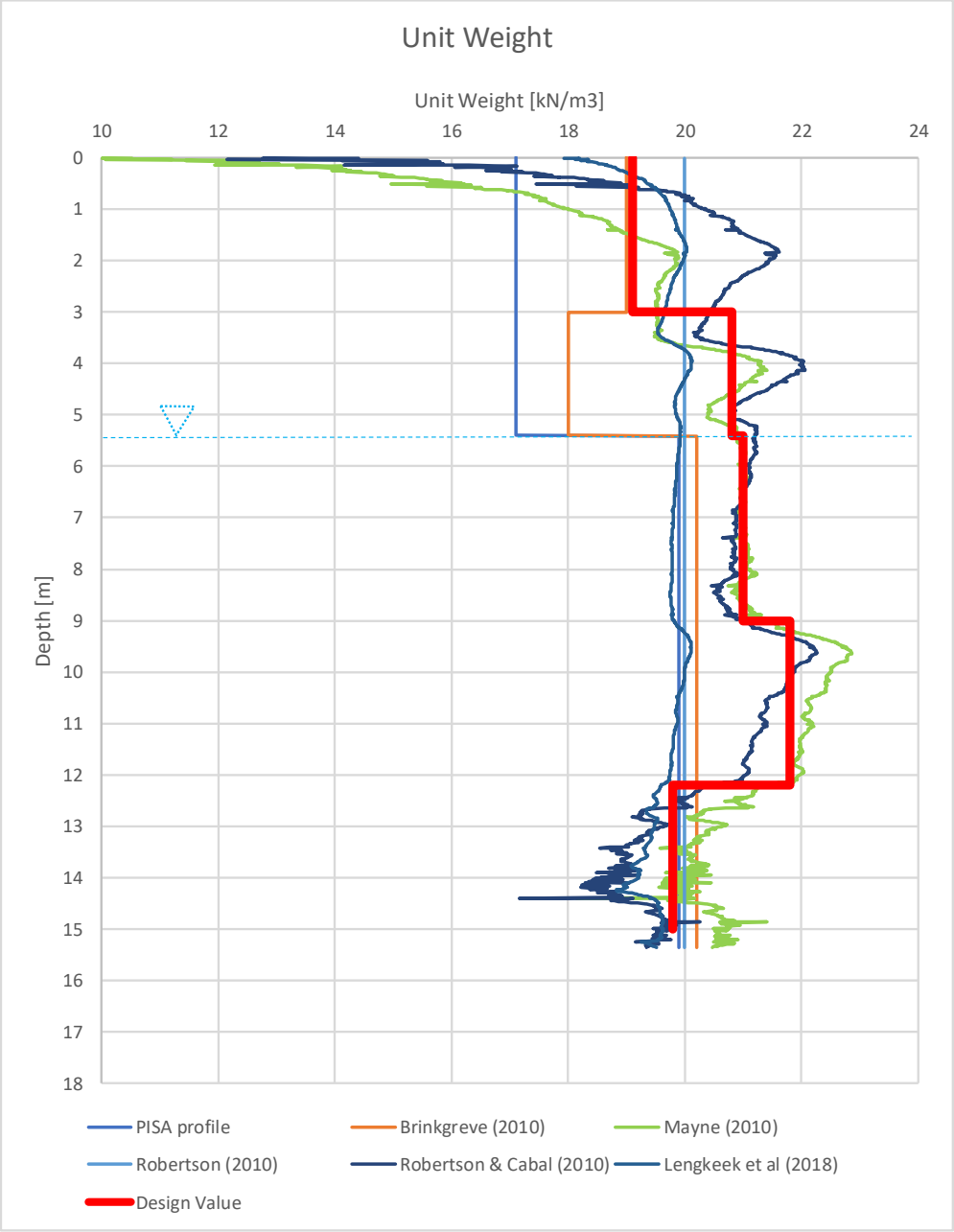

Figure I- 1 Unit weight

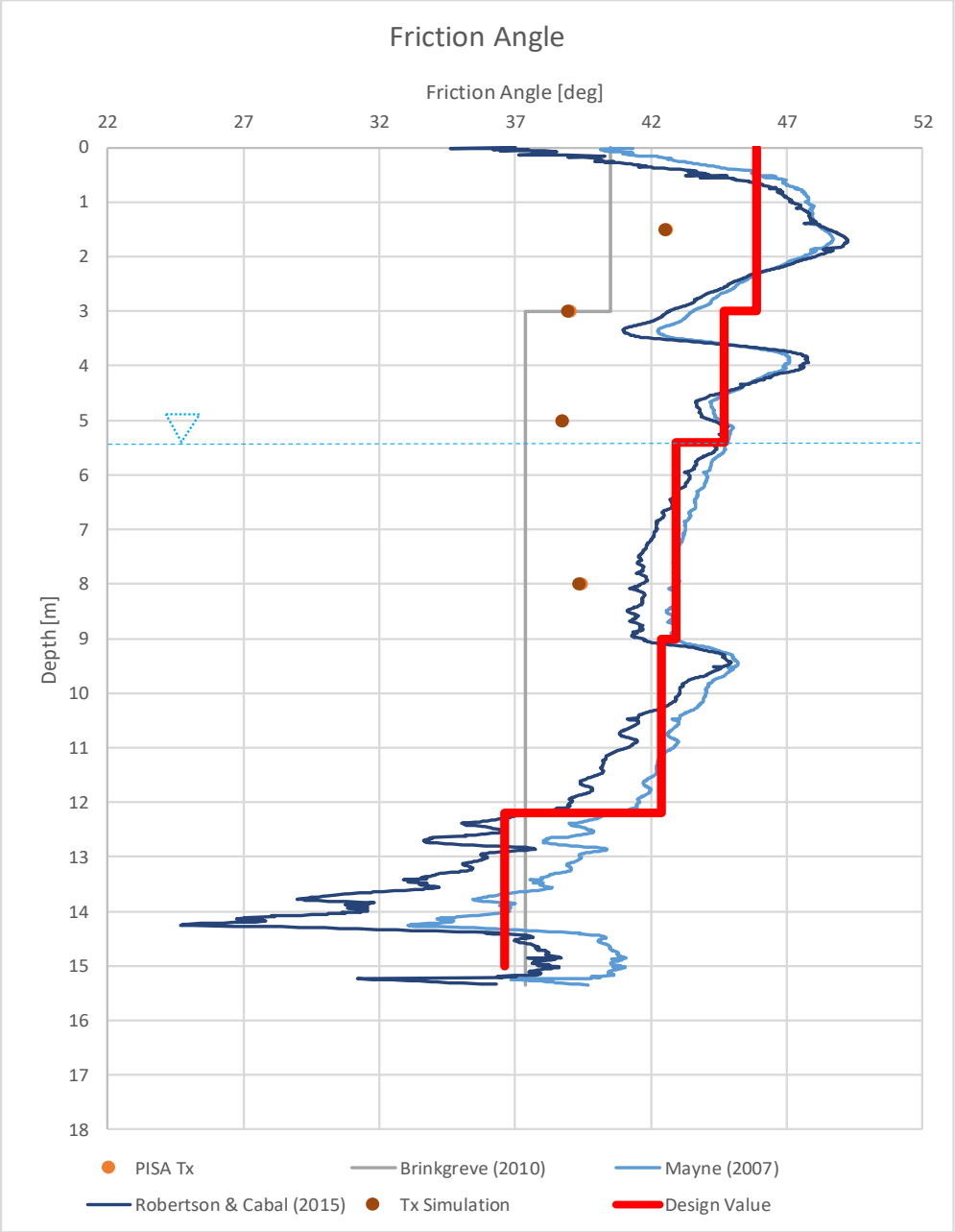

Figure I- 2 Friction angle

Notes:

- 'PISA Tx' corresponds to the triaxial tests included in the PISA report (see subchapter 3.2.2 of this thesis)
- 'Tx Simulation' corresponds to the triaxial test simulations considering the hardening soil model through the Soil Test add-on included in PLAXIS 3D (see subchapter 3.2.2. of this thesis)

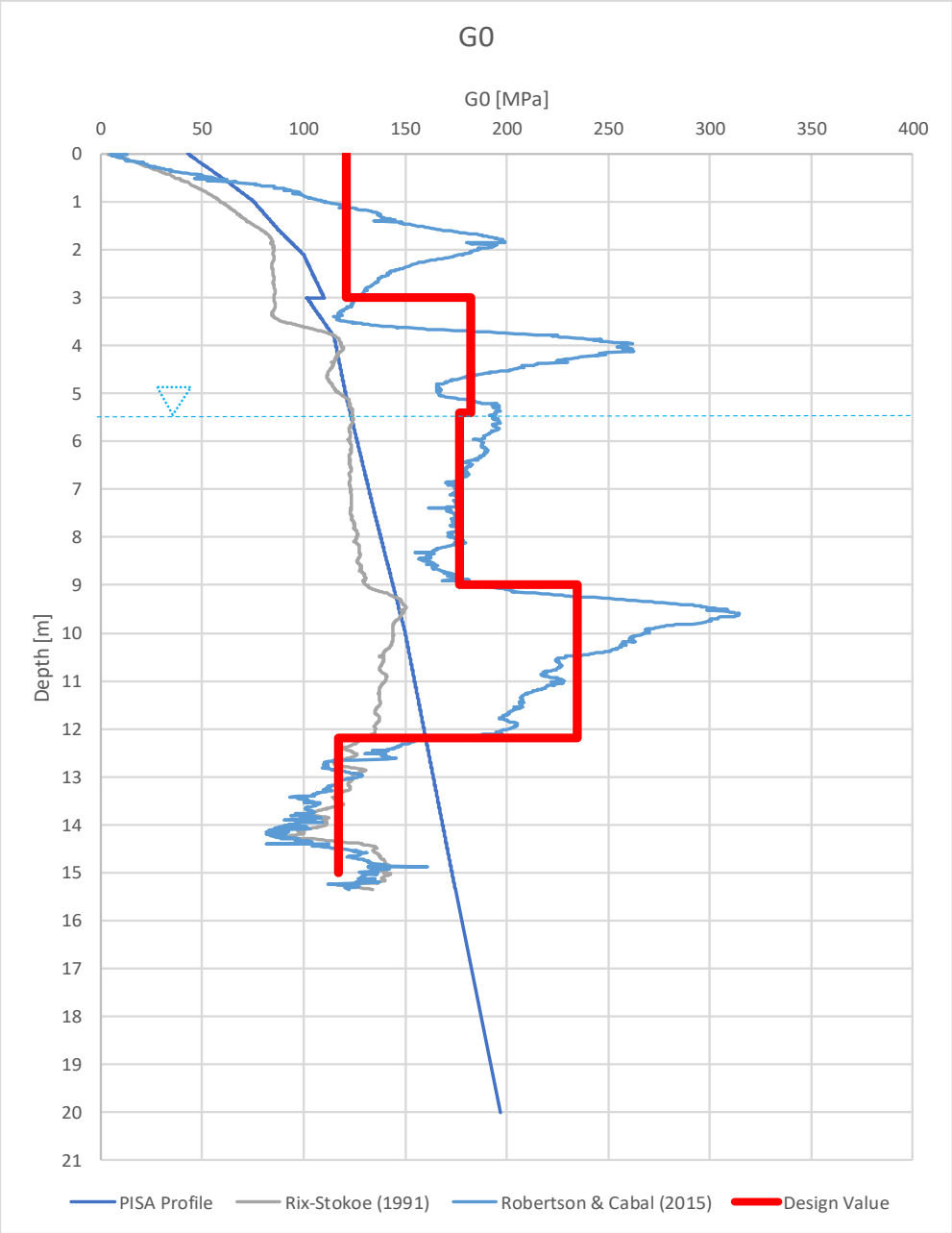

Figure I- 3 Small strain shear modulus

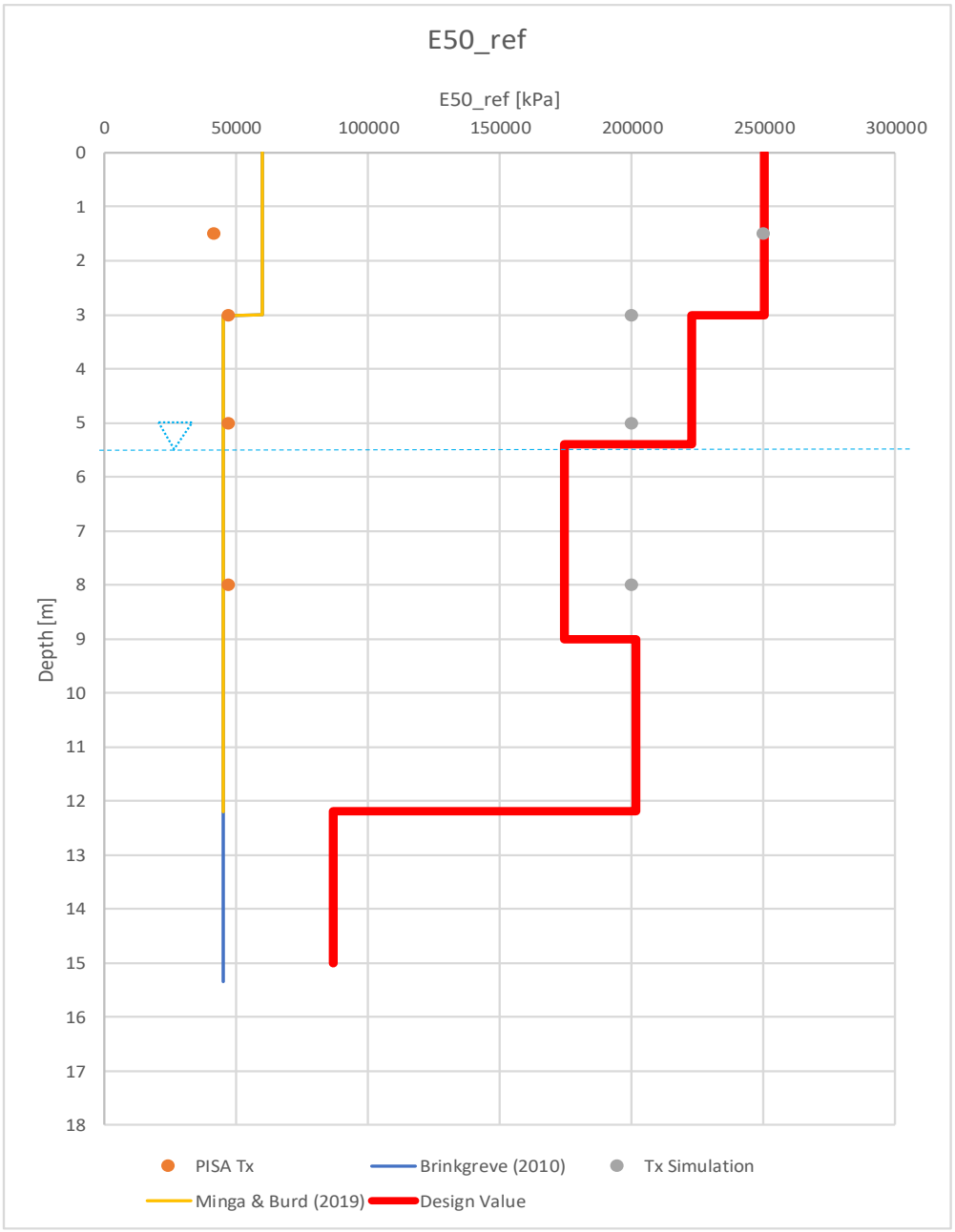

Figure I- 4 E_{50}^{ref}

Notes:

- 'PISA Tx' corresponds to the triaxial tests included in the PISA report (see subchapter 3.2.2 of this thesis)
- 'Tx Simulation' corresponds to the triaxial test simulations considering the hardening soil model through the Soil Test add-on included in PLAXIS 3D (see subchapter 3.2.2. of this thesis)

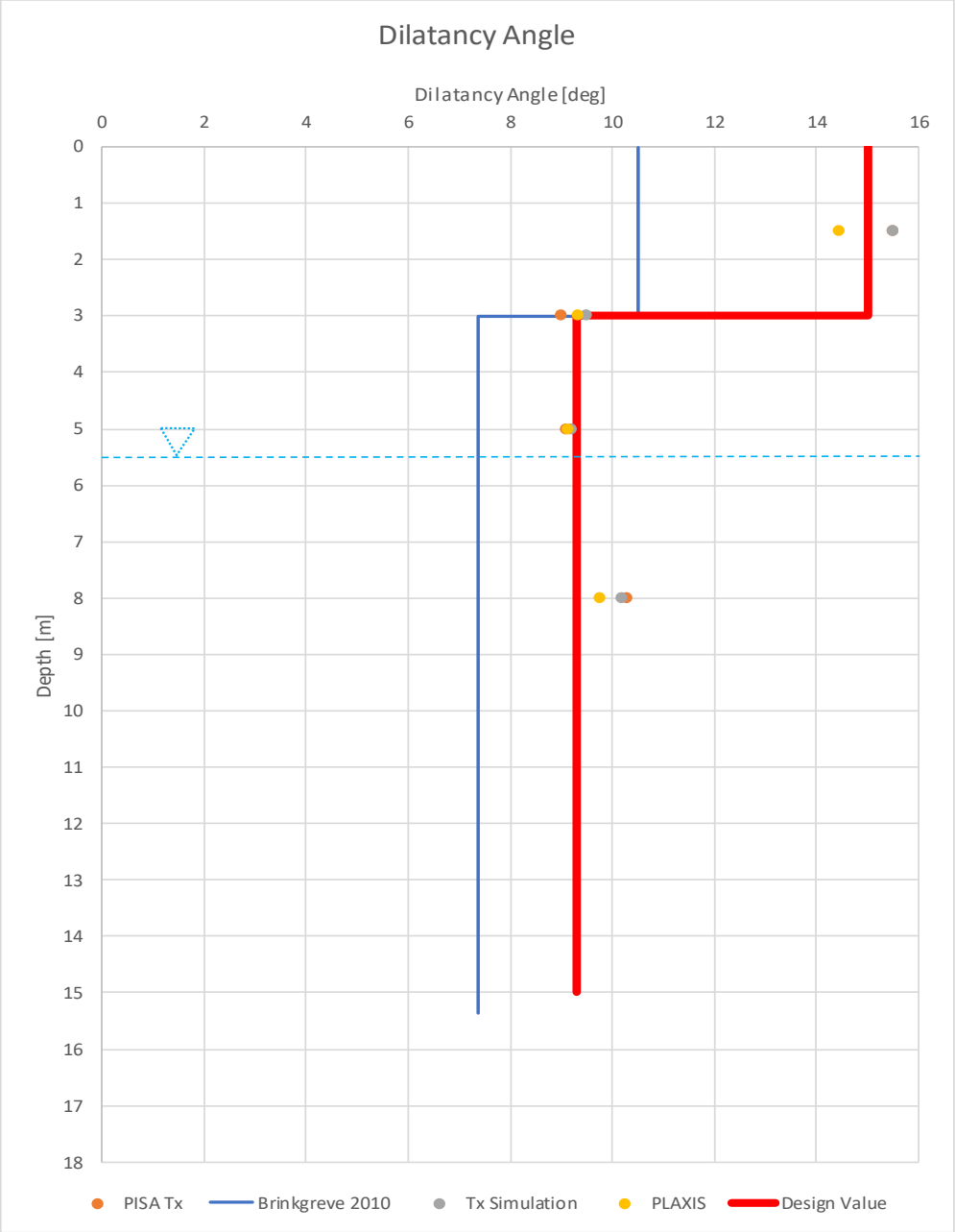

Figure I- 5 Dilatancy angle

Notes:

- 'PISA Tx' corresponds to the triaxial tests included in the PISA report (see subchapter 3.2.2 of this thesis)
- 'Tx Simulation' corresponds to the triaxial test simulations considering the hardening soil model through the Soil Test add-on included in PLAXIS 3D (see subchapter 3.2.2. of this thesis)
- 'PLAXIS' corresponds to an internal dilatancy angle calculation included in PLAXIS manual (2018).

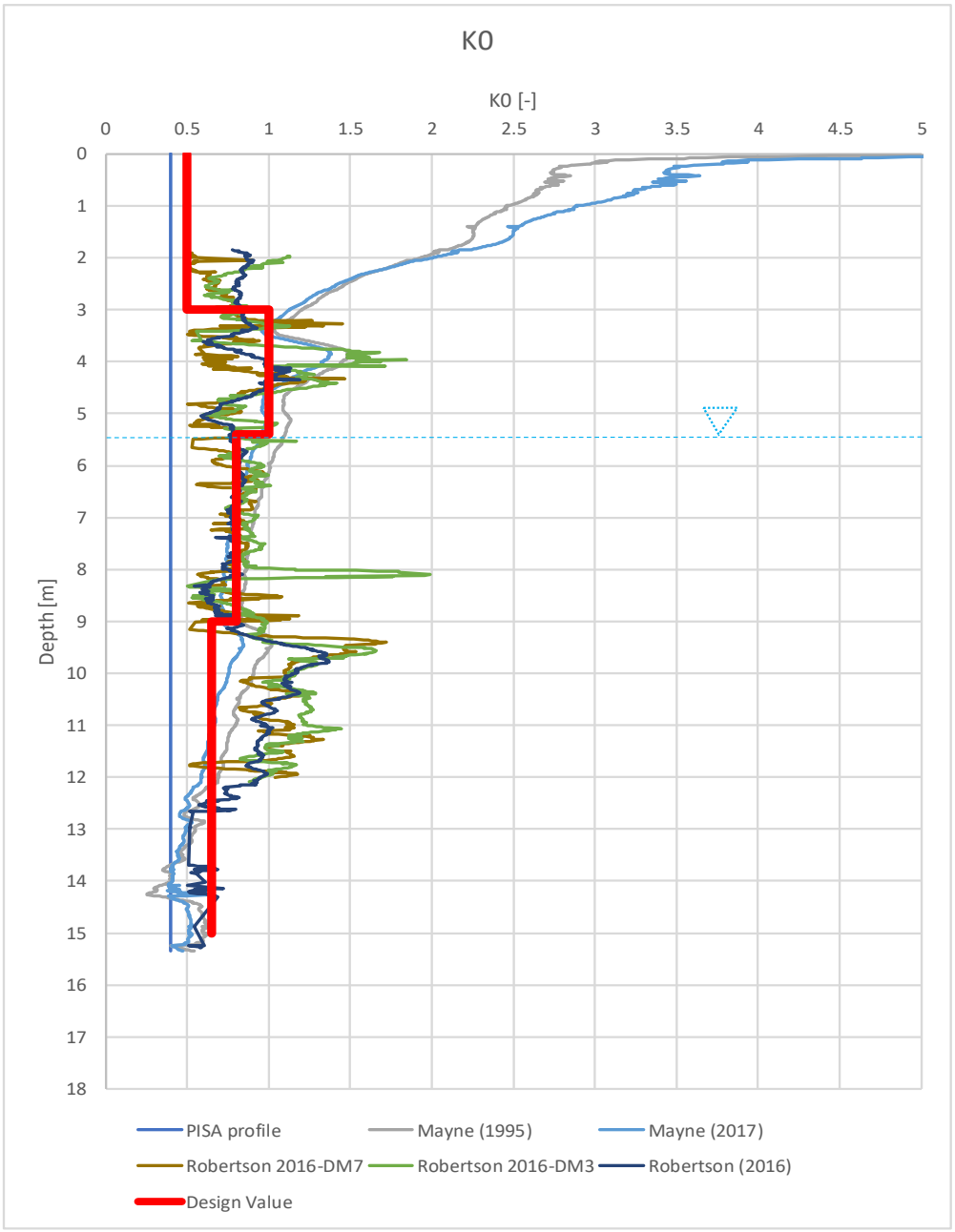
K0
K0 [-]
0
0.5
1
1.5
2
2.5
3
3.5
4
4.5
5
Depth [m]
0
1
2
3
4
5
6
7
8
9
10
11
12
13
14
15
16
17
18
PISA profile
Mayne (1995)
Mayne (2017)
Robertson 2016-DM7
Robertson 2016-DM3
Robertson (2016)
Design Value

Figure I- 6 K_0

II. APPENDIX: General Lateral Response (Tables)

Table II-1 General lateral response - Pile DM3

PILE	**DM3**						
Case		All reactions		Only p-y		p-y + m-psi	
Load [kN]	Depth [m]	Deflection [m]	Rotation [deg]	Deflection [m]	Rotation [deg]	Deflection [m]	Rotation [deg]
	0.001	0.002310035	0.076438549	0.002381637	0.078493416	0.002318585	0.076818148
	1	0.000977265	0.044819877	0.001013038	0.046639542	0.000979197	0.045211717
	2	0.00019501	0.020751997	0.000199024	0.022181643	0.000190103	0.021162699
50	3	-0.00016718	0.005263581	-0.000188118	0.006157791	-0.000179256	0.00564438
	4.2	-0.000277421	-0.00115524	-0.000317087	-0.00107694	-0.000297471	-0.000684922
	5.4	-0.000253225	-0.001916128	-0.000294531	-0.002483372	-0.000283126	-0.001350392
	6.1	-0.000229815	-0.001916128	-0.000264191	-0.002483372	-0.000266628	-0.001350392
Load [kN]	Depth [m]	Deflection [m]	Rotation [deg]	Deflection [m]	Rotation [deg]	Deflection [m]	Rotation [deg]
	0.001	0.007396711	0.224254507	0.007934797	0.233474588	0.007440497	0.225538936
	1	0.003486645	0.142713443	0.003863972	0.151800662	0.003508036	0.14404517
	2	0.000995826	0.076993552	0.00121455	0.086449509	0.000993974	0.078457287
125	3	-0.000347965	0.029921402	-0.000294278	0.041174603	-0.000375364	0.031601738
	4.2	-0.000974638	0.00616692	-0.001156637	1.93E-02	-0.001037229	7.85E-03
	5.4	-0.001103797	0.001043641	-0.001561794	0.014838	-0.001201701	0.002652578
	6.1	-0.001116548	0.001043641	-0.001743075	0.014838	-0.001234108	0.002652578
Load [kN]	Depth [m]	Deflection [m]	Rotation [deg]	Deflection [m]	Rotation [deg]	Deflection [m]	Rotation [deg]
	0.001	0.011541576	0.334510525	0.012445412	0.34991738	0.01161424	0.336235606
	1	0.005709104	0.220174306	0.006344308	0.235463508	0.00575169	0.22199239
	2	0.001866338	0.126917178	0.002234695	0.142866879	0.001877192	0.129016643
174	3	-0.000348785	0.059055965	-0.000258803	0.077640526	-0.000374573	0.061740293
	4.2	-0.00158565	0.023599137	-0.001884902	0.045661692	-0.001667659	0.027102603
	5.4	-0.002079909	0.015232676	-0.002841238	0.038973447	-0.002235295	0.01927889
	6.1	-0.002266012	0.015232676	-0.003317389	0.038973447	-0.002470831	0.01927889
Load [kN]	Depth [m]	Deflection [m]	Rotation [deg]	Deflection [m]	Rotation [deg]	Deflection [m]	Rotation [deg]
	0.001	0.018865312	0.521205756	0.020433386	0.548247005	0.0189912	0.52388856
	1	0.009777652	0.355749547	0.010874239	0.382690453	0.009856764	0.358539585
	2	0.003568651	0.219347792	0.004195031	0.247276162	0.003599067	0.222460588
250	3	-0.00025969	0.118715561	-0.000120753	0.150291846	-0.000283602	0.122494442
	4.2	-0.002746063	0.065454401	-0.003268458	1.02E-01	-0.00284912	7.02E-02
	5.4	-0.004116937	0.052722025	-0.005405756	0.091853937	-0.00431849	0.058039406
	6.1	-0.004761058	0.052722025	-0.006527963	0.091853937	-0.005027575	0.058039406
Load [kN]	Depth [m]	Deflection [m]	Rotation [deg]	Deflection [m]	Rotation [deg]	Deflection [m]	Rotation [deg]
	0.001	0.028030377	0.746769733	0.030364269	0.788579446	0.028156295	0.749464614
	1	0.015009819	0.524552668	0.016614724	0.566241869	0.015088751	0.527367949
	2	0.005854648	0.339841565	0.006731939	0.382744369	0.005884444	0.343024185
334	3	-7.67E-05	0.202041406	5.18E-05	0.249382759	-1.02E-04	0.205978586
	4.2	-0.004308251	0.128483194	-0.005171271	0.182394512	-0.004416463	0.133443733
	5.4	-0.006999197	0.110751525	-0.008991332	0.168149876	-0.007211302	0.116409441
	6.1	-0.008352282	0.110751525	-0.011045671	0.168149876	-0.008633512	0.116409441
Load [kN]	Depth [m]	Deflection [m]	Rotation [deg]	Deflection [m]	Rotation [deg]	Deflection [m]	Rotation [deg]
	0.001	0.035810607	0.935608087	0.038939145	0.989738314	0.036002115	0.939392741
	1	0.019497495	0.668594794	0.021682227	0.722646711	0.019623014	0.672510352
	2	0.007828314	0.445418474	0.009069663	0.501063916	0.007885494	0.449734522
400	3	5.43E-05	0.277578512	0.000324447	0.338644509	3.61E-05	0.282722007
	4.2	-0.005759295	0.187573432	-0.006768107	2.56E-01	-0.00588517	1.94E-01
	5.4	-0.009687824	0.165792847	-0.012138945	0.238836127	-0.009944765	0.172818962
	6.1	-0.011713366	0.165792847	-0.015056879	0.238836127	-0.012056147	0.172818962
Load [kN]	Depth [m]	Deflection [m]	Rotation [deg]	Deflection [m]	Rotation [deg]	Deflection [m]	Rotation [deg]
	0.001	0.048542319	1.234808841	0.052778914	1.305070714	0.048728932	1.238701574
	1	0.027012391	0.899789668	0.030023911	0.97004684	0.027131131	0.903799957
	2	0.011308098	0.618051239	0.0130934	0.690417543	0.011356846	0.622416956
500	3	0.000521069	0.404336063	1.04E-03	0.483411108	4.94E-04	0.409438892
	4.2	-0.007947325	0.289042003	-0.009081198	3.78E-01	-0.008081647	2.95E-01
	5.4	-0.014001007	0.261074372	-0.016989805	0.354757174	-0.014264169	0.267960211
	6.1	-0.017190632	0.261074372	-0.021323981	0.354757174	-0.01753792	0.267960211
Load [kN]	Depth [m]	Deflection [m]	Rotation [deg]	Deflection [m]	Rotation [deg]	Deflection [m]	Rotation [deg]
	0.001	0.058665572	1.467179117	0.063761385	1.549833686	0.058855095	1.471130421
	1	0.033084073	1.080542071	0.036738734	1.163324648	0.033204701	1.084609827
	2	0.014225056	0.754290436	0.016434888	0.839684406	0.014274689	0.758702914
576	3	1.06E-03	0.505537887	1.78E-03	0.598745615	1.03E-03	0.510662045
	4.2	-0.009527756	0.370732415	-0.010760468	4.75E-01	-0.009662456	3.77E-01
	5.4	-0.017292358	0.337933652	-0.020705743	0.44795308	-0.017556005	0.344821579
	6.1	-0.021420996	0.337933652	-0.026178522	0.44795308	-0.021768796	0.344821579

Table II-2 General lateral response - Pile DM3B

PILE	**DM3B**						
Case		All reactions		Only p-y		p-y + m-psi	
Load [kN]	Depth [m]	Deflection [m]	Rotation [deg]	Deflection [m]	Rotation [deg]	Deflection [m]	Rotation [deg]
	0.001	0.007194378	0.185271992	0.01046307	0.209064263	0.00940461	0.189919375
	1	0.004964006	0.152804664	0.00681786	0.175687702	0.006093207	0.157573026
	2	0.002897061	0.125456022	0.003751531	0.147342271	0.003343039	0.130541937
200	3	0.00080744	0.104147375	0.001179923	0.125582391	0.001064652	0.109844629
	4.2	-0.000773817	0.091952867	-0.001450268	0.11386499	-0.001235929	0.098510499
	5.4	-0.001596735	0.088661519	-0.003835051	0.111207898	-0.003299128	0.095798903
	6.1	-0.001782878	0.088661519	-0.005193712	0.111207898	-0.004469532	0.095798903
Load [kN]	Depth [m]	Deflection [m]	Rotation [deg]	Deflection [m]	Rotation [deg]	Deflection [m]	Rotation [deg]
	0.001	0.016080726	0.386543682	0.022520152	0.45625126	0.019474222	0.396351294
	1	0.010341013	0.321867436	0.014565029	0.389378983	0.012563504	0.331823375
	2	0.006023366	0.267927028	0.007769083	0.333001686	0.006772094	0.278307937
400	3	0.001547157	0.226803411	0.001957107	0.29049258	0.001914704	0.237990451
	4.2	-0.002003002	0.204332389	-0.004126955	2.68E-01	-0.003069756	2.17E-01
	5.4	-0.00508253	0.198705329	-0.009747103	0.263505218	-0.00760521	0.211571507
	6.1	-0.006410173	0.198705329	-0.012966427	0.263505218	-0.010190043	0.211571507
Load [kN]	Depth [m]	Deflection [m]	Rotation [deg]	Deflection [m]	Rotation [deg]	Deflection [m]	Rotation [deg]
	0.001	0.025261767	0.654704475	0.039160425	0.780224186	0.032732159	0.665289822
	1	0.016846445	0.556826072	0.025556562	0.679168347	0.021132272	0.567548544
	2	0.009127997	0.47511326	0.013702838	0.593441391	0.011226682	0.486206696
600	3	0.002035706	0.413242808	0.003345332	0.528444254	0.002740774	0.425049192
	4.2	-0.004819231	0.379811174	-0.007722379	0.494450449	-0.006161435	0.392583631
	5.4	-0.008773978	0.371609182	-0.018078125	0.487007232	-0.014383688	0.385027028
	6.1	-0.01031404	0.371609182	-0.024028041	0.487007232	-0.01908768	0.385027028
Load [kN]	Depth [m]	Deflection [m]	Rotation [deg]	Deflection [m]	Rotation [deg]	Deflection [m]	Rotation [deg]
	0.001	0.049537226	0.976336173	0.059321044	1.15936454	0.05007767	0.988560023
	1	0.032513986	0.845688562	0.039106551	1.024614788	0.032841296	0.858074665
	2	0.017753936	0.736301013	0.021223649	0.910211981	0.017865068	0.749121377
800	3	0.004903059	0.652844551	0.005337453	0.823042208	0.004790434	0.666476348
	4.2	-0.008770085	0.607711976	-0.011900303	7.77E-01	-0.009168214	6.22E-01
	5.4	-0.021497975	0.596783633	-0.028182671	0.76744928	-0.022204036	0.612176442
	6.1	-0.028789063	0.596783633	-0.037558832	0.76744928	-0.029683182	0.612176442
Load [kN]	Depth [m]	Deflection [m]	Rotation [deg]	Deflection [m]	Rotation [deg]	Deflection [m]	Rotation [deg]
	0.001	0.068300129	1.326911891	0.082025549	1.582064341	0.068910318	1.34153806
	1	0.045164307	1.163553213	0.054440929	1.413195054	0.045519476	1.178326435
	2	0.024856472	1.026933357	0.029776023	1.269853219	0.0249538	1.04212152
1000	3	6.93E-03	0.922808458	7.61E-03	1.160650548	6.77E-03	0.938780393
	4.2	-0.012394151	0.866659981	-0.016695705	1.103499281	-0.012896422	0.883692032
	5.4	-0.030545435	0.853120079	-0.03980734	1.091011557	-0.031404425	0.870864095
	6.1	-0.040968263	0.853120079	-0.053136561	1.091011557	-0.042044037	0.870864095
Load [kN]	Depth [m]	Deflection [m]	Rotation [deg]	Deflection [m]	Rotation [deg]	Deflection [m]	Rotation [deg]
	0.001	0.088534197	1.703692768	0.107062024	2.045391063	0.08918722	1.719382028
	1	0.058828883	1.507330663	0.071398914	1.842450426	0.059208352	1.523178383
	2	0.032521	1.343272244	0.039242088	1.670121328	0.032623874	1.359562409
1200	3	9.08E-03	1.218460878	0.010092972	1.538819842	8.90E-03	1.235584159
	4.2	-0.016442908	1.15129832	-0.022135996	1.47E+00	-0.016982981	1.17E+00
	5.4	-0.040555644	1.135168963	-0.052924755	1.455001997	-0.041477911	1.154178823
	6.1	-0.054424349	1.135168963	-0.070700958	1.455001997	-0.055578865	1.154178823
Load [kN]	Depth [m]	Deflection [m]	Rotation [deg]	Deflection [m]	Rotation [deg]	Deflection [m]	Rotation [deg]
	0.001	0.111393576	2.121620421	0.134863181	2.548635473	0.112202316	2.140271724
	1	0.074401344	1.892348113	0.090425583	2.311566167	0.074884883	1.91116426
	2	0.041373639	1.700740755	0.050081142	2.110228779	0.041528774	1.720015919
1400	3	0.011690113	1.55497127	1.33E-02	1.956546268	1.15E-02	1.575104624
	4.2	-0.020877129	1.476557382	-0.027727107	1.88E+00	-0.021480081	1.50E+00
	5.4	-0.051802075	1.457738116	-0.067014334	1.858081313	-0.052851042	1.479837995
	6.1	-0.069611706	1.457738116	-0.08971508	1.858081313	-0.070930674	1.479837995
Load [kN]	Depth [m]	Deflection [m]	Rotation [deg]	Deflection [m]	Rotation [deg]	Deflection [m]	Rotation [deg]
	0.001	0.130079123	2.459478794	0.156911072	2.944639507	0.130923443	2.478902235
	1	0.087196046	2.204987542	0.105568811	2.681380007	0.087701702	2.224574043
	2	0.048711753	1.99234975	0.058769901	2.457659244	0.04887556	2.012395437
1553	3	1.39E-02	1.830496567	1.59E-02	2.28660723	1.38E-02	1.851406259
	4.2	-0.02439914	1.743377861	-0.032014934	2.20E+00	-0.025023128	1.77E+00
	5.4	-0.060912361	1.722466343	-0.078019656	2.176711562	-0.061998942	1.745379469
	6.1	-0.081956257	1.722466343	-0.104613204	2.176711562	-0.083322775	1.745379469

Table II-3 General lateral response - Pile DM3D

PILE	**DM3D**						
Case		All reactions		Only p-y		p-y + m-psi	
Load [kN]	Depth [m]	Deflection [m]	Rotation [deg]	Deflection [m]	Rotation [deg]	Deflection [m]	Rotation [deg]
	0.001	0.009252708	0.167869006	0.012705505	0.214188766	0.011019533	0.185448528
	1	0.007125771	0.157370198	0.008970944	0.203409688	0.007786083	0.175061887
	2	0.004279143	0.148446959	0.005420775	0.194296271	0.004730676	0.166451867
300	3	0.001788255	0.141255152	0.002029666	0.187228496	0.001825543	0.159842617
	4.2	-0.000900186	0.136797372	-0.001891639	0.183383197	-0.001522193	0.156188516
	5.4	-0.003535264	0.135340228	-0.005732408	0.182503174	-0.004793397	0.155292032
	6.1	-0.005088757	0.135340228	-0.007962105	0.182503174	-0.006690647	0.155292032
Load [kN]	Depth [m]	Deflection [m]	Rotation [deg]	Deflection [m]	Rotation [deg]	Deflection [m]	Rotation [deg]
	0.001	0.019289124	0.353746542	0.02564618	0.434015488	0.022108105	0.37267917
	1	0.014121256	0.332863622	0.018078756	0.412475628	0.015610131	0.351916272
	2	0.00901169	0.315337323	0.010879698	0.394313457	0.009468034	0.334724733
600	3	0.003508015	0.301548721	0.00399763	0.380303794	0.003625985	0.321556927
	4.2	-0.002307607	0.293452699	-0.003967434	3.73E-01	-0.003108688	3.14E-01
	5.4	-0.008053666	0.291107838	-0.011774945	0.371112729	-0.00969163	0.312552886
	6.1	-0.011210219	0.291107838	-0.016308942	0.371112729	-0.013510184	0.312552886
Load [kN]	Depth [m]	Deflection [m]	Rotation [deg]	Deflection [m]	Rotation [deg]	Deflection [m]	Rotation [deg]
	0.001	0.031107734	0.558269042	0.041508842	0.72328854	0.034316008	0.587611972
	1	0.021373845	0.527038319	0.0288977	0.690800001	0.0240705	0.556498922
	2	0.012175291	0.501071135	0.016840965	0.663562966	0.014357762	0.530914222
900	3	0.00512995	0.481006557	0.005259607	0.642785881	0.00509156	0.511554429
	4.2	-0.004244228	0.469651613	-0.008202869	0.631815039	-0.00562241	0.501123829
	5.4	-0.012480588	0.46654627	-0.021435573	0.629392857	-0.016117923	0.498633808
	6.1	-0.017518053	0.46654627	-0.029125057	0.629392857	-0.022209885	0.498633808
Load [kN]	Depth [m]	Deflection [m]	Rotation [deg]	Deflection [m]	Rotation [deg]	Deflection [m]	Rotation [deg]
	0.001	0.04864651	0.836477202	0.062655197	1.090118164	0.050162843	0.87148583
	1	0.034061828	0.794529297	0.043648072	1.046569656	0.034967756	0.829641301
	2	0.020194676	0.759710933	0.025381986	1.009991774	0.020487784	0.795158331
1200	3	0.006935219	0.732981315	0.007754304	0.981997326	0.006609653	0.7690619
	4.2	-0.008416306	0.71809139	-0.0128126	9.67E-01	-0.009497542	7.55E-01
	5.4	-0.023455977	0.71414873	-0.033070234	0.96398868	-0.0253109	0.751689483
	6.1	-0.03218095	0.71414873	-0.044847577	0.96398868	-0.03449452	0.751689483
Load [kN]	Depth [m]	Deflection [m]	Rotation [deg]	Deflection [m]	Rotation [deg]	Deflection [m]	Rotation [deg]
	0.001	0.068324351	1.168775431	0.087653228	1.524419367	0.070073322	1.208740253
	1	0.047945771	1.116240197	0.061073697	1.469835892	0.048997921	1.156325483
	2	0.028463704	1.072670549	0.035420221	1.42410135	0.028816234	1.113140884
1500	3	9.74E-03	1.039143743	1.06E-02	1.389019677	9.39E-03	1.080317618
	4.2	-0.012021704	1.020552509	-0.018526596	1.370520036	-0.013237858	1.062661044
	5.4	-0.033396106	1.01572057	-0.047230701	1.366452871	-0.035494179	1.058467143
	6.1	-0.045805474	1.01572057	-0.063925072	1.366452871	-0.048425795	1.058467143
Load [kN]	Depth [m]	Deflection [m]	Rotation [deg]	Deflection [m]	Rotation [deg]	Deflection [m]	Rotation [deg]
	0.001	0.089847496	1.538365688	0.114446477	1.989457719	0.091826838	1.584048469
	1	0.0630248	1.47521309	0.079758612	1.923738005	0.064207624	1.520998073
	2	0.037277474	1.422973408	0.04618305	1.868773606	0.037661199	1.469127198
1800	3	1.24E-02	1.382782104	0.013566798	1.826581329	1.20E-02	1.429618664
	4.2	-0.016519018	1.360616764	-0.024689032	1.80E+00	-0.017921771	1.41E+00
	5.4	-0.045015709	1.354931033	-0.062479184	1.799463721	-0.047418415	1.403309586
	6.1	-0.061569314	1.354931033	-0.08446378	1.799463721	-0.064563076	1.403309586
Load [kN]	Depth [m]	Deflection [m]	Rotation [deg]	Deflection [m]	Rotation [deg]	Deflection [m]	Rotation [deg]
	0.001	0.113163959	1.934159091	0.145421758	2.518691371	0.115301325	1.584048469
	1	0.079440272	1.860299888	0.10150626	2.441815317	0.08070439	1.520998073
	2	0.046971914	1.799340914	0.058888543	2.377652266	0.047360068	1.469127198
2100	3	0.015567491	1.752496044	1.74E-02	2.328398761	1.51E-02	1.429618664
	4.2	-0.021136701	1.726714431	-0.031375187	2.30E+00	-0.022704293	1.41E+00
	5.4	-0.057300923	1.720152333	-0.079597233	2.296729249	-0.05996141	1.403309586
	6.1	-0.078316548	1.720152333	-0.107657074	2.296729249	-0.081622644	1.403309586
Load [kN]	Depth [m]	Deflection [m]	Rotation [deg]	Deflection [m]	Rotation [deg]	Deflection [m]	Rotation [deg]
	0.001	0.134551296	2.294617316	0.172595356	2.981442446	0.136933445	2.349707026
	1	0.094542718	2.211891988	0.120611405	2.895288621	0.095964331	2.267081173
	2	0.05593792	2.14372214	0.070079085	2.823535461	0.0563963	2.199289135
2349	3	1.85E-02	2.091373081	2.08E-02	2.768459285	1.80E-02	2.147638302
	4.2	-0.025278705	2.062613518	-0.037183381	2.74E+00	-0.026968568	2.12E+00
	5.4	-0.068477982	2.05531479	-0.094557797	2.73305124	-0.071366347	2.113231698
	6.1	-0.093588389	2.05531479	-0.127948317	2.73305124	-0.097184343	2.113231698

Table II-4 General lateral response - Pile DM7

PILE	**DM7**						
Case		All reactions		Only p-y		p-y + m-psi	
Load [kN]	Depth [m]	Deflection [m]	Rotation [deg]	Deflection [m]	Rotation [deg]	Deflection [m]	Rotation [deg]
10	0.001	0.00093969	0.036401535	0.001074578	0.052933081	0.001043363	0.046169183
	1.145	0.000112876	0.026150034	1.76861E-05	0.043409446	4.51078E-05	0.037028418
	2.29	-0.00040971	0.026150034	-0.00084981	0.043409446	-0.00075301	0.037028418
Load [kN]	Depth [m]	Deflection [m]	Rotation [deg]	Deflection [m]	Rotation [deg]	Deflection [m]	Rotation [deg]
20	0.001	0.002557908	0.103208505	0.00308659	0.150368953	0.002818562	0.122324004
	1.145	0.000197188	0.083296167	8.42386E-05	0.130935379	0.000111711	0.103778222
	2.29	-0.0010674	0.083296167	-0.00253238	0.130935379	-0.00207976	0.103778222
Load [kN]	Depth [m]	Deflection [m]	Rotation [deg]	Deflection [m]	Rotation [deg]	Deflection [m]	Rotation [deg]
30	0.001	0.005290097	0.201509814	0.006020004	0.279120657	0.005671465	0.226825018
	1.145	0.000266638	0.171976317	0.000146923	0.249777297	0.000186581	0.198732809
	2.29	-0.00317014	0.171976317	-0.00484463	0.249777297	-0.00395848	0.198732809
Load [kN]	Depth [m]	Deflection [m]	Rotation [deg]	Deflection [m]	Rotation [deg]	Deflection [m]	Rotation [deg]
40	0.001	0.008284349	0.322458017	0.010924574	0.435723629	0.010259233	0.352916973
	1.145	0.00034597	0.283209018	0.000224669	0.396339068	0.000212693	0.315222784
	2.29	-0.00531369	0.283209018	-0.00769578	0.396339068	-0.00608673	0.315222784
Load [kN]	Depth [m]	Deflection [m]	Rotation [deg]	Deflection [m]	Rotation [deg]	Deflection [m]	Rotation [deg]
50	0.001	0.012849418	0.461725624	0.017447566	0.607061079	0.015225645	0.497298739
	1.145	0.000430343	0.412702423	0.00032664	0.557450215	0.000296296	0.449879311
	2.29	-0.00781711	0.412702423	-0.01081346	0.557450215	-0.0086941	0.449879311
Load [kN]	Depth [m]	Deflection [m]	Rotation [deg]	Deflection [m]	Rotation [deg]	Deflection [m]	Rotation [deg]
60	0.001	0.018777199	0.613228347	0.026222953	0.788668311	0.023412195	0.651217844
	1.145	0.000533134	0.55431834	0.000475955	0.728485562	0.00040961	0.593831236
	2.29	-0.01054437	0.55431834	-0.01408212	0.728485562	-0.01145752	0.593831236

Table II-5 General lateral response - Pile DM7B

PILE	**DM7B**						
Case		All reactions		Only p-y		p-y + m-psi	
Load [kN]	Depth [m]	Deflection [m]	Rotation [deg]	Deflection [m]	Rotation [deg]	Deflection [m]	Rotation [deg]
25	0.001	0.002484876	0.086163612	0.002769504	0.110934174	0.002335401	0.094308292
	1	0.000682541	0.057371468	0.000835273	0.081499565	0.000691057	0.066358199
	2	-0.00031878	0.044592761	-0.00058716	0.069329282	-0.00046711	0.055016467
	3	-0.001097071	0.044592761	-0.00179719	0.069329282	-0.00142733	0.055016467
Load [kN]	Depth [m]	Deflection [m]	Rotation [deg]	Deflection [m]	Rotation [deg]	Deflection [m]	Rotation [deg]
50	0.001	0.006371909	0.235001259	0.007525215	0.298222571	0.006225693	0.248446542
	1	0.001874464	0.176784007	0.002325454	0.238209839	0.001893819	0.191095557
	2	-0.001210999	0.151955459	-0.00183209	0.21333546	-0.00144143	0.167787327
	3	-0.003863122	0.151955459	-0.0055555	0.21333546	-0.00436987	0.167787327
Load [kN]	Depth [m]	Deflection [m]	Rotation [deg]	Deflection [m]	Rotation [deg]	Deflection [m]	Rotation [deg]
75	0.001	0.012008509	0.433293702	0.013949301	0.541765587	0.011536948	0.450939715
	1	0.003653669	0.345765451	0.004503164	0.451251489	0.003674436	0.364308039
	2	-0.002381076	0.30889801	-0.00337266	0.413564333	-0.00268394	0.329007
	3	-0.007772363	0.30889801	-0.01059072	0.413564333	-0.00842619	0.329007
Load [kN]	Depth [m]	Deflection [m]	Rotation [deg]	Deflection [m]	Rotation [deg]	Deflection [m]	Rotation [deg]
100	0.001	0.01855623	0.663327898	0.021744278	0.834376823	0.01900034	0.686335214
	1	0.005790552	0.546404556	0.007196218	0.713188648	0.00583351	0.57034104
	2	-0.003746007	0.497308751	-0.00525127	0.662596339	-0.00412082	0.522884033
	3	-0.012425682	0.497308751	-0.01681576	0.662596339	-0.01324687	0.522884033
Load [kN]	Depth [m]	Deflection [m]	Rotation [deg]	Deflection [m]	Rotation [deg]	Deflection [m]	Rotation [deg]
125	0.001	0.026075357	0.931495614	0.030222912	1.149945878	0.027527758	0.955581887
	1	0.008333949	0.785173165	0.01017264	0.99821239	0.008366386	0.810228428
	2	-0.005369908	0.723919468	-0.00724945	0.934656928	-0.00577477	0.750680997
	3	-1.80E-02	0.723919468	-2.36E-02	0.934656928	-1.89E-02	0.750680997
Load [kN]	Depth [m]	Deflection [m]	Rotation [deg]	Deflection [m]	Rotation [deg]	Deflection [m]	Rotation [deg]
150	0.001	0.034531449	1.216217007	0.039592519	1.49151899	0.037869129	1.243574896
	1	0.011125685	1.040393598	0.013586634	1.308686752	0.011186357	1.068703655
	2	-0.007032609	0.966692033	-0.00925426	1.23156963	-0.00746604	0.99673637
	3	-2.39E-02	0.966692033	-0.0307492	1.23156963	-2.49E-02	0.99673637

Table II-6 General lateral response - Pile DM7D

PILE	**DM7D**						
Case		All reactions		Only p-y		p-y + m-psi	
Load [kN]	Depth [m]	Deflection [m]	Rotation [deg]	Deflection [m]	Rotation [deg]	Deflection [m]	Rotation [deg]
50	0.001	0.004389206	0.13014173	0.004900031	0.145767802	0.004433206	0.131569401
	1	0.001120076	0.063927071	0.001358447	0.075920498	0.001139183	0.0655492
	2	4.33808E-06	0.021640646	3.3384E-05	0.03003985	-4.86625E-06	0.0237104
	3	-0.000373362	0.003681624	-0.00049091	0.01062432	-0.000418691	0.00609324
	3.8	-0.000424768	-0.00111075	-0.000639254	0.005337265	-0.000503768	0.001352313
	4.65	-0.000408289	-0.00111075	-0.000718434	0.005337265	-0.00052383	0.001352313
Load [kN]	Depth [m]	Deflection [m]	Rotation [deg]	Deflection [m]	Rotation [deg]	Deflection [m]	Rotation [deg]
100	0.001	0.009529221	0.304525781	0.010871615	0.34193657	0.009760646	0.308088934
	1	0.003219559	0.167554173	0.003909664	0.198735667	0.003288857	0.171517596
	2	0.000295187	0.075249566	0.000441072	0.100730107	0.00029531	0.080287269
	3	-0.001018166	0.033311556	-0.001317	0.057502128	-0.001105967	0.039840555
	3.8	-0.001483283	0.0203564	-0.002119881	4.52E-02	-0.001662246	2.82E-02
	4.65	-0.001785276	0.0203564	-0.002791053	0.045241524	-0.002079986	0.02815848
Load [kN]	Depth [m]	Deflection [m]	Rotation [deg]	Deflection [m]	Rotation [deg]	Deflection [m]	Rotation [deg]
150	0.001	0.016080089	0.507482449	0.018300097	0.569890978	0.017118823	0.511577429
	1	0.006131707	0.299367231	0.007363569	0.35288576	0.006199041	0.303901076
	2	0.000906763	0.156896434	0.001204551	0.202092542	0.000894967	0.162593139
	3	-0.001831596	0.091319037	-0.002322629	0.134458869	-0.001942819	0.098612504
	3.8	-0.003106651	0.070991323	-0.004200029	0.114978841	-0.003319709	0.079641355
	4.65	-0.004159828	0.070991323	-0.005905775	0.114978841	-0.004501212	0.079641355
Load [kN]	Depth [m]	Deflection [m]	Rotation [deg]	Deflection [m]	Rotation [deg]	Deflection [m]	Rotation [deg]
200	0.001	0.024362813	0.730436215	0.02782339	0.820058455	0.025573845	0.736201123
	1	0.009627045	0.450777154	0.011524982	0.528533215	0.009737561	0.457010899
	2	0.001759499	0.257559084	0.002300338	0.323689599	0.001761216	0.265035596
	3	-0.002735755	0.167927455	-0.003349112	0.230562955	-0.002864528	0.177137472
	3.8	-0.005080464	0.140123034	-0.006568378	2.04E-01	-0.005337834	1.51E-01
	4.65	-0.007159231	0.140123034	-0.009588448	0.203573292	-0.007576115	0.150875373
Load [kN]	Depth [m]	Deflection [m]	Rotation [deg]	Deflection [m]	Rotation [deg]	Deflection [m]	Rotation [deg]
250	0.001	0.03358616	0.969520046	0.037080968	1.08267307	0.0350244	0.975737185
	1	0.013681765	0.617623034	0.016203654	0.716378513	0.013811603	0.624315405
	2	0.002902209	0.372519533	0.00370049	0.456775418	0.002915244	0.380495952
	3	-3.60E-03	0.257874875	-4.27E-03	0.337368102	-3.73E-03	0.267684884
	3.8	-0.007200096	0.222263034	-0.008982292	0.302509621	-0.00746325	0.233754188
	4.65	-0.010497434	0.222263034	-0.013470113	0.302509621	-0.010931063	0.233754188
Load [kN]	Depth [m]	Deflection [m]	Rotation [deg]	Deflection [m]	Rotation [deg]	Deflection [m]	Rotation [deg]
300	0.001	0.04320985	1.214679951	0.048707912	1.3503912	0.045463614	1.221118198
	1	0.018030885	0.790698176	0.021162708	0.909692045	0.018172393	0.797636144
	2	0.004230599	0.493702046	0.005285587	0.595515885	0.004251016	0.501975538
	3	-4.39E-03	0.3538659	-0.005108126	0.449691628	-4.51E-03	0.364062851
	3.8	-0.009327027	0.310328903	-0.011387006	4.07E-01	-0.009593386	3.22E-01
	4.65	-0.013930849	0.310328903	-0.01742272	0.406848166	-0.014375341	0.322336309

Table II-7 General lateral response - Pile DM7E

PILE	**DM7E**						
Case		All reactions		Only p-y		p-y + m-psi	
Load [kN]	Depth [m]	Deflection [m]	Rotation [deg]	Deflection [m]	Rotation [deg]	Deflection [m]	Rotation [deg]
45	0.001	0.003696877	0.127749801	0.004054616	0.148510168	0.003751274	0.131807397
	1	0.001169452	0.069620549	0.001465216	0.088206709	0.001213102	0.074225481
	2	-4.5656E-05	0.035485742	-7.42811E-05	0.053327657	-8.23772E-05	0.041466936
	3	-0.000664999	0.024100247	-0.001005024	0.043005068	-0.000806112	0.031522245
	3.8	-0.001001502	0.024100247	-0.001605488	0.043005068	-0.001246245	0.031522245
Load [kN]	Depth [m]	Deflection [m]	Rotation [deg]	Deflection [m]	Rotation [deg]	Deflection [m]	Rotation [deg]
90	0.001	0.009456825	0.320164567	0.010987379	0.375434409	0.009691365	0.327923068
	1	0.003574488	0.201826725	0.004441365	0.252805728	0.003673751	0.210267404
	2	5.19467E-05	0.13140239	2.90729E-05	0.180232698	3.89295E-06	0.141447462
	3	-0.002241458	0.108422053	-0.003116581	0.158349434	-0.002464831	0.120051297
	3.8	-0.003755315	0.108422053	-0.005327556	1.58E-01	-0.004141063	1.20E-01
Load [kN]	Depth [m]	Deflection [m]	Rotation [deg]	Deflection [m]	Rotation [deg]	Deflection [m]	Rotation [deg]
135	0.001	0.017593133	0.556122254	0.019771222	0.6536588	0.018003981	0.566173766
	1	0.006796675	0.377132951	0.008374132	0.468212747	0.006932266	0.387932802
	2	0.000214463	0.269694964	0.000202278	0.357146024	0.000161561	0.282231636
	3	-0.004492602	0.23483178	-0.006031096	0.32339015	-0.00476431	0.249054108
	3.8	-0.007771472	0.23483178	-0.010546474	0.32339015	-0.008241761	0.249054108
Load [kN]	Depth [m]	Deflection [m]	Rotation [deg]	Deflection [m]	Rotation [deg]	Deflection [m]	Rotation [deg]
180	0.001	0.027060099	0.825852687	0.030165152	0.975974231	0.028022918	0.838248192
	1	0.010660665	0.585958837	0.013148222	0.727479539	0.010807357	0.599108697
	2	0.000433754	0.441230805	0.000451309	0.577548005	0.000350938	0.456129205
	3	-0.007267177	0.394392018	-0.009628805	0.53176586	-0.007610019	0.411029684
	3.8	-0.012773928	0.394392018	-0.017053657	5.32E-01	-0.013349076	4.11E-01
Load [kN]	Depth [m]	Deflection [m]	Rotation [deg]	Deflection [m]	Rotation [deg]	Deflection [m]	Rotation [deg]
225	0.001	0.037805519	1.126480169	0.041935778	1.334661613	0.039028136	1.140855403
	1	0.015164392	0.825626026	0.018664833	1.022993665	0.015336365	0.840801764
	2	0.000754499	0.643684398	0.000810225	0.834174293	0.000661606	0.660684216
	3	-1.05E-02	0.58491692	-1.37E-02	0.776321482	-1.09E-02	0.603716442
	3.8	-0.018646894	0.58491692	-0.024588356	0.776321482	-0.019298981	0.603716442
Load [kN]	Depth [m]	Deflection [m]	Rotation [deg]	Deflection [m]	Rotation [deg]	Deflection [m]	Rotation [deg]
270	0.001	0.049960843	1.453429386	0.05481094	1.721115866	0.051543493	1.545392645
	1	0.020219082	1.091533984	0.024801841	1.345966642	0.021598276	1.170708042
	2	0.00116822	0.872211029	0.001310291	1.117657512	0.001165566	0.944866531
	3	-1.41E-02	0.801355007	-0.018196512	1.047246623	-1.53E-02	0.873165931
	3.8	-0.025243761	0.801355007	-0.032818833	1.05E+00	-0.027517163	8.73E-01

Table II-8 General lateral response - Pile DM4

PILE	**DM4**						
Case		All reactions		Only p-y		p-y + m-psi	
Load [kN]	Depth [m]	Deflection [m]	Rotation [deg]	Deflection [m]	Rotation [deg]	Deflection [m]	Rotation [deg]
40	0.001	0.002492479	0.08933587	0.0027928	0.102045358	0.002593678	0.092915909
	1	0.000834833	0.061376204	0.001013554	0.073363081	0.000873611	0.06512669
	1.33	0.000481332	0.044611312	0.000591013	0.056042625	0.000498508	0.048680239
	2	-4.03398E-05	0.026087918	-6.43335E-05	0.037109329	-7.07444E-05	0.031024869
	3	-0.00049566	0.016705985	-0.000712013	0.028253931	-0.000612231	0.022766593
	4	-0.000787234	0.016705985	-0.001205138	0.028253931	-0.001009583	0.022766593
Load [kN]	Depth [m]	Deflection [m]	Rotation [deg]	Deflection [m]	Rotation [deg]	Deflection [m]	Rotation [deg]
80	0.001	0.006690635	0.224856108	0.007479762	0.255093296	0.006998711	0.231566852
	1	0.00257008	0.168202133	0.003031997	0.197042352	0.002661148	0.175129332
	1.33	0.001601305	0.13393804	0.001897114	0.161550818	0.001652476	0.141276517
	2	3.5073E-05	0.09592606	7.98642E-06	0.122177409	4.29814E-07	0.104373995
	3	-0.001639153	0.077116023	-0.002124412	1.04E-01	-0.00182124	8.70E-02
	4	-0.002985081	0.077116023	-0.003934483	0.103709458	-0.00333885	0.086952641
Load [kN]	Depth [m]	Deflection [m]	Rotation [deg]	Deflection [m]	Rotation [deg]	Deflection [m]	Rotation [deg]
120	0.001	0.012214104	0.389821099	0.013529177	0.439258274	0.012525441	0.397108046
	1	0.005017246	0.304067534	0.00587034	0.351447876	0.005101529	0.311551063
	1.33	0.003265943	0.251863837	0.003846146	0.297258547	0.003307124	0.259711294
	2	0.000320721	0.193702743	0.000370092	0.236514608	0.000270136	0.202561239
	3	-0.003060029	0.165341439	-0.003757867	0.20811696	-0.003265224	0.175602471
	4	-0.005945782	0.165341439	-0.007390193	0.20811696	-0.006330065	0.175602471
Load [kN]	Depth [m]	Deflection [m]	Rotation [deg]	Deflection [m]	Rotation [deg]	Deflection [m]	Rotation [deg]
160	0.001	0.018859923	0.569633618	0.020323296	0.638728991	0.019009303	0.577988006
	1	0.007927882	0.455059635	0.00918652	0.521391643	0.008031597	0.463626103
	1.33	0.005306927	0.385204772	0.006183519	0.448868309	0.005361302	0.394160309
	2	0.000802456	0.307326495	0.000934585	0.367501956	0.000752107	0.317363306
	3	-0.004561404	0.269850432	-0.005479534	3.30E-01	-0.004786927	2.81E-01
	4	-0.009271182	0.269850432	-0.011237297	0.329895506	-0.009698676	0.281422493
Load [kN]	Depth [m]	Deflection [m]	Rotation [deg]	Deflection [m]	Rotation [deg]	Deflection [m]	Rotation [deg]
200	0.001	0.025659846	0.761684148	0.027829942	0.852677147	0.026551659	0.770987981
	1	0.011179243	0.617947967	0.0129628	0.705501981	0.011308836	0.62745249
	1.33	0.007620118	0.530220735	0.0088994	0.614341316	0.007694969	0.540103595
	2	1.42E-03	0.432518933	1.72E-03	0.511947857	1.38E-03	0.443485182
	3	-0.006129006	0.386045789	-0.007219702	0.464912894	-0.00636112	0.39861485
	4	-0.012866776	0.386045789	-0.015333963	0.464912894	-0.013318261	0.39861485
Load [kN]	Depth [m]	Deflection [m]	Rotation [deg]	Deflection [m]	Rotation [deg]	Deflection [m]	Rotation [deg]
240	0.001	0.033781542	0.967315104	0.036086386	1.080274571	0.035002039	0.977283981
	1	0.014915592	0.794350032	0.017250892	0.903201686	0.015062273	0.804510131
	1.33	0.010340464	0.688588008	0.012048824	0.793299811	0.010428627	0.699120167
	2	2.29E-03	0.570700455	0.002772209	0.669648543	2.25E-03	0.582323604
	3	-0.007672284	0.514933916	-0.008915363	6.13E-01	-0.007910142	5.28E-01
	4	-0.016659576	0.514933916	-0.019613036	0.612931527	-0.017129378	0.528223284

III. APPENDIX: Partial Lateral Response (Plots)

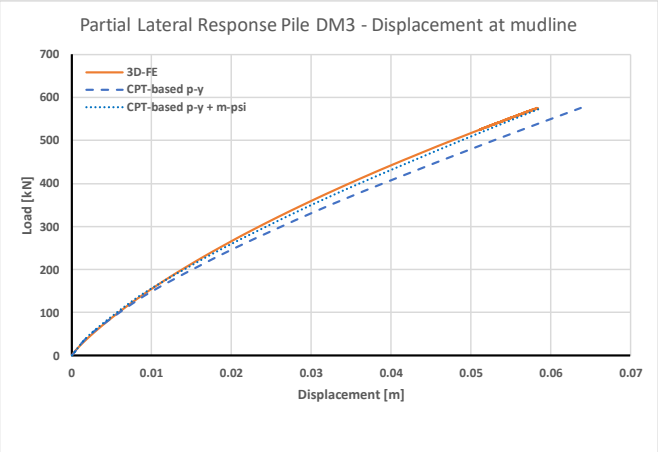

Figure III- 1 Partial Lateral Response Pile DM3

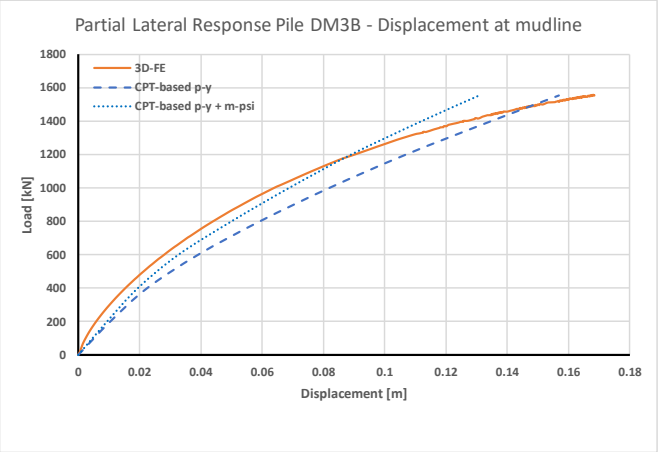

Figure III- 2 Partial Lateral Response Pile DM3B

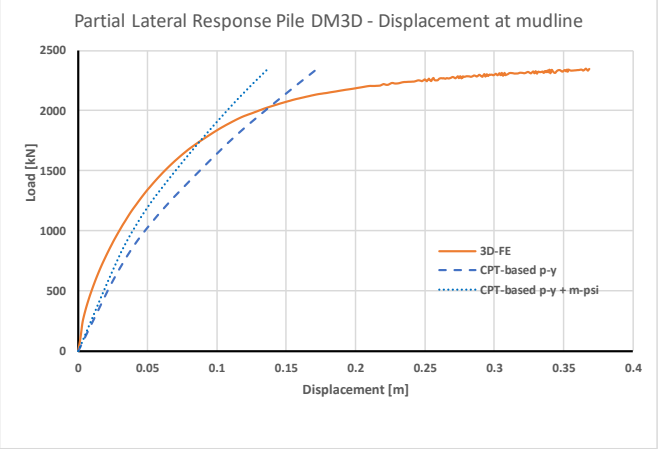

Figure III- 3 Partial Lateral Response Pile DM3D

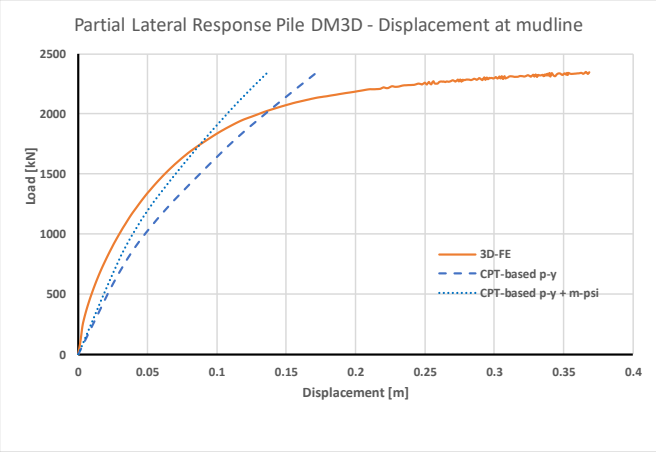

Figure III- 4 Partial Lateral Response Pile DM7

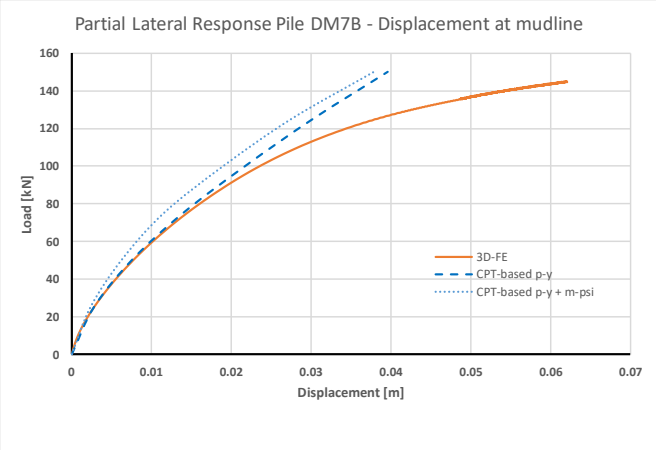

Figure III- 5 Partial Lateral Response Pile DM7B

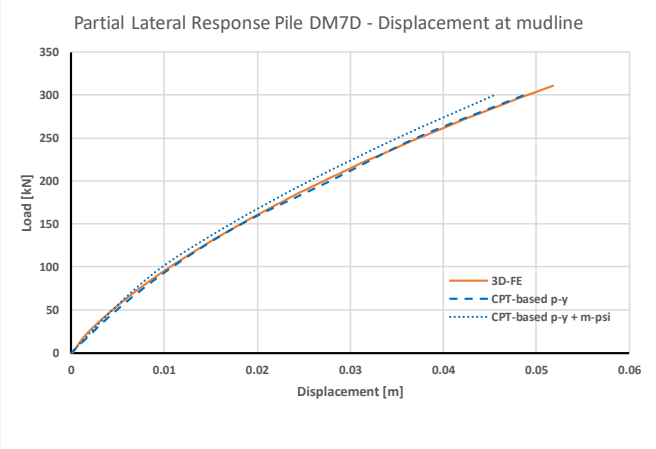

Figure III- 6 Partial Lateral Response Pile DM7D

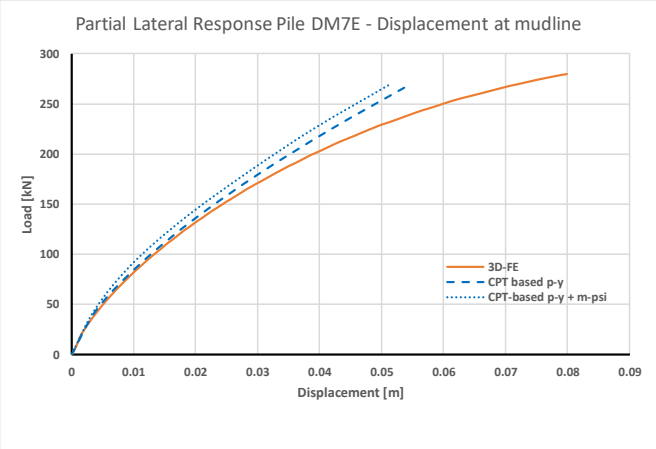

Figure III- 7 Partial Lateral Response Pile DM7E

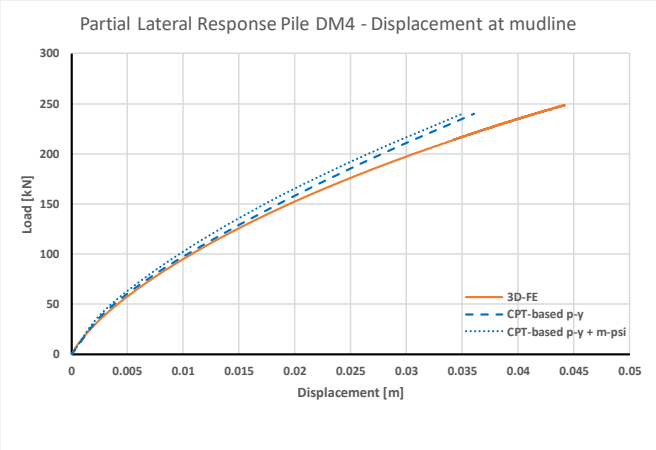

Figure III- 8 Partial Lateral Response Pile DM4

List of Tables and Figures